technische universität dortmund

thermodynamik

Department of Biochemical and Chemical Engineering

Laboratory of thermodynamics

Prof. Dr. Gabriele Sadowski

Oxalic Acid – Phase Behavior of a Cocrystal and Hydrate Forming Component

Master-Thesis

Miko Schleinitz

March 29, 2016

Examiner: Prof. Dr. Gabriele Sadowski

Coexaminer: Prof. Dr.-Ing. Gerhard Schembecker

Supervisor: Dipl.-Ing. Linda Lange

Declaration of Authorship

I hereby declare that this submission is my own work and that, to my best knowledge and belief, it contains neither materials previously published or written by another person nor any contribution made to the research by others except where special acknowledgement is made in this bachelor thesis.

Dortmund, March 29, 2016

Miko Schleinitz

Table of Contents

List of Symbols and Abbreviations

Symbols

Symbol	Meaning	Unit
a	Activity	-
A	Absorbance	-
A^{assoc}	Helmholtz energy of association	J
A^{DH}	Helmholtz energy of Debye-Hückel	J
A^{disp}	Helmholtz energy of dispersion	J
A^{hc}	Helmholtz energy of hard chain	J
ARD	Average relative deviation	%
A^{res}	Residual Helmholtz energy	J
c	Concentration	mol L^{-1}
d	Cuvette thickness	mm
f	Fugacity	Pa
k	Boltzmann constant	J K^{-1}
K_a	Dissociation constant	-
k_{ij}	Binary interaction parameter of i and j	-
$k_{ij,b}$	Intrinsic binary interaction parameter	-
$k_{ij,m}$	Temperature-dependent binary interaction	K^{-1}
K_s	Solubility product	-
K_x	Mole fraction product	-
K_γ	Activity coefficient product	-
l	Lattice plane	nm
$\bar{m}$	Mean segment number	-
m_{seg}	Segment number	-
M	Molecular mass	g mol^{-1}
N	Number of molecules	-
N_A	Avogardo constant	mol^{-1}
p^+	Standard pressure	Pa
pH	pH value	-
pK_a	Logarithm of acid constant	-

Symbol	Meaning	Unit
q	Charge	e
$\dot{q}$	Mass specified heat flow	W g^{-1}
R	Ideal gas constant	J mol^{-1} K^{-1}
t	Time	hours
T	Temperature	K
u	Dispersion energy	K
w	Weight fraction	wt.%
x	Mole fraction	mol mol^{-1}
Z	Compressibility factor	-
γ	Activity coefficient	-
Δc_p	Heat capacity difference	J mol^{-1} K^{-1}
Δg	Gibbs energy	J mol^{-1}
Δh	Enthalpy difference	J mol^{-1}
Δs	Entropy difference	J mol^{-1} K^{-1}
ε	Molar extinction	mm^{-1}
ε^{AiBi}	Association energy of component i	K
ε^{AiBj}	Association energy of the mixture of i and j	K
ε^{AjBj}	Association energy of component j	K
θ	Diffraction angle	°
κ^{AiBi}	Association volume of component i	-
κ^{AiBj}	Association volume of the mixture of i and j	-
κ^{AjBj}	Association volume of component j	-
λ	Wave length	nm
μ	Chemical potential	J mol^{-1}
ν	Stoichiometric coefficient	-
ν_{sp}	Specific molar volume	m^3 mol^{-1}
ρ	Density	kg m^{-3}
σ	Segment diameter	Å
φ	Fugacity coefficient	-
$\dot{\vartheta}$	Heat-up rate	°C min^{-1}

Subscripts and Exponents

Subscript	Meaning
0i	Property of pure component i
0	Neutral non-dissociated component
208	Wave length of 208 nm
208 Cal	Recalibration at 208 nm
273	Wave length of 273 nm
273 Cal	Recalibration at 273 nm
buffer	Phosphate buffer as the solvent
C	Caffeine
C hydrate	Caffeine hydrate (1:0.8)
CC	Cocrystal
exp	Experimental
H_2O	Water
$H_2C_2O_4 \cdot 2\ H_2O$	Oxalic acid dihydrate
i	Component i
ij	Interaction of component i and component j
j	Component j
m	Melting
n	Number of components
$Na_2C_2O_4$	Disodium oxalate
$NaHC_2O_4 \cdot H_2O$	Sodium hydrogen oxalate monohydrate
OxA	Oxalic acid ($H_2C_2O_4$)
range	Temperature range
total	Total

Exponents	Meaning
id	Ideal
L	Liquid phase
ref	Reference
res	Residual
S	Solid phase
SL	Solid-liquid interaction

Abbreviations

Abbreviations	Meaning
A	Neutral solute
A^-	Dissociated acid or anion of a salt
ACN	Acetonitrile
AI	Non-dissociated salt
API	Active pharmaceutical ingredient
API^+	Protonated active pharmaceutical ingredient
BCS	Biopharmaceutics class system
CC	Cocrystal
CF	Coformer
CF^-	Dissociated coformer
CF^{2-}	Twice dissociated coformer
CH_3OH	Methanol
COD	Crystallography open database
CSD	Cambridge structural database
DSC	Differential scanning calorimetry
EA	Ethyl acetate
GRAS	General recognized as safe
H_2O	Water
H^+	Hydrogen proton
HA	Non-dissociated acid
HCl	Hydrogen chloride
$HOxA^-$	Hydrogen oxalate ($HC_2O_4^-$)
HPLC	High performance liquid chromatography
I_2	Iodine
I^+	Cation of a salt
KF-T	Karl-Fischer Titration
L	Liquid Phase
NaOH	Sodium hydroxide
OxA	Oxalic acid ($H_2C_2O_4$)
OxA^{2-}	Oxalate ($C_2O_4^{2-}$)

Abbreviations	**Meaning**
PC-SAFT	Perturbed-chain statistical associating fluid theory
PXRD	Powder X-ray diffraction
Ref.	Reference
RN	Alkyl part with nitrogen (e.g. imidazole)
[RNH]I	Alkyl, nitrogen iodine complex
$[RNH]SO_3CH_3$	Alkyl, nitrogen sulfur complex
$[RNH]SO_4CH_3$	Alkyl, nitrogen sulfur complex
SO_2	Sulfur dioxide
UV/VIS	Ultra violet and visible light

1. Introduction

One of the greatest challenges in pharmaceutical industry is the improvement of physico-chemical properties of active pharmaceutical ingredient (API) [1]. More than 40% of available API's have a good permeability but a low solubility [1]. Therefore, the solubility of API's has to be optimized without the reduction of its pharmaceutical properties. An attractive method for solubility improvement is the formation of cocrystals. In this case, the API and a coformer are forming a stoichiometric crystal structure, interacting via weak interactions [2]. By dissolution of the cocrystal, the pharmaceutical properties of the API remain constant but the solubility can be increased drastically [2]. However, the physicochemical properties that can be achieved depend on the composition of the cocrystal and therefore the selection of coformer for an API has to be based on the desired properties [3]. For example, the focus can be set on stability improvement because most API's have a limited storage stability which can be enhanced by cocrystal formation [3].

Usually coformer and API have basic or acidic properties [4] and thus dissociated species have to be considered as well. By alteration of the pH value, the concentration of proton donors or proton acceptors of API and coformer can change. Due to the dissociation, the solubility of API and coformer can alter by pH variation and the measured solubility is always the concentration of all dissociated and non-dissociated species. Therefore, the cocrystal solubility also depends on the pH value which is investigated within this work.

The cocrystal solubility in a solvent can be illustrated in a ternary phase diagram of coformer, API and the solvent. This diagram allows a complete presentation of all occuring solid phases and solubility points. Especially the pH-dependent cocrystal solubility is of major interest for the pharmaceutical industry. By its knowledge, cocrystals can be applied more easily in pharmaceutical industry. However, the determination of ternary phase diagrams for a component system is time consuming and cost intensive. Therefore, it is required to develop thermodynamic models to reduce the experimental effort and achieve results more quickly.

The aim of this work is the investigation of oxalic acid as a hydrate and cocrystal forming component. Therefore, the cocrystal system consisting of the coformer oxalic acid and the API caffeine shall be examined. In this case, the API caffeine is also a hydrate forming component. The experimental results within this work shall be model with perturbed-chain statistical association fluid theory (PC-SAFT). In the first part of this work, PC-SAFT pure component parameters of oxalic acid shall be determined by solubility experiments within organic solvents.

Afterwards, the temperature-dependent solubility of oxalic acid and caffeine within water shall be modeled via PC-SAFT and hydrate solubility products. Then the pH-dependent binary solubility of oxalic acid and caffeine within water shall be examined at 298.15 K. In addition, the pH-dependent cocrystal solubility of oxalic acid, caffeine and water at 298.15 K and pH values 1, 2, 4, 5 and 7 shall be investigated by experiments. Afterwards, the cocrystal solubility shall be modeled for one pH value and predicted for the remaining pH values via PC-SAFT. In addition, the salt and hydrate solubility of caffeine in presence of oxalic acid shall be predicted and vice versa.

2. Theory

This chapter starts with a short introduction to cocrystals, their formation and benefits in chemical processes and their fields of application (2.1). Afterwards, the determination of the solid-liquid equilibrium is presented in chapter 2.2. The chapter is subdivided in the temperature-dependent solubility of pure components (2.2.1), the pH-dependent solubility of pure components (2.2.2) and the determination of the cocrystal solubility (2.2.3). Then the modeling with PC-SAFT is introduced for the determination of the activity coefficients in mixtures (2.3). At last, the modeling procedure for the determination of the PC-SAFT parameters for oxalic acid and modeling of the phase diagrams is introduced (2.4).

2.1. Cocrystals

At first, a short introduction to cocrystals, their advantages in comparison to sole active pharmaceutical ingredients (API), solvates and hydrates are presented (2.1.1). Furthermore, the fields of application for cocrystals are presented within this chapter. Second, the cocrystal formation for an API and a coformer (CF) in water is presented and illustrated in a ternary diagram. In addition, the focus is set on the non-ideality of the API and CF solubility and the illustration of hydrate forming components (2.1.2).

2.1.1. Introduction to Cocrystals

This chapter focuses on the introduction to cocrystals. Therefore, the necessity of product improvement in pharmaceutical industry is shown. Afterwards, the application of solvates and hydrates is discussed briefly. Then the focus is set on the properties and advantages of cocrystals in comparison to solvates and hydrates. At last, the fields of application are presented.

In the first section, the necessity of product improvement for pharmaceutical products is described. A challenge for the application of pharmaceutical products and medicines is the improvement of the solubility of pure API's [5]. The API's in the biopharmaceutics class system (BCS) class II are of major interest because these API's have a high permeability and a low solubility [6]. This class represents 40% of all manufactured API's [1]. The other classes I and III have a high solubility and class III is only limited in its permeability [1]. Hence, an improvement of the solubility of API's in BCS class II would lead to better bioavailability of these pharmaceutical products and would also enhance the product quality.

For the improvement of the solubility and bioavailability of API's, crystal structures of the API's such as salts, solvates or hydrates can be formed [5]. However, the application of solvates is difficult due to the toxicity of many solvents which are part of the crystal structure [2]. An alternative could be the application of API hydrates but these components could show significant pharmacological property changes [2]. The hydrates are especially sensitive to temperature, pressure or changes in relative humidity [2], [7]. Therefore, a stable complex structure of API's has to be developed to ensure improved solubility and stability of the complex to humidity exhibition.

An attractive method for property improvement is the formation of cocrystals. On the one hand, its application results in an improvement of the physicochemical properties and therefore can enhance the solubility of the API [5]. On the other hand, the API keeps its pharmacological properties [5]. According to *Jones et al.*, a cocrystal is "a crystalline complex of two or more neutral molecular constituents bound together in the crystal lattice through noncovalent interactions, often including hydrogen bonding" [2]. Furthermore, a cocrystal can be formed theoretically with all API's and therefore this method exploits a large field of application [2]. For the cocrystal formation, the API and a coformer (CF) are forming a stoichiometric crystal structure, interacting via weak interactions [2]. The stoichiometry of the crystal structure depends on the component system of API and CF. The advantage of cocrystals is the simple formation of supramolecular structures and the modularity of API and CF in comparison to solvates and hydrates [8]. Based on the diversity of cocrystals that can be achieved, the properties of the various cocrystals can be different. On the one hand, the solubility of the API can be improved. On the other hand, the main focus can be set on the stability of the cocrystal to protect the API from hydration exhibiting to humidity. Hence, the physicochemical properties of the cocrystal and the API can be adjusted by the selection of the coformer. For this purpose, the coformer should have a "general recognized as safe (GRAS)" status to be a non-toxic component and can be applied in pharmaceutical cocrystals [5].

The last section focuses on the fields of application for cocrystals. Cocrystal formation is a preferred method in pharmaceutical industry to improve physicochemical properties compared to pure API's [8]. Therefore, the solubility of API's can be increased to improve the absorption capacity of the API into the human body. Furthermore, the stability can be improved by cocrystal formation to enhance the storage stability. In this case, the cocrystal has a high stability against temperature, pressure or humidity changes. Another example can be that the API is released over a long period of time ("slow releasing tablets") [1]. In addition, cocrystals

are applied as molecular semiconductors in electric circuits as transistors [8]. Furthermore, cocrystals can be applied as optical materials in photochemical processes and are used as catalysts in media for stereocontrolled synthesis of other components [8]. The growing fields of application lead to emerging markets for cocrystals and therefore the field of cocrystal formation and cocrystal screening is a growing research topic [2].

2.1.2. Cocrystal Formation

This chapter focuses on the determination of the cocrystal solubility in ternary phase diagrams and cocrystal formation methods. At first, cocrystal formation techniques are discussed briefly. Then the illustration of the cocrystal solubility in a ternary phase diagram is described. Afterwards, the ternary phase diagram becomes more complex in two steps. In the first step, the cocrystal stoichiometry is adjusted to the examined system of caffeine and oxalic acid and a non-ideality of the active pharmaceutical ingredient (API) solubility is presented. In the second step, the solubilities of API and coformer (CF) hydrates are included in the ternary phase diagram, due to the hydrate formation of oxalic acid and caffeine in water. Afterwards, the conversion of the ternary phase diagram into a binary diagram is presented. In this work, the binary illustration is applied to present the results of the cocrystal experiments.

In the first section, the cocrystal formation methods are discussed briefly. Cocrystal formation can be achieved by solution-based methods (e.g. solvent evaporation, slurry conversion, cooling crystallization or precipitation) or solid-based-techniques (e.g. dry co-grinding, wet co-grinding, crystallization from melt) [5]. In this work, the cocrystal is formed in the solution by oversaturation of the solvent. The other techniques are not used in this work.

In this section, the ternary phase diagram for a cocrystal (CC) with a 1:1 stoichiometry of API to (CF) is described. For a better insight, the system is presented in Figure 2-1. By a presentation of the ternary diagram in mole fractions, the stoichiometry of the cocrystal is shown on the axis between the API and CF. Additionally, the pure API and CF solubilities in water on the axes between API, CF and water are shown. If the water concentration is high and the solutes are completely dissolved in water, a solubility point in the concentration range (L) can be achieved.

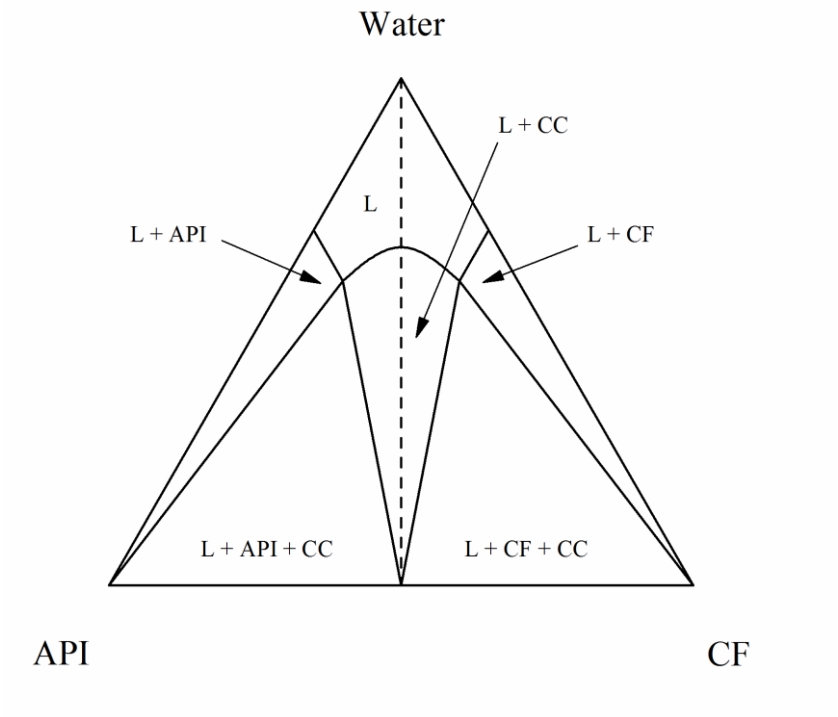

Figure 2-1: Ternary phase diagram consisting of the active pharmaceutical ingredient (API), the coformer (CF) and water. L corresponds to the liquid phase while the concentration ranges represents the equilibria of L with solid phases (e.g. "L+CF+CC" corresponds to the liquid phase L in equilibrium with a solid mixture of CF and cocrystal CC). In this case, a complete solid phase of CC can be achieved by a solid mixture of API and CF with a 1:1 mole ratio by adding water to the solid mixture

By mixing API and CF in a 1:1 mole ratio and add water to the solids (black dashed line), pure cocrystal formation is achieved which is in equilibrium with the liquid phase (L+CC). In addition, the solubility line of the API and CF are shown. In this case, the solubility and the activity coefficients of API (or CF) are not influenced by the presence of CF (or API) in the ideal solution [9]. If the solids API and CF are mixed in a 2:1 mole ratio and water is added to the solids, a mixture in the solid phase can be achieved (L+API+CC). In this case, the liquid phase L is in equilibrium with the solid mixture of API and CC. By adding only small amounts of CF to an API and water mixture, pure API in the solid phase can be recovered and vice versa. Therefore, the liquid phase L is in equilibrium with the solid phase of the pure API (or CF).

In the next section, the ternary phase diagram becomes more complex. Therefore, the stoichiometry for the 2:1 cocrystal of caffeine and oxalic acid is applied instead of the 1:1 stoichiometry. Additionally, a non-ideality of the API solubility is introduced. The example for a non-ideal ternary phase diagram is shown in Figure 2-2. It is shown that the API solubility line is curved and therefore the activity coefficients and the solubility of the API are influenced by the presence of CF [9].

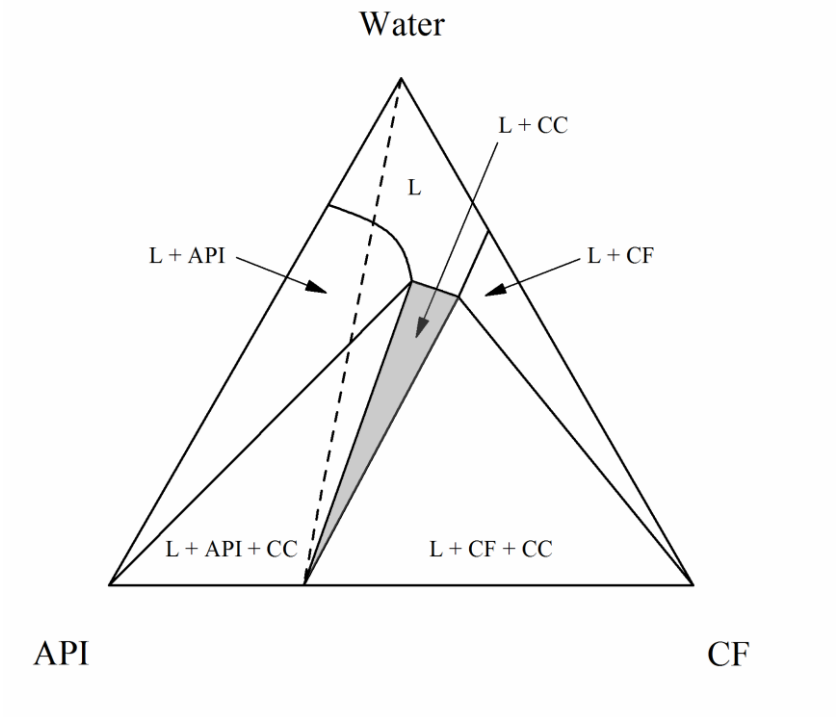

Figure 2-2: Non-ideal ternary phase diagram consisting of the active pharmaceutical ingredient (API), the coformer (CF) and water. L corresponds to the liquid phase while the concentration ranges represents the equilibria of L with solid phases (e.g. "L+CF+CC" corresponds to the equilibrium of the liquid phase L and a solid mixture of CF and cocrystal CC). For example, a complete solid phase of CC can be achieved by a solid mixture of API and CF with a 1:2 mole ratio by adding water to the solid mixture

By adding water to the solid mixture with a 2:1 mole ratio of API to CF, mostly API and small amounts of the cocrstal can be recovered (black dashed line). In this case, pure cocrystal formation can only be achieved by mole ratios with higher CF amount (e.g. API:CF mole ratio of 1:2) to reach a mixture within the grey section. Therefore, water is added to the solid mixture with a 1:2 mole ratio of API to CF. The other equilibria can be determined with the same procedure as described in the previous section for the simplified ternary diagram with 1:1 stoichiometry of API to CF.

In the following section, the ternary phase diagram becomes more complex due to hydrate formation of API and CF in water. At first, the ternary diagram is presented and discussed. Afterwards, the ternary phase diagram is converted into a binary diagram that is used in this work for the illustration of the API, CF and water system at various pH values. The ternary phase diagram is presented in Figure 2-3. This diagram is based on Figure 2-2 with the same concentration range for the cocrystal (L+CC) and the liquid phase L. In this case, API and CF are forming hydrates in water. Therefore, the hydrate stoichiometry can be identified on the axes of API with water and CF with water. Due to the hydrate formation, the solubility line of API hydrate and CF hydrate are shown instead of the solubility of pure API and CF.

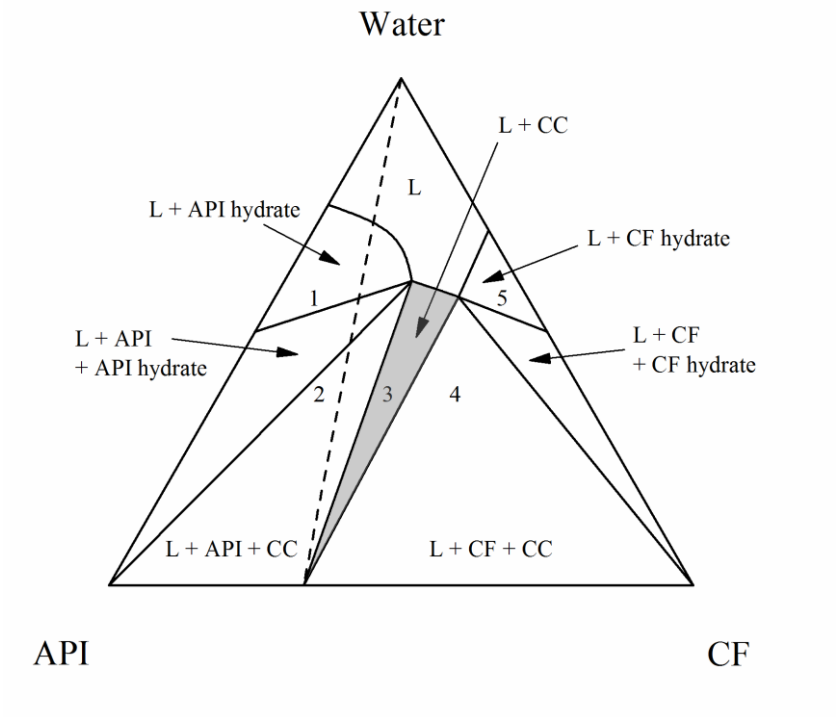

Figure 2-3: Ternary phase diagram of active pharmaceutical ingredient (API), coformer (CF) and water. In addition, API and CF are hydrate forming components and therefore the concentration ranges are divided. L corresponds to the liquid phase while the concentration ranges represents the equilibria of L with solid phases (e.g. "L+CF+CC" corresponds to an equilibrium between the liquid phase L and a solid mixture of CF and cocrystal CC). The numbers (1) to (5) correspond to equilibria illustrated in the same concentration range and these equilibria are also taken into account for the conversion into the binary diagram

In comparison to Figure 2-2 (L+API), the concentration range is divided in (L+API hydrate) and (L+API+API hydrate). For CF, the concentration range of (L+CF) is divided in (L+CF hydrate) and (L+CF+CF hydrate). The numbers for the various phase equilibria correspond to the phases in the same concentration range. These numbers are applied for the conversion of the ternary phase diagram into the binary diagram. For a better illustration, the equilibria of (L+API+API hydrate) and (L+CF+CF hydrate) are not presented in the binary diagram. These equilibria are of minor importance due to the difficult determination of the solubility point at the intersection of the concentration ranges of (1), (2), (3) and (3), (4), (5).

The following section focuses on the conversion of the ternary phase diagram into the binary diagram because the results of this work are presented in binary diagrams. This illustration allows an easier understanding of the examined system and identification of the cocrystal and hydrate concentration ranges. The binary diagram is presented in Figure 2-4. In this diagram, the mole fraction of the API is presented as a function of CF. The numbered concentration ranges shown in the ternary diagram correspond to the concentration ranges in the binary diagram. In this case, the concentration range (1) corresponds to the equilibrium of the liquid

phase L with API hydrate, concentration range (2) corresponds to the equilibrium between the liquid phase L and a solid mixture of API hydrate and CC and concentration range (3) to the equilibrium of the liquid phase with pure cocrystal formation. Furthermore, the liquid phase L is in equilibrium with a solid mixture of CC and CF hydrate (4) and with pure CF hydrate formation (5).

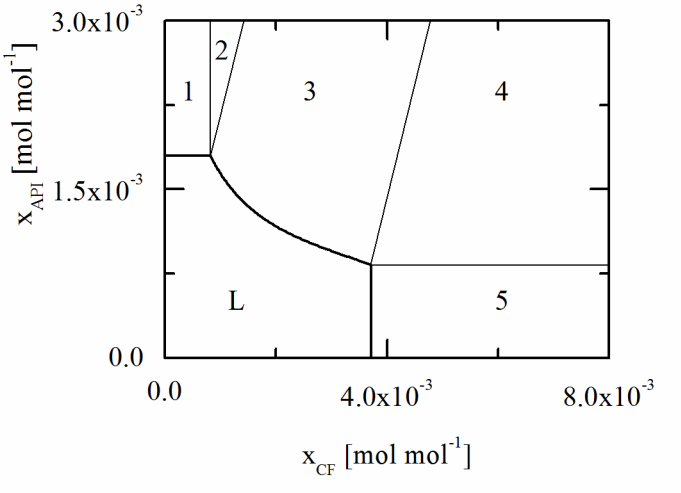

Figure 2-4: Illustration of ternary phase diagram in a binary diagram. The mole fraction of the active pharmaceutical ingredient (API) is shown as a function of the mole fraction of the coformer CF. The cocrystal and hydrate solubility is presented by bold black solid lines. The thin black solid lines correspond to phase boundaries between two solid phases. The liquid phase L is in equilibrium with API hydrate (1), a solid mixture of cocrystal (CC) and API hydrate (2), pure CC formation (3), a solid mixture of CC and CF hydrate (4) and CF hydrate (5)

2.2. Solid-Liquid-Equilibrium

The aim of this work is the determination and modeling of the solid-liquid equilibria. Therefore, this chapter is divided into the temperature-dependent solubility (2.2.1), the pH-dependent solubility of pure components (2.2.2) and the pH-dependent solubility of the cocrystals and hydrates (2.2.3).

2.2.1. Solubility of Pure Components

This chapter focuses on the determination of the solubility of pure components. The solubility of pure components depends on the temperature, the pressure and the chemical equilibrium. The chemical equilibrium between the solid phase μ_i^S and the liquid phase μ_i^L can be described with the following equation:

$$\mu_i^S = \mu_i^L \tag{2-1}$$

The chemical potential μ_i can be calculated by equation (2-2) [10]. In this case, μ_{0i}^{id} corresponds to the ideal chemical potential at the reference pressure p^+ and the desired temperature T. The ideal potential is independent of the concentration of the component. The second term contains the ideal gas constant R and the fugacity f_i.

$$\mu_i(T,p) = \mu_{0i}^{id}(T,p^+) + R \cdot T \cdot \ln\left(\frac{f_i}{p^+}\right) \tag{2-2}$$

Due to the equal term of μ_{0i}^{id} in the solid and liquid phase, equation (2-2) can be simplified. A chemical equilibrium is reached, when the fugacity of the solid phase f_i^S is equal to the fugacity of the liquid phase f_i^L (2-3).

$$f_i^S = f_i^L \tag{2-3}$$

The fugacity of each phase can be described by the activity coefficient γ_i, the mole fraction x_i and the standard fugacity of the pure component f_{0i} with equation (2-4).

$$x_i^S \cdot \gamma_i^S \cdot f_{0i}^S = f_{0i}^L \cdot x_i^L \cdot \gamma_i^L \tag{2-4}$$

Furthermore, the chemical potential can be equated with the Gibbs energy and therefore, the solid-liquid equilibrium can be determined with equation (2-5) [11].

$$\Delta g^{SL} = R \cdot T \cdot \ln\left(\frac{f_{0i}^{L}}{f_{0i}^{S}}\right) \tag{2-5}$$

In addition, the difference of the Gibbs energy Δg^{SL} between the solid and liquid phase can be calculated by equation (2-6) [11]. In this case, Δh^{SL} corresponds to the specific enthalpy and Δs^{SL} to the specific entropy difference which can be replaced by the equations mentioned in Appendix in (A-1) and (A-2).

$$\Delta g^{SL} = \Delta h^{SL} - T \cdot \Delta s^{SL} \tag{2-6}$$

By combination of equation (2-4) to (2-6), the mole fraction of the liquid phase x_i^L can be calculated as a function of the activity coefficient γ_i^L, the melting temperature T_{0i}^{SL}, the specific melting enthalpy Δh_{0i}^{SL} and the difference in the heat capacity $\Delta c_{p,i}^{SL}$ of the pure component with equation (2-7) [12].

$$\ln\left(\frac{x_i^L \cdot \gamma_i^L}{x_i^S \cdot \gamma_i^S}\right) = -\frac{\Delta h_{0i}^{SL}}{R \cdot T} \cdot \left(1 - \frac{T}{T_{0i}^{SL}}\right) - \frac{\Delta c_{p,i}^{SL}}{R} \cdot \left(\ln\left(\frac{T_{0i}^{SL}}{T}\right) - \frac{T_{0i}^{SL}}{T} + 1\right) \tag{2-7}$$

Furthermore, the assumption is made that only the pure solute crystallizes and therefore, the mole fraction of the solid phase x_i^S and the activity coefficient γ_i^S are equal to one. Under this assumption, equation (2-7) can be simplified to equation (2-8). The PC-SAFT model for the determination of the activity coefficient is presented in chapter 2.3.

$$x_i^L = \frac{1}{\gamma_i^L} \cdot \exp\left(-\frac{\Delta h_{0i}^{SL}}{R \cdot T} \cdot \left(1 - \frac{T}{T_{0i}^{SL}}\right) - \frac{\Delta c_{p,i}^{SL}}{R} \cdot \left(ln\left(\frac{T_{0i}^{SL}}{T}\right) - \frac{T_{0i}^{SL}}{T} + 1\right)\right) \tag{2-8}$$

2.2.2. pH-Dependent Solubility of Pure Components

This chapter focuses on the pH-dependent solubility of the active pharmaceutical ingredient (API) and the coformer (CF). The API and CF usually have acidic or basic properties and therefore the variation of the pH has a significant influence on the solubility [13]. As an introduction, the equilibrium constant for an acid dissociation is shown in equation (2-9) [10].

$$HA \overset{K_a}{\leftrightarrow} A^- + H^+ \tag{2-9}$$

In this case, HA corresponds to the non-dissociated acid and A^- to the dissociated form with H^+ as the released proton. On the basis of this dissociation, it is possible to determine the equilibrium constant K_a with equation (2-10).

$$K_a = \frac{a_{A^-} \cdot a_{H^+}}{a_{HA}} \quad \textbf{(2-10)}$$

The activity a_{A^-} corresponds to the dissociated form, where a_{HA} corresponds to the non-dissociated form of the acid. The activity a_{H^+} corresponds to the activity of the released proton. This equation can be reformulated by the separation of the activity into mole fractions x_i and activity coefficients γ_i. The result of this separation is shown in equation (2-11), where K_x is based on the mole fractions of all species and K_γ corresponds to their activity coefficients [11].

$$K_a = K_x \cdot K_\gamma \quad \text{with } K_x = \frac{x_{A^-} \cdot x_{H^+}}{x_{HA}} \quad \text{and } K_\gamma = \frac{\gamma_{A^-} \cdot \gamma_{H^+}}{\gamma_{HA}} \quad \textbf{(2-11)}$$

In comparison to the equilibrium constant of an acid, the equilibrium constant for a base can be determined by the dissociation shown in (2-12) [10].

$$AH^+ \overset{K_a}{\leftrightarrow} A + H^+ \quad \textbf{(2-12)}$$

AH^+ corresponds to the protonated base, where A represents the neutral species of the base. The corresponding equilibrium constant is shown in (2-13).

$$K_a = \frac{a_A \cdot a_{H^+}}{a_{AH^+}} \quad \textbf{(2-13)}$$

In addition to the equilibrium constant of the dissociation of species, salt solubility products have to be considered. For an acid, at least two different salts can be measured [14], one for each dissociation step. The difference in the solubility of these salts can be substantial [14] and hence, the solid phase of a solid-liquid experiment has to be identified. The identification is required because each concentration range has to be modeled independently. For an illustration of the substantial difference in the solubility, Figure 2-5 presents the concentration profile of an acid and a base over the pH value qualitatively.

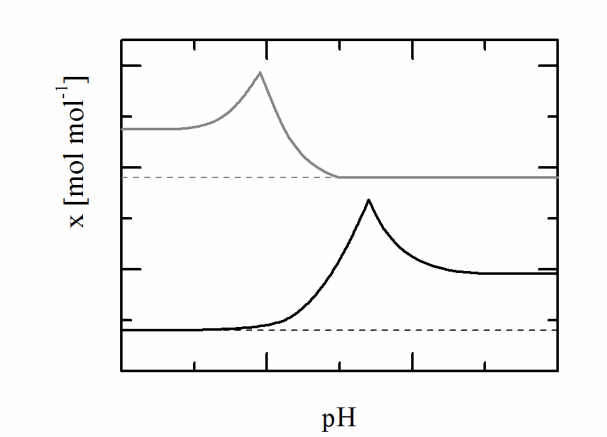

Figure 2-5: pH-dependent solubility of a base (light grey solid line) and an acid (black solid line) with the intrinsic concentrations of the neutral species of the acid or the base (dashed lines)

The concentration for an acid (black solid line) is small at a low pH value and is increased with increasing pH value. The peak in the concentration profile corresponds to the transition point from one salt to another. The increasing concentration manifests due to a higher dissociation of the examined species. In comparison to the profile of an acid, the concentration of a base is small at a higher pH value and the concentration increases with decreasing pH value. In this case, the dissociation is increased with a reduction of the pH value.

The salt solubility for an acid can be determined by the following equation, where AI corresponds to the salt form and A^- and I^+ to the anion and cation of the salt:

$$AI \overset{K_S}{\leftrightarrow} A^- + I^+ \qquad \textbf{(2-14)}$$

The salt equilibrium constant K_s can be determined exactly as shown in equation (2-10) on the basis of the activities of the species mentioned in (2-14) according to *Lange*:

$$K_s = \frac{a_{A^-} \cdot a_{I^+}}{a_{AI}} \qquad \textbf{(2-15)}$$

Based on the salt and dissociation solubility products, a determination of the pH-dependent solubility of the API and CF should be possible. However, pK_a values are published in literature instead of K_s values which usually neglect the amount of water and the activity coefficients of all species are set to one [4], [15]. In this case, the concentration of the ions can be theoretically calculated with the Henderson-Hasselbalch equation shown in (2-16) [10]. The assumption is made that for small concentrations, c_i can be equated to the mole fraction x_i.

$$pH = pK_a + \log_{10}\left(\frac{c_{A^-}}{c_{HA}}\right) = pK_a + \log_{10}\left(\frac{x_{A^-}}{x_{HA}}\right) \qquad \textbf{(2-16)}$$

However, the determination of the ion species with the Henderson-Hasselbalch equation was already investigated by *Lange* and it was shown that this approach alone does not achieve accurate results. The reason is that this attempt does not consider the activity coefficients of the ions and all species and therefore this attempt is only used for the generation of starting values. Furthermore, the concentration of the dissociated species cannot be measured separately and the measured value is always the total concentration. For an accurate determination of the ion concentration, *Lange* developed a modeling approach for PC-SAFT parameters for ion species. This approach is presented in the modeling procedure in chapter 2.4.

2.2.3. pH-Dependent Solubility of Cocrystals

This chapter is focused on the pH-dependent solubility of cocrystals. For its formation, the API and coformer are in equilibrium with the cocrystal according to a specific stoichiometry which depends on the component system [2]. The equilibrium between the cocrystal and its single components can be described by the following equilibrium [9], [16]:

$$CC^S \overset{K_{s,CC}}{\longleftrightarrow} \nu_{API} \cdot API^L + \nu_{CF} \cdot CF^L \qquad \textbf{(2-17)}$$

In this case, CC corresponds to the cocrystal species, API to the pharmaceutical ingredient and CF to the coformer. The stoichiometric factors correspond to the stoichiometry of the cocrystal itself. The solubility product $K_{s,CC}$ for the cocrystal can be determined with equation (2-18) [9].

$$K_{s,CC} = \frac{{a_{API}}^{\nu_{API}} \cdot {a_{CF}}^{\nu_{CF}}}{a_{CC}} \quad \text{with} \quad a_i = x_i \cdot \gamma_i \qquad \textbf{(2-18)}$$

The activity a_i is calculated by the multiplication of the mole fraction x_i and the activity coefficient γ_i of each component. The activity coefficients are modeled via PC-SAFT which is introduced in chapter 2.3. Under the condition that the activity of the cocrystal is equal to one, equation (2-18) can be simplified to equation (2-19). In addition, this equation is also used for hydrate and salt calculation with water as the coformer [9].

$$K_{s,CC} = (x_{API} \cdot \gamma_{API})^{\nu_{API}} \cdot (x_{CF} \cdot \gamma_{CF})^{\nu_{CF}} \qquad \textbf{(2-19)}$$

Furthermore, only the mole fractions of the neutral species of the API and CF are used to determine the solubility product of the cocrystal CC [9]. The dissociated forms of the API and CF are considered to be not able to form a cocrystal. Based on this theory, the mole fraction of

the neutral species are calculated from the dissociation constants of CF and API. The dissociation of CF is shown in equation (2-20) for a dicarboxylic acid.

$$CF \overset{K_{a1,CF}}{\longleftrightarrow} CF^- + H^+ \overset{K_{a2,CF}}{\longleftrightarrow} CF^{2-} + 2\,H^+ \quad \textbf{(2-20)}$$

In this case, two equilibria between the neutral and the dissociated species CF^- and CF^{2-} have to be considered. Depending on the pH value, the concentration of these three species changes. For a basic API, the dissociation can be described by the following equation:

$$API^+ \overset{K_{a,API}}{\longleftrightarrow} API + H^+ \quad \textbf{(2-21)}$$

API^+ corresponds to the protonated form of the API at a low pH value which can be determined by the solubility product of the dissociation. At a higher pH value, the concentration of the dissociated species is lower.

For the modeling of the cocrystal solubility line, the neutral concentration of API and CF are calculated by using one experimental value for 298.15 K. The neutral concentrations are calculated by the dissociation constants of API and CF according to equations (2-10) and (2-13). After the determination of the neutral cocrystal solubility line, the concentration of the dissociated species are added to the neutral concentration. Based on the determination of $K_{s,CC}$ in equation (2-19), the solubility product is independent of the pH value and therefore it is possible to determine the solubility line for every pH value based on one experimental solubility point.

The solubility product $K_{s,CC}$ only depends on the temperature. To model the solubility for another temperature, one additional experimental value is required. Then the Gibbs-Helmholtz equation is used to determine the temperature-dependency of the solubility product by the calculation of the reference enthalpy Δh^{ref} with equation (2-22) [9].

$$\ln(K_s) = ln\left(K_s^{ref}\right) + \frac{\Delta h^{ref}}{R} \cdot \left(\frac{1}{T^{ref}} - \frac{1}{T}\right) \quad \textbf{(2-22)}$$

In this case, K_s^{ref} represents the reference solubility product and T^{ref} its reference temperature. With the second experimental value, equation (2-22) can be reformulated to calculate the reference enthalpy Δh^{ref}. Hence, only three reference parameters are required to determine the solubility product for every desired temperature. Then the concentration can be determined by the solubility product with equation (2-19).

As an alternative, the reference enthalpy Δh^{ref} can be determined based on the melting properties of the pure components, the reference temperature and the mole fractions in the mixture.

2.3. Modeling with PC-SAFT

The solubility of the API and the CF can be determined by the equations, mentioned in chapter 2.2. Especially for the pH-dependent solubility modeling, the determination of the activity coefficients for each substance has to be modeled. Therefore, the PC-SAFT model is used [17]. This model is based on the residual Helmholtz enthalpy A^{res}, which consists of three contributions as it is shown in equation (2-23) [18].

$$A^{res} = A^{hc} + A^{disp} + A^{assoc} + A^{DH} \quad \textbf{(2-23)}$$

In this case, A^{hc} corresponds to the contribution of the hard chain, which represents the fraction of repulsive forces. Furthermore, attractive forces for the dispersion A^{disp} and the association A^{assoc} are applied, which represents the Van-der-Waals forces and the fraction of hydrogen bonds, respectively. Additionally, the ion charge is considered with the Debye-Hückel contribution A^{DH}. For a better illustration, these forces are presented in the Figure 2-6.

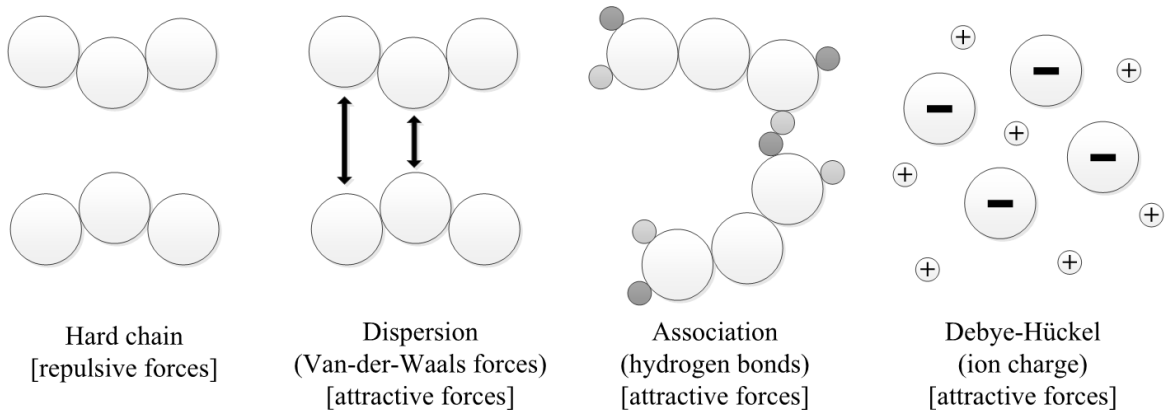

Figure 2-6: Illustration of the contributions of the hard chain, dispersion, association and Debye-Hückel to the residual Helmholtz enthalpy for the PC-SAFT model.

For the determination of the activity coefficients, it is required to determine the mean segment number of all components $\bar{m}$ in the desired mixture [12]. Therefore, the segment number of each pure component $m_{seg,i}$ is weighted with its mole fraction x_i (equation (2-24)).

$$\bar{m} = \sum_{i=1}^{n} x_i \cdot m_{seg,i} \qquad \textbf{(2-24)}$$

Afterwards, the segment diameter σ_{ij} of the mixture is calculated based on the segment diameters of the pure components σ with equation (2-25) [12].

$$\sigma_{ij} = \frac{1}{2} \cdot (\sigma_{ii} + \sigma_{jj}) \qquad \textbf{(2-25)}$$

The dispersion energy u_{ij} of the mixture is determined by equation (2-26) based on the dispersion energy of the pure components u_{ii} and u_{jj} and the binary interaction parameter k_{ij} [18].

$$u_{ij} = \sqrt{u_{ii} \cdot u_{jj}} \cdot (1 - k_{ij}) \qquad \textbf{(2-26)}$$

The association energy ε^{AiBj} of the mixture is calculated analogous to the segment diameter based on the association energy of the pure components ε^{AiBi} and ε^{AjBj} with equation (2-27).

$$\varepsilon^{AiBj} = \frac{1}{2} \cdot (\varepsilon^{AiBi} + \varepsilon^{AjBj}) \qquad \textbf{(2-27)}$$

At last, the association volume κ^{AiBj} of the mixture is determined by equation (2-28), where κ^{AiBi} and κ^{AjBj} corresponds to the association volume of the pure components. Additionally, the segment diameter σ of each pure component i and j has an impact on the associating volume [19].

$$\kappa^{AiBj} = \sqrt{\kappa^{AiBi} \cdot \kappa^{AjBj}} \cdot \left(\frac{\sqrt{\sigma_{ii} \cdot \sigma_{jj}}}{\frac{1}{2} \cdot (\sigma_{ii} + \sigma_{jj})} \right)^3 \qquad \textbf{(2-28)}$$

The aim of the previous calculations is the determination of the fugacity coefficients φ_i as a function of the mole fraction x_i with equation (2-29) [11].

$$\gamma_i = \frac{\varphi_i(x_i)}{\varphi_{0i}(x_i = 1)} \qquad \textbf{(2-29)}$$

Thereby, the activity coefficient represents the ratio of the real behavior of the components in the mixture to the ideal behavior [19]. The fugacity coefficient is calculated by the following equation:

$$\ln(\varphi_i) = \frac{\mu_i^{res}(T, v_{sp})}{k \cdot T} - \ln(Z) \quad \textbf{(2-30)}$$

In this equation, μ_i^{res} corresponds to the chemical potential, k to the Boltzmann constant and T to the temperature of the mixture. The compressibility factor Z can be calculated with equation (2-31).

$$Z = \frac{p \cdot v_{sp}}{k \cdot N_A \cdot T} \quad \textbf{(2-31)}$$

For the determination of the compressibility factor, v_{sp} corresponds to the specific molar volume, p to the pressure and N_A to the Avogadro constant. The formula for the compressibility factor can be derived from the ideal gas law [18].

The remaining term $\frac{\mu_i^{res}(T,v)}{k \cdot T}$ for the determination of the fugacity coefficient in equation (2-30) is calculated by the PC-SAFT model with equation (2-32) [18]. In this case, A^{res} corresponds to the residual Helmholtz enthalpy and N to the number of molecules. Therefore, it is possible to describe the interaction between all existing species in the mixture and to determine the activity coefficients based on fugacity coefficients.

$$\frac{\mu_i^{res}(T,v)}{k \cdot T} = \frac{A^{res}}{N \cdot k \cdot T} + Z - 1 + \left(\frac{\partial \left(\frac{A^{res}}{N \cdot k \cdot T} \right)}{\partial x_i} \right)_{T,v,x_{l \neq j}} - \sum_j \left(x_j \cdot \left(\frac{\partial \left(\frac{A^{res}}{N \cdot k \cdot T} \right)}{\partial x_j} \right)_{T,v,x_{l \neq i}} \right) \quad \textbf{(2-32)}$$

2.4. Modeling Procedure

This chapter is focused on the modeling procedure for the determination of PC-SAFT parameters and the modeling of temperature- and pH-dependent solubility of oxalic acid and caffeine in water. At first, the oxalic acid PC-SAFT parameter segment number $m_{seg,i}$, the segment diameter σ_{ii}, the dispersion energy u_{ii}, the association volume ε^{AiBi} and the association volume κ^{AiBi} are adjusted to temperature-dependent solubility data of oxalic acid in organic solvents. This determination is not required for caffeine because PC-SAFT parameters already exist and are used in this work [9]. Afterwards, the modeling of temperature-

dependent solubilities of oxalic acid and caffeine in water is described. At last, the pH-dependent solubilities of oxalic acid and caffeine in water and the cocrystal solubility is modeled.

The PC-SAFT parameter set is adjusted by the temperature-dependent solubility of oxalic acid in the organic solvents. Therefore, the PC-SAFT parameter for the solvents are presented in Appendix in chapter A.4.1 in Table A-18. For the determination, a heuristic is applied to set the associating volume κ^{AiBi} to 0.02 to equalize the volume of caffeine and oxalic acid. After the determination of oxalic acid pure component parameters, binary interaction parameter k_{ij} between oxalic acid and the organic solvents are introduced:

$$k_{ij}(T) = k_{ij,m} \cdot T + k_{ij,b} \quad \textbf{(2-33)}$$

To determine a robust parameter set, the parameters are additionally validated by liquid densities of oxalic acid dissolved in water for five different temperatures. For the hydrate solubility modeling of oxalic acid and caffeine in water, the required PC-SAFT parameters are presented in Table 2-1. The melting properties of oxalic acid, the melting temperature $T_{m,i}$, the melting enthalpy Δh_{0i}^{SL} and the heat capacity difference $\Delta c_{p,i}$ are based on literature data as shown in the following table.

Table 2-1: PC-SAFT pure component parameters of caffeine, oxalic acid and water for the determination of the solubility of caffeine and oxalic acid in water and melting properties these solutes (*parameter is determined within this work)

Component	**Caffeine** [9]	**Oxalic Acid**	**Water** [20]
M_i [g mol^{-1}]	194.19	90.04	18.02
$m_{seg,i}$ [-]	9.56	3.36*	1.20
σ_{ii} [Å]	2.96	2.75*	2.79
u_{ii} [K]	428.51	180.14*	353.94
ε^{AiBi} [K]	827.69	1654.78*	2425.67
κ^{AiBi} [-]	0.02	0.02*	0.05
$as.scheme$ [-]	2/2	2/2	1/1
$\Delta c_{p,i}$ [J mol^{-1} K^{-1}]	101.52 [21]	93.00 [22]	0.00
Δh_{0i}^{SL} [J mol^{-1}]	21600.00 [23]	18578.00 [22]	0.00
$T_{m,i}$ [K]	509.15 [24]	462.65 [25]	273.15

In the second step, the modeling of the hydrate solubility of oxalic acid and caffeine is described. The modeling is based on the equations (2-19) and (2-22) mentioned in chapter 2.2.3. Therefore, the hydrate structures of oxalic acid and caffeine have to be taken into account for the determination of their hydrate solubility products. Furthermore, the binary interaction parameter k_{ij} (2-33) between oxalic acid and water is adjusted to experimental data of previous work and literature data [26], [27]. The same procedure as for oxalic acid can be applied for caffeine. At first, the binary interaction parameter between caffeine and water is determined by modeling the anhydrous caffeine solubility in water based on the experimental data of *Dischlov* and *Suzuki et al.* [26], [28]. Afterwards, the hydrate solubility line is modeled until the melting temperature of the hydrate is reached. Above the melting point of the hydrate, the solubility is modeled with its anhydrous form which is described in chapter 2.2.1 with equation (2-8). Based on the literature and modeling data, it is possible to determine the complete binary phase diagrams of oxalic acid and caffeine in water, respectively. The activity coefficients in the hydrate solubility calculations and the pH dependent solubility calculations are determined via PC-SAFT [17].

In the third step, the pH-dependent solubilities of oxalic acid and caffeine in water are modeled based on the equations (2-10), (2-13) and (2-15) presented in 2.2.2. For this purpose, experimental data from previous work is used [29]. Additionally, pH-dependent solubility points are measured based on this work. A challenge in modeling of the pH-dependency of oxalic acid and caffeine is the determination of the ion concentration. Therefore, an ion concept is set up [16]. This concept uses the PC-SAFT parameters presented in Table 2-1 and modifies its values as shown in Table 2-2 [16]. In this case, the molecular mass of the dissociated species M_i is adjusted due to a release or addition of a hydrogen atom. Furthermore, the dissociation has an influence on the charge q_i of the ions and on the associating scheme ($as.scheme$) as shown in Table 2-2. The remaining PC-SAFT parameters are not changed. After the application of the ion concept, the pH-dependency of oxalic acid and caffeine can be modeled (equations (2-10), (2-13) and (2-15)). For oxalic acid, one experimental point is used in the pH range of sodium hydrogen oxalate monohydrate and one in the range of the disodium oxalate. The dissociation constants are adjusted to the experimental values. In case of caffeine, the dissociation constants are adjusted to one experimental value.

Table 2-2: PC-SAFT parameters of protonated caffeine, hydrogen oxalate and oxalate for modeling the pH-dependent solubility (*parameter is determined within this work)

Component	**(Caffeine)$^+$** [9]	**(Caffeine)$^-$** [9]	**HOxA$^-$**	**OxA^{2-}**
M_i [g mol^{-1}]	195.19*	193.19*	89.04	88.04
$m_{seg,i}$ [-]	9.56	9.56	3.36*	3.36*
σ_{ii} [Å]	2.96	2.96	2.75*	2.75*
u_{ii} [K]	428.51	428.51	180.14*	180.14*
ε^{AiBi} [K]	827.69	827.69	1654.78*	1654.78*
κ^{AiBi} [-]	0.02	0.02	0.02*	0.02*
q_i [e]	1*	-1*	-1*	-2*
$as.scheme$ [-]	1/1*	1/1*	1/1*	0/0*

In the last modeling section, the cocrystal system consisting of caffeine, oxalic acid and water is modeled. The cocrystal solubility is modeled according to chapter 2.2.3 [9]. Therefore, one experimental cocrystal point is used at the temperature of 298.15 K to determine the solubility product at this temperature. The neutral species of oxalic acid and caffeine are calculated via dissociation constants with equation (2-10) and (2-13). Afterwards, the solubility line of the neutral components can be calculated which is independent of the pH-value. On the basis of the dissociation constants for oxalic acid and caffeine in water, the complete cocrystal solubility line is calculated. Afterwards, it is possible to model the complete cocrystal line for every pH value. In addition, the pH-dependent hydrate solubility lines of oxalic acid and caffeine are calculated with the same equations as for the cocrystal (2-19). For these calculations, small amounts of caffeine are added to the mixture of oxalic acid in water at the desired pH value and vice versa. Finally, the complete ternary phase diagram of oxalic acid, caffeine and water can be modeled for every pH value.

3. Materials and Methods

The following chapter starts with an introduction to the examined substances of this master thesis (3.1). Afterwards, the procedure for the experiments is presented to determine the solubility of oxalic acid in organic solvents and the setup of the pH-dependent solubility experiments (3.2). The last chapter consist of the analysis of the solid and liquid phase for each experiment (3.3).

3.1. Examined Substances

This chapter focuses on the selection and presentation of the considered pharmaceutical ingredient (API) caffeine and the coformer (CF) oxalic acid. At first, the criteria for the cocrystal selection and the cocrystal of these two substances are presented with its properties (3.1.1). Then each substance is introduced with its characteristics (3.1.2 and 3.1.3). Afterwards, the selected solvents for the temperature-dependent solubility measurements of oxalic acid are introduced (3.1.4). At last, the buffer system used in the analysis of oxalic acid concentrations as well as in the pH-dependent solubility experiments are presented (3.1.5). A detailed list of the chemicals and the equipment is presented in the Appendix in Table A-1 and Table A-2.

3.1.1. Criteria for Cocrystal Selection of Oxalic Acid and Caffeine

The basic condition for the cocrystal selection is that oxalic acid is used as the coformer (CF) of the cocrystal which was set by *Lange*. This substance is suitable for cocrystal formation in water with many API's [30]. Then criteria have to be defined to determine a suitable cocrystal system. The selected criteria are the pharmacologic properties of the API, the formation of a non-hydrated cocrystal, the availability and the price of the API. In Table 3-1 three possible cocrystals with the API's caffeine, theophylline and nicotinamide and oxalic acid as the coformer are presented. The cocrystals have a similar chemical structure but a different API to CF ratio.

Table 3-1: Suitable API and CF cocrystals

API	CF	Ratio	Reference
Caffeine	Oxalic acid	2:1	[31]
Theophylline	Oxalic acid	2:1	[32]
Nicotinamide	Oxalic acid	1:1	[33], [34]

These API's build cocrystals easily and have pharmacological properties [30], [31]. However, studies with nicotinamide were successfully performed at this chair by *Lange* and therefore this system is not examined [35]. Theophylline and caffeine form cocrystals easily in a slurry but in comparison to caffeine which forms an anhydrous cocrystal, theophylline forms a cocrystal pentahydrate [30]. The system that was selected by *Lange* is an anhydrous cocrystal system consisting of caffeine and oxalic acid.

The system consisting of caffeine and oxalic acid fulfills all the criteria in comparison to the other systems and was already investigated at this chair by *Lange*, *Rela* and *Dischlov* [26], [29]. However, the determination of robust PC-SAFT parameters for oxalic acid was not achieved. Therefore, this system is examined within this work.

Caffeine forms an anhydrous cocrystal and due to this formation it is possible to avoid hydration of caffeine [36]. The cocrystal is also stable against humidity for over 7 weeks and therefore the analysis can be performed easily [31], [36]. At the end of this chapter, the cocrystal structure of caffeine and oxalic acid with a 2:1 stoichiometry is presented in Figure 3-1.

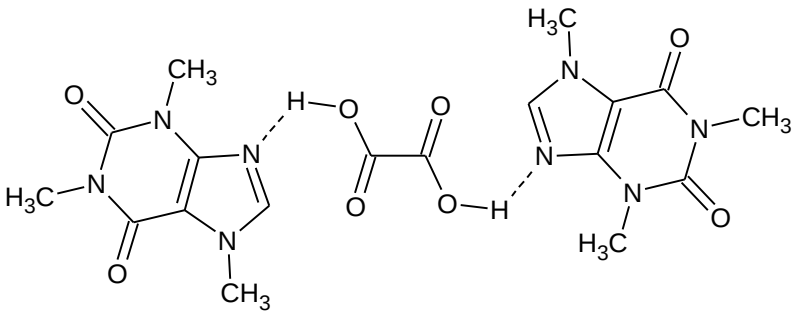

Figure 3-1: Cocrystal structure of caffeine and oxalic acid (2:1)

3.1.2. Oxalic Acid

The chemical structure of oxalic acid is presented in Figure 3-2 a). It is shown, that two carboxylic groups are directly connected and therefore, oxalic acid is a strong organic acid with a high acidity [37]. Additionally, it is the simplest dicarboxylic acid. Due to the direct connection of the carboxylic groups, oxalic acid is dissociated completely in water which results in a pH value below 1 [29]. Furthermore, the temperature stability of oxalic acid substances is presented in Figure 3-2 b).

a)

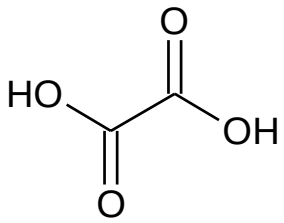

b)

Substance	T_{range} [K]		Ref.
Oxalic acid dihydrate	273.15	373.15	[38], this work
β-oxalic acid	373.15	393.20	[38], [39]
α-oxalic acid	393.20	462.65	[39], [25]

Figure 3-2: a) Chemical structure of oxalic acid and b) temperature stability range of oxalic acid substances

It is shown that oxalic acid dihydrate is stable below 373.15 K and above that temperature the anhydrous forms are stable. There exist two polymorphs of oxalic acid, β-oxalic acid which is stable within a small temperature range and α-oxalic acid which is stable from the transition temperature 393.20 K [39] to the decomposition temperature of 462.65 K [25].

The pK_a values for oxalic acids are 1.27 and 4.2 [40]. For a pH value between both pK_a values, oxalic acid is present as sodium hydrogen oxalate monohydrate. The hydrogen oxalate is formed due to the addition of sodium hydroxide which is used for the adjustment of the pH value. The formed hydrogen oxalate shows a lower solubility in comparison to the oxalic acid solubility without a pH adjustment. This phenomenon can be confirmed by *Rela's* measurements [29].

Furthermore, oxalic acid is very hygroscopic [41]. If oxalic acid is exhibited to air with a relative humidity above 20%, oxalic acid dihydrate is formed [41]. Therefore, it is very difficult to determine the solubility data of anhydrous oxalic acid in various solvents. Additionally, the analysis of oxalic acid in the liquid phase and the solid phase is complex, due to the dihydrate formation. Due to oxalic acid's reactivity, it is used as an additive for bleaching components, for bee protection of mites, removing of rust and production of ester [42], [43]. The aim of this work is to model the formation of cocrystals with oxalic acid as a coformer. The considered pharmaceutical ingredient (API) is often hygroscopic and would form hydrates [36]. Therefore, the formation of cocrystals is a meaningful method to avoid hydration of caffeine. Hence, oxalic acid represents an attractive coformer which can be used for several API's [30].

3.1.3. Caffeine

In this work, caffeine represents the active pharmaceutical ingredient (API). The chemical structure of this component is shown in Figure 3-3 a). Furthermore, the temperature stability for caffeine substances is presented in Figure 3-3 b).

a)

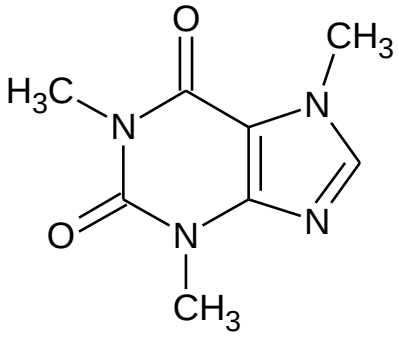

b)

Substance	T_{range} [K]		Ref.
Caffeine hydrate	273.15	353.15	[28]
β-caffeine	353.15	414.15	[28], [24]
α-caffeine	414.15	509.15	[24]

Figure 3-3: a) Chemical structure of caffeine and b) temperature stability range of caffeine substances

In comparison to oxalic acid, caffeine has a lower solubility in water [44]. Additionally, caffeine is forming hydrates which are stable for temperatures below 353.15 K [28]. Above temperatures of 353.15 K, anhydrous caffeine is built. There exist two anhydrous forms of caffeine at higher temperatures. At temperatures below 414.15 K, β-caffeine is the stable anhydrous form and above this temperature, α-caffeine is the stable anhydrous form [24]. In this case, only the crystal structures of both components are different. Furthermore, caffeine has two pK_a values of 1 and 14 and after contact with water it forms caffeine hydrate [45]. Additionally, it has to be mentioned that the stoichiometry of caffeine hydrate is not 1:1 but 1 to 0.8 mole of water [28], [46]. Caffeine occurs naturally in several teas and in coffee [47]. In addition, caffeine has pharmacologic properties and therefore is able to increase the heart rate and stimulate the nervous system [47]. These properties show that it is reasonable to use it as an API.

3.1.4. Solvent Selection

In this chapter, the solvent selection for the temperature-dependent solubility experiments with oxalic acid is presented. The most important criterion is that the solvents are free of water. This is required, because a high water content would result in the measurement of the solubility of oxalic acid dihydrate in an organic solvent and not the solubility of the anhydrous form. Additionally, the assumption is made that oxalic acid is not dissociated in the organic solvents

and the purpose for these experiments are the determination of PC-SAFT parameters for non-dissociated oxalic acid. Furthermore, the analysis of the oxalic acid concentration shall be easy and simple. The possible solvents which can be used to determine the solid-liquid equilibria are presented in the following table:

Table 3-2: Water content for several organic solvents

Solvent	w_{H2O} **[wt.%]**	**Solvent**	w_{H2O} **[wt.%]**
Ethanol	0.1060	Ethyl acetate	0.0006
Isopropanol	0.0317	Butyl acetate	0.0237
Butanol	0.0256	Acetonitrile	0.0050

It is shown, that the water content for all examined solvents is below 0.1 wt.% which correspond to a very low water content for the pure solvents. Due to the fact that the water content of ethanol is the highest with 0.106 wt.%, it will not be used for the temperature-dependent solubility experiments. In addition, the reaction of oxalic acid with ethanol has been observed at room temperature by *Chen et al.* [48]. Another criterion is the selection of different types of solvents to achieve a robust PC-SAFT parameter set for oxalic acid. Therefore, all organic solvents except of ethanol are examined and additionally a mixture of acetonitrile and ethyl acetate is examined as well.

3.1.5. Solutions and Buffer System

For the solubility experiments of the examined cocrystal system, consisting of oxalic acid, caffeine and water, the pH value is adjusted by the addition of 2 M HCl and 1 M NaOH solution. These solutions are used to adjust the pH value in a small scale to the desired set point. For great pH variations, pure sodium hydroxide cookies are required and added directly to the solubility vessel. Due to the addition of NaOH and HCl, Na^+ and Cl^- ions are added to the solution. However, these ions do not have an influence on the analysis of the liquid and solid phase which was investigated by *Lehmkemper* [49].

The analysis of the liquid phase is carried out at a pH value of 7 due to the fact that the absorbance of oxalic acid is dependent on the pH value [29]. Therefore, the buffer system consisting of disodium hydrogen phosphate dihydrate (3.6341 g) and potassium dihydrogen phosphate (1.7611 g) in 500 g water is used. The calibration of oxalic acid in the buffer solution is also based on this pH value.

3.2. Experiments for Solubility Determination

This chapter focuses on the experimental setup of the solubility measurements. The setup for temperature-dependent solubility experiments are presented in 3.2.1. Afterwards, the pH-dependent solubility experiments are presented in chapter 3.2.2 and 3.2.3 for the pure components and the mixtures.

3.2.1. Temperature-Dependent Solubility

In the following chapter, the temperature-dependent solubility experiments of oxalic acid within the organic solvents acetonitrile, butanol, isopropanol and ethyl acetate and butyl acetate are explained. The aim of these experiments is the determination of PC-SAFT pure component parameters for oxalic acid. With this parameter set, the cocrystal system consisting of oxalic acid, caffeine and water is modeled. These experiments are not required for caffeine because model parameters were already determined by *Lange* [9] and the component was already investigated by *Dischlov* [26]. The temperature-dependent experiments are carried out for five temperatures (20, 25, 30, 37, 45 °C) for oxalic acid.

The experimental setup for the temperature-dependent solubility of oxalic acid is presented in Figure 3-4. The double-walled solubility vessel (1) is tempered by water as a heating and cooling medium. Additionally, the solubility vessel is equipped with a magnetic stirrer for mixing and is placed on a magnetic plate from *IKA Labortechnik*.

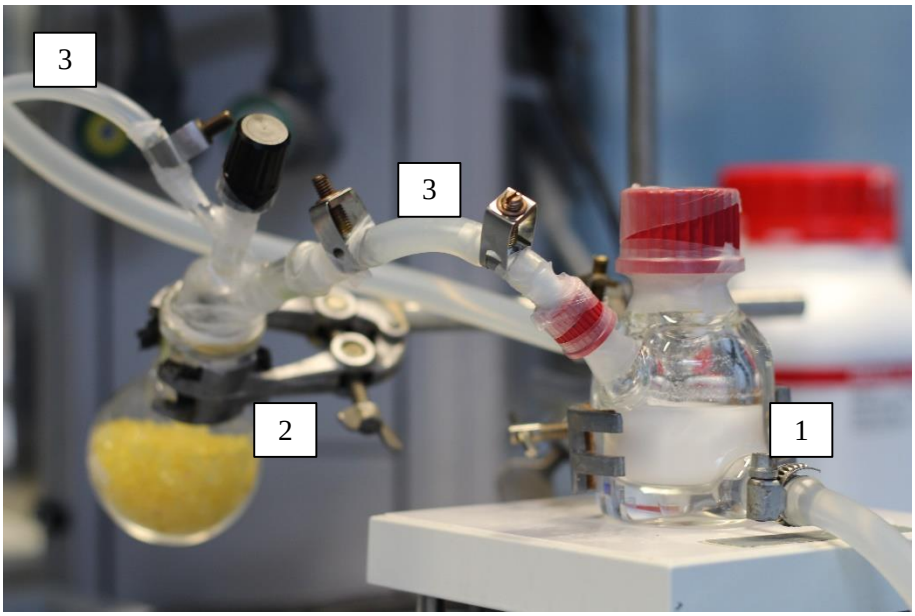

Figure 3-4: Temp.-dependent solubility experiment of oxalic acid in organic solvents with the solubility vessel (1), *silica gel orange*® in a glass flask (2) and a nitrogen connection (3)

The thermostat for temperature adjusting is a *Lauda Ecoline Staredition RE 304*. This equipment is used to ensure that the equilibrium is reached.

In order to avoid humidity above the mixture, a flask with the drying agent *silica gel orange*® is connected to the solubility vessel. At the start of each experiment, it is required to purge the solubility vessel with nitrogen for 15 minutes. Then oxalic acid is added to the solubility vessel and the solid remains at 45 °C for 60 minutes. During that time, the vessel is purged with nitrogen (1 bar) to remove the humidity from the solid particles due to input procedure. To determine the solubility of oxalic acid in the organic solvents, it is required to add 10 g of oxalic acid into the solubility vessel. Afterwards, the organic solvent is added (15 g) to the solubility vessel in countercurrent nitrogen flow with a syringe through the semipermeable membrane. With this procedure, it is possible to avoid that humid air moves into the vessel. Finally, the nitrogen flow is turned off, the vessel is closed and all connections are sealed with *PARAFILM*® and the grindings are daubed with vacuum grease. A nitrogen flow over several hours would lead to a complete evaporation of the solvent and therefore the nitrogen is used only during the sample taking. Then the vessel is stirred for at least 48 hours to achieve a solid-liquid equilibrium. This procedure is required because the formation of oxalic acid dihydrate would have an impact on the results.

For the sample taking, the stirrer is turned off and the particles are sedimented for a few minutes. Then the vessel lid is opened and the fluid phase is removed in countercurrent nitrogen flow with a syringe. Three 1 ml samples of the liquid phase are taken for each solubility point. Afterwards, the liquid phase is filtered with a syringe filter holder (0.2 µm) and then diluted with additional solvent to avoid that solid particles precipitate. The diluted solutions are analyzed in the *UV/VIS Biospectrometer*®. Additionally, the liquid phase is analyzed with the *Karl-Fischer-Titration* to examine the water content in the liquid phase.

For the analysis of the solid phase, the suspension of the vessel is sampled with a syringe in countercurrent nitrogen flow with an approximate mass ratio of solid to liquid of 2:1.The analysis of the solid phase is explained in detail in chapter 3.3.2.

3.2.2. pH-Dependent Solubility of Pure Components

The aforementioned experimental setup is not required for the pH-dependent solubility experiments because the solubility measurements are carried out in water. The experimental setup is shown in Figure 3-5. For this setup, a magnetic plate with a magnetic stirrer is used and in addition, the same thermostats as for the previous experiments for temperature adjusting are used.

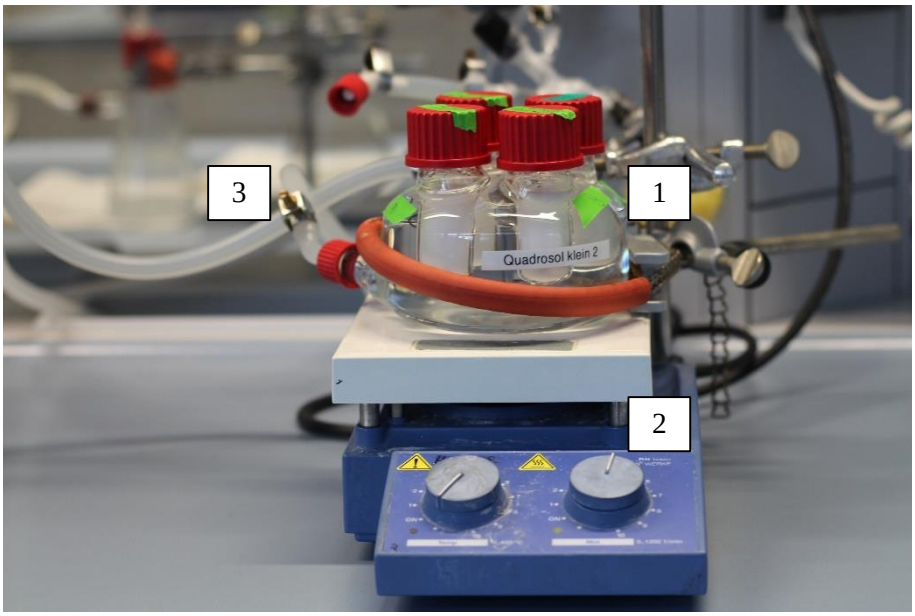

Figure 3-5: pH-dependent solubility of pure components and mixtures with a quadrosol as the solubility vessel (1), the magnetic plate stirrer (2) and the heating medium connection (3)

The experiments for the pH-dependent solubility for pure components are carried out in the same way as for the mixtures (3.2.3) consisting of oxalic acid, caffeine and water. In this case, only oxalic acid and water or caffeine and water are examined at a temperature of 25 °C. The pH value is set with NaOH or HCl solutions mentioned in chapter 3.1.5. The analysis is performed with the same phosphate buffer system as for the pH-dependent solubility of the mixtures and the same calibration curves are used as for the cocrystal system.

3.2.3. pH-Dependent Solubility of Mixtures

For the pH-dependent solubility experiments in the mixture, the procedure is not as difficult as mentioned in chapter 3.2.1. In this case, the components oxalic acid and caffeine are added to the solubility vessels in specific mass ratios of oxalic acid to caffeine (12:1 to 1:4).

With these mass ratios it is possible to determine solubility points along the complete cocrystal solubility line. Afterwards, water is added to the vessel and the pH value is adjusted with NaOH or HCl solution or NaOH cookies mentioned in chapter 3.1.5. The desired pH values are 1, 2, 4, 5 and 7. When the desired pH value and the set temperature of 25 °C are reached, the vessels are stirred for at least 48 hours to achieve a solid-liquid equilibrium. Then three samples of the liquid phase are taken with a syringe after particle settlement and filtered with a syringe filter holder (0.2 µm). The samples are diluted with the phosphate buffer solution presented in chapter 3.1.5.

The diluted solution is analyzed in the *UV/VIS Biospectrometer*® with a specific analysis method which is explained in detail in the following chapter 3.3.1. The liquid phase is analyzed twice per sample and hence six measurements are made for each solubility point to achieve its standard deviation. The solid phase is dried over a nutsch filter and analyzed using X-ray diffraction (PXRD). In this case, the PXRD can be used due to the stability of the cocrystal and the hydrates of caffeine and oxalic acid in contact with humid air. The analysis, of the binary and ternary system is presented in the following chapter.

3.3. Analysis

In this chapter, the analysis methods for the binary and ternary systems are presented. At first, the analysis methods for the liquid phase (3.3.1) using UV/VIS spectroscopy (3.3.1.1) and the *Karl-Fischer-Titration* (3.3.1.2) are explained. At last, the analysis methods for the solid phase (3.3.2) with the usage of the differential scanning calorimetry (DSC) and the powder X-ray diffraction (PXRD) are shown.

3.3.1. Analysis of the Liquid Phase

The analysis of the liquid phase is performed via UV/VIS spectroscopy and *Karl-Fischer-Titration*. At first, the UV/VIS spectroscopy for the binary and ternary component system is explained and at last the qualitative analysis by *Karl-Fischer-Titration*.

3.3.1.1. UV/VIS-Spectroscopy

This analysis method is used to determine the mass fraction of the substances in diluted solutions. Therefore, light is sent from the *UV/VIS BioSpectrometer*® to the sample. The generated light goes through an aperture and then through a monochromator to adjust the desired wave length. The monochromatic light is sent afterwards through the cuvette (10 mm) with the sample to an exit aperture and then to a detector which measures the absorbance. The apparatus is presented schematically in Figure 3-6.

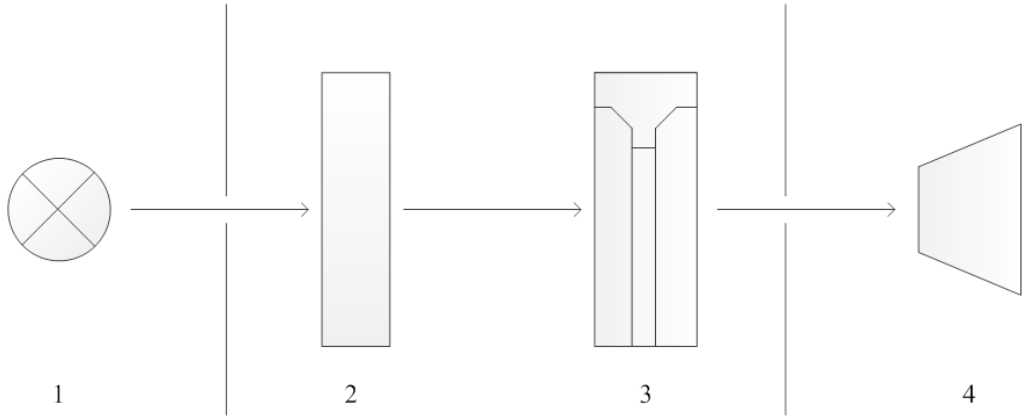

Figure 3-6: Schematically UV/VIS measurement procedure with the lamp (1), the monochromator (2), the cuvette with the sample (3) and the detector (4)

At first, the absorption of the "blank" solution consisting of pure solvent is measured with the same cuvette which is used to measure the sample. Therefore, the influence of solvent itself and the cuvette is assumed to be neglectable. Afterwards, the sample is measured in the same cuvette to determine the absorbance between the sample and the "blank" solution. During the measurement of "blank" solution or the samples, the cuvette is cleaned with water and acetone.

For a sufficient accuracy, the absorbance of the diluted solution has to follow a linear trend according to the Lambert-Beer law. Therefore, the absorbance has to be within a range of 0.1 to 1.0 for the analysis [50]. The Lambert-Beer law is shown in equation (3-1).

$$A = \varepsilon_{i,solvent} \cdot d \cdot x_i \qquad \textbf{(3-1)}$$

In this equation, A corresponds to the absorbance, x_i to the mole fraction of the examined component, d to the thickness of the cuvette (10 mm) and ε to the molar extinction in mm^{-1}. The molar extinction is in this case independent of the mole fraction, the thickness of the cuvette and the intensity of the incoming light.

However, this equation exhibits several assumptions and boundary conditions. The underlying assumptions for this method are a strongly diluted solution and that the absorbing functional

groups are not influencing each other [50]. Furthermore, the influence of dust particles and reflections at the cuvette can be neglected [50].

For the determination of the mass fraction, it is necessary to set up calibration curves for oxalic acid and each organic solvent mixture. To reduce the influence of the organic solvent the absorbance is measured at characteristic wave lengths. An example for this procedure is shown in Figure 3-7 where the absorbance of oxalic acid in acetonitrile is shown.

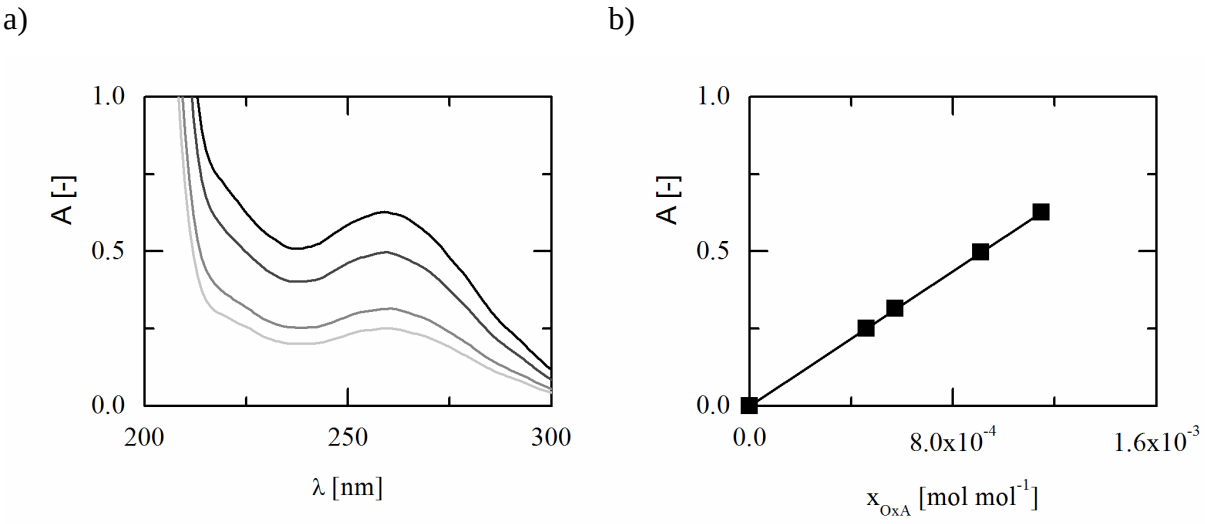

Figure 3-7: a) Absorbance spectra for oxalic acid in acetonitrile for four different mole fractions ($1.15 \cdot 10^{-3}$, $9.11 \cdot 10^{-4}$, $5.73 \cdot 10^{-4}$, $4.60 \cdot 10^{-4}$) and b) absorbance of oxalic acid at $\lambda = 260$ nm depending on the mole fraction of oxalic acid with a molar extinction $\varepsilon_{OxA,acetonitrile} = 54.54$ mm^{-1}

It is shown that a relative maximum exists at a wave length of 260 nm. Therefore, the calibration curve is also based on this wave length to determine the mole fraction for the unknown solubility of oxalic acid in acetonitrile at the five temperatures mentioned in chapter 3.2.1. To avoid any fluctuations in the absorption of the "blank" solution, it is required to be at least 5 nm away from the cut-off absorption of the solvent which is 200 nm in the case of acetonitrile. This analysis method can be used for the temperature-dependent solubility experiments and the pH-dependent binary component solubility experiments. The calibration curves for oxalic acid in the other organic solvents are presented in Appendix in Figure A-1 to Figure A-4.

For the system consisting of oxalic acid, caffeine and water, a more difficult analysis method has to be applied. Therefore, the absorbance of oxalic acid and caffeine has to be measured simultaneously. To identify the two components based on the total absorbance, the following equations are used:

$$A_{208} = d \cdot \left(\varepsilon_{OxA,buffer,208} \cdot x_{OxA} + \varepsilon_{caffeine,buffer,208} \cdot x_{caffeine}\right) \quad \textbf{(3-2)}$$

$$A_{273} = d \cdot \left(\varepsilon_{OxA,,buffer,273} \cdot x_{OxA} + \varepsilon_{caffeine,buffer,273} \cdot x_{caffeine}\right) \quad \textbf{(3-3)}$$

The equations represent the addition of the absorbance of oxalic acid and caffeine in water at a wave length of 208 nm and 273 nm. In Figure 3-8 it is shown that caffeine has two characteristic wave lengths at 208 nm and 273 nm. Therefore, both equations mentioned above are designated with the same values and the calibration curves are also shown with a good accuracy for both wave lengths.

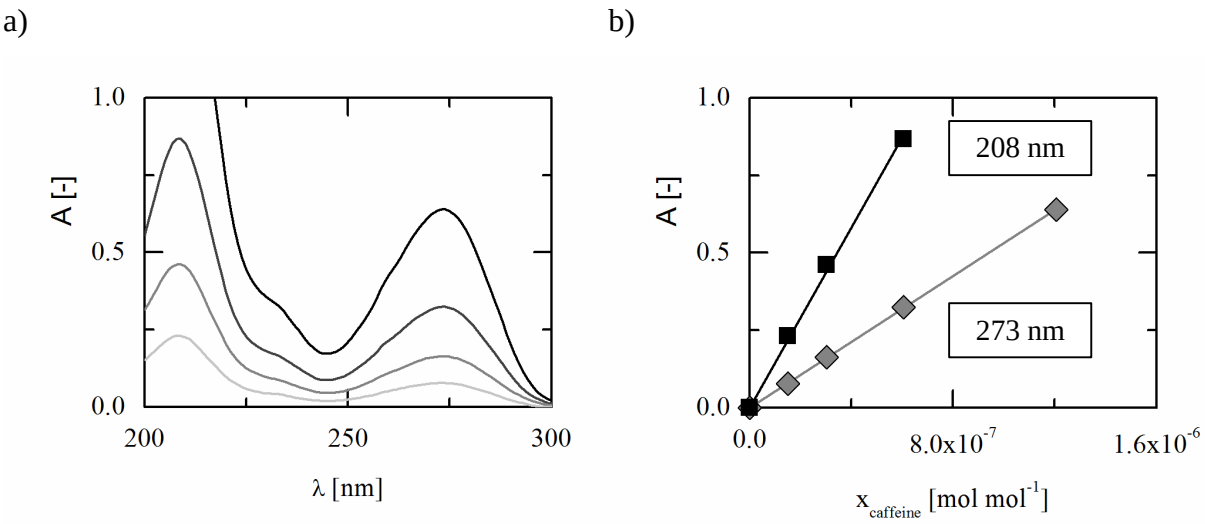

Figure 3-8: a) Absorbance spectra for caffeine in water for four different mole fractions ($1.21 \cdot 10^{-6}$, $6.04 \cdot 10^{-7}$, $3.02 \cdot 10^{-7}$, $1.51 \cdot 10^{-7}$) and b) absorbance of caffeine at λ_1 = 208 nm with a molar extinction $\varepsilon_{caffeine,buffer,208}$ = 145506 $mm^{-1}$and λ_2 = 273 nm with a molar extinction $\varepsilon_{caffeine,buffer,273}$ = 53073 mm^{-1} depending on the mole fraction of caffeine

The absorbance spectra of oxalic acid in water and the calibration curves are shown in Figure 3-9. A challenge is that the absorption of oxalic acid depends on the pH value and therefore the analysis has to be carried out at a pH value of 7. This is achieved with the phosphate buffer system. It can be seen that the absorbance of oxalic acid has only one characteristic peak at 208 nm. Therefore, the calibration is set on this wave length and also at 273 nm to achieve an equation system which is solved analytically. It can also be seen that the accuracy is only high at a low absorbance rate (Figure 3-9 b)).

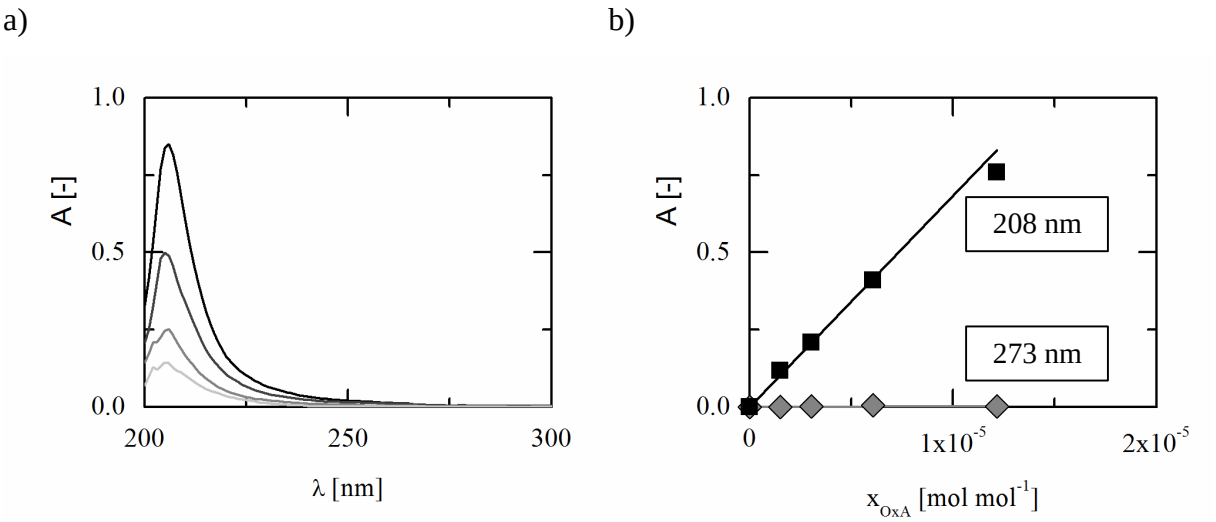

Figure 3-9: a) Absorbance spectra for oxalic acid in water buffered to pH = 7 for four different mole fractions ($1.22 \cdot 10^{-5}$, $6.07 \cdot 10^{-6}$, $3.03 \cdot 10^{-6}$, $1.52 \cdot 10^{-6}$) and b) absorbance of oxalic acid at λ_1 = 208 nm with a molar extinction $\varepsilon_{OxA,buffer,208}$ = 6823 mm^{-1} and λ_2 = 273 nm with a molar extinction $\varepsilon_{OxA,buffer,273}$ = 31.74 mm^{-1} depending on the mole fraction of oxalic acid

By combination of these two calibration curves, it is possible to determine the mole fractions of oxalic acid and caffeine in water simultaneously. A schematically analysis is presented in Figure 3-10. The mole fraction of caffeine can be identified by a wave length of 273 nm. Whereas, oxalic acid can be identified over the addition of the absorbance of caffeine and oxalic acid at the wave length of 208 nm.

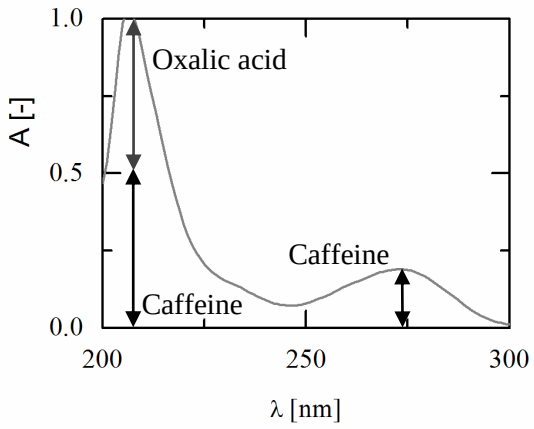

Figure 3-10: Absorbance spectrum of oxalic acid, caffeine and water buffered to pH = 7 with a mass ratio of oxalic acid to caffeine of 10:1

To confirm this method, several mass ratios of oxalic acid to caffeine were tested which are presented in the Appendix from Table A-3 to Table A-4 with the recalibration of the analysis method. These experiments show that after a recalibration for several mass ratios of oxalic acid to caffeine of 5:1 to 15:1 an average deviation of 2.61% for caffeine and 6.56% for oxalic acid can be achieved. Therefore, a good analysis method for the cocrystal system is applied without using High Performance Liquid Chromatography (HPLC).

3.3.1.2. Karl-Fischer-Titration

This analysis method is used to determine the water content in the liquid phase of the temperature-dependent solubility experiments. The *Karl-Fischer-Titration* (KF-T) is based on the following two main reactions [51]:

$$CH_3OH + SO_2 + RN \rightarrow [RNH]SO_3CH_3$$

$$[RNH]SO_3CH_3 + I_2 + H_2O + 2\,RN \rightarrow [RNH]SO_4CH_3 + 2\,[RNH]I$$

For this purpose, methanol dry is put in the analysis vessel and the titer is measured. Therefore, a titrant mixture is used which consist of SO_2, RN and I_2 and forms a complex with methanol according to reaction one. R represents the alkyl part of the base. If water is present in the sample, this water reacts with iodine and water to form an iodide complex shown in the second reaction. If all water is removed, the reaction is stopped. The titer represents the amount of *CombiTitrant 5* which is necessary to neutralize all present water molecules. After the titer is measured and the injection of *CombiTitrant 5* into the vessel is stable so that no water is present, the sample can be injected with a syringe. Therefore, a few droplets are injected and the weight loss of the syringe is measured. Based on the weight of the droplets, the KF-T apparatus calculates automatically the water content of the sample.

In this work, the *915 KF Ti-Touch* (by Metrohm) is used for the analysis. As mentioned before, *CombiTitrant 5* is used which is a single component reagent. For the analysis, the sample is injected after a stable system within the vessel is reached. This analysis is only required for the temperature-dependent solubility analysis. It is only used for a qualitative analysis of existing water in the liquid phase and not for quantification purposes.

3.3.2. Analysis of the Solid Phase

In this chapter, the analysis of the solid phase for the temperature-dependent solubility experiments based on the differential scanning calorimetry (DSC) is introduced in 3.3.2.1. The solid phase for the pH-dependent experiments is examined via (PXRD) which is presented in 3.3.2.2.

3.3.2.1. Differential Scanning Calorimetry

The differential scanning calorimetry (DSC) is often used to determine material properties of solid substances [52]. "Differential Scanning Calorimetry (DSC) means the measurement of the change of the difference in the heat flow rate to the sample and to a reference sample while they are subjected to a controlled temperature program" [52]. For this purpose, the weight of the substance is determined and put on a pan. Then, the difference in the heat absorption of the sample and an empty reference pan is measured. The result of this analysis is a weight specified heat flow which depends on the temperature.

In this work, the DSC is used qualitatively to identify the composition of the solid phase for the temperature-dependent solubility experiments. Therefore, it is required to develop an analysis method to differentiate between oxalic acid and oxalic acid dihydrate. The different heat absorption between oxalic acid dihydrate and oxalic acid is confirmed with an endothermal peak. A challenge in the analysis of the solid is that the hydration of oxalic acid particles is fast [41]. This phenomenon is shown in Figure 3-11 where the mass specified heat flow $\dot{q}$ is depending on the temperature T.

The anhydrous form of oxalic acid corresponds to the black solid line. For these experiments, oxalic acid is put into a climate chamber with a temperature of 25 °C and relative humidity of 60%, which is achieved by a sodium bromide solution. It is shown, that with increasing exposure time the endothermal peak is increased until complete hydration of oxalic acid (black dashed line) is reached. For the DSC procedure, only the heating of the sample is considered due to the evaporation of water. The analysis is started at 45 °C with a heat-up rate of 2 °C min^{-1} to 105 °C and then the temperature remains at this temperature for two minutes. Afterwards, the temperature is raised up to 125 °C with the same heat-up rate. With this procedure it is possible to develop a characteristic trend for the analysis of oxalic acid samples at various exposure times.

a)

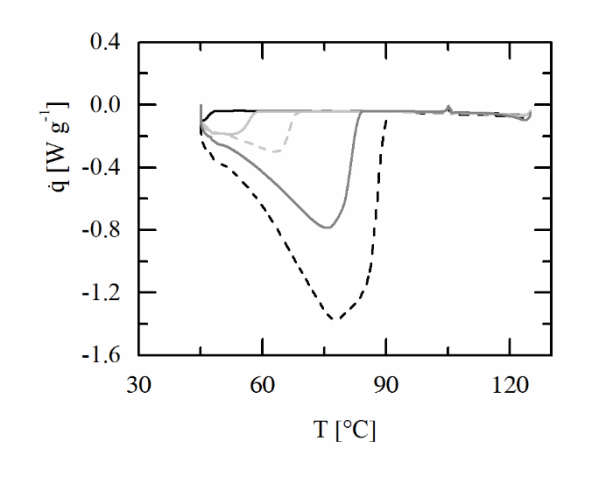

b)

DSC procedure
Equilibration at 45 °C
Heat-up 2 °C min^{-1} to 105 °C
Isothermal for 2 min
Heat-up 2 °C min^{-1} to 125 °C

Figure 3-11: a) Mass specified heat flow $\dot{q}$ of oxalic acid (black solid line), oxalic acid after 0.5 h (light grey solid line), oxalic acid after 1.5 h (light grey dashed line), oxalic acid after 3.0 h (grey solid line) and oxalic acid dihydrate after 3 days (black dashed line) of exposition in a climate chamber at 25 °C and 60% relative humidity depending on the temperature. b) DSC procedure for the analysis of the samples

If oxalic acid particles are dried after the solubility experiments in organic solvents, the analysis would show that dihydrate is formed which would lead to false results. Due to the presented fast hydration of oxalic acid within a few hours, the sample cannot be dried and analyzed. Instead of drying, the oxalic acid particles have to be protected. For this purpose, the sample of oxalic acid has to be analyzed with the organic solvent in a hermetic pan with a hole in the lid. Due to the wetted particles, oxalic acid is protected during the preparation of the pan and with the hole in the lid it is possible that the solvent and the water of the formed dihydrate can be removed. As the reference mass, the average mass ($\approx$ 8 mg) of the sample mass before and after the analysis is used. Additionally, it is required to avoid purging of the DSC analysis chamber. Otherwise, the difference between solvent evaporation and the removal of water cannot be identified. As an example, the characteristic trend for anhydrous oxalic acid (black solid line) and oxalic acid dihydrate (black dashed line) with the organic solvent acetonitrile is presented in Figure 3-12. As mentioned before, the mass specified heat flow $\dot{q}$ is depending on the temperature T.

a)

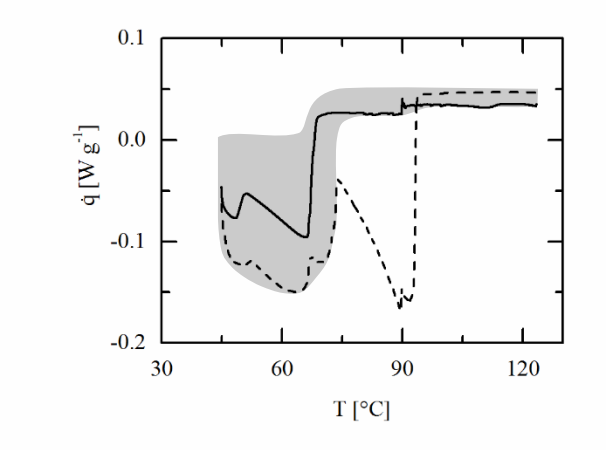

b)

DSC procedure
Equilibration at 45 °C
Heat-up 2 °C min^{-1} to 90 °C
Isothermal for 4 min
Heat-up 1 °C min^{-1} to 125 °C

Figure 3-12: a) Mass specified heat flow $\dot{q}$ of oxalic acid in acetonitrile(black solid line) and oxalic acid dihydrate in acetonitrile (black dashed line) depending on the temperature T. b) DSC procedure for the analysis of the samples

In this case, only the heating process is used for a qualitative analysis. The analysis is started at 45 °C with a heat-up rate of 2 °C min^{-1} to 90 °C. Then the temperature remains constant for 4 minutes and afterwards the sample is heated up with 1 °C min^{-1} to 125 °C. During this process, no nitrogen purge is used to achieve a better identification of the two endothermal peaks. It is shown that oxalic acid dihydrate has 2 peaks in comparison to anhydrous oxalic acid. The first peak belongs to the evaporation of the organic solvent, while the second peak corresponds to the evaporation of water bounded to oxalic acid. If the mass ratio of solvent to particles is high, the first peak would become larger with a broader temperature range but no additional peak would occur. When the sample of oxalic acids particles wetted with organic solvent shows a curve within the grey section, only organic solvent evaporation takes place and no oxalic acid dihydrate is formed. Oxalic acid dihydrate was formed during solubility measurement, if a second peak is shown in the curve with a maximum at 90 °C. Thus, a method for the qualitative analysis of the solid phase in the temperature-dependent solubility experiments is developed.

3.3.2.2. Powder X-Ray-Diffraction

In this chapter, the analysis with the powder X-ray diffraction (PXRD) is introduced. The PXRD is used to determine the crystal and molecular structure of powders or single crystals. Thereby, the geometry, symmetry and the content of the elemental cell of a crystal is examined [53]. For the examination, X-rays are sent to a crystalline sample with a specific wave length. The sample is placed on a silicon wafer and the angle on which the X-rays are sent to the sample is changed between 2° to 50°. The reason for this procedure is that the X-rays are scattered on the crystalline surface of the sample and therefore the measured intensity is a function of the diffraction angle ($2\,\theta$). The generated diffraction spectrum can be described by the Bragg equation [53].

$$\lambda = 2 \cdot d \cdot sin(\theta) \qquad \textbf{(3-4)}$$

In this equation, λ corresponds to the wave length of the X-rays, d to the lattice plane and θ to the diffraction angle. Therefore, a characteristic diffraction spectrum can be measured for every crystal structure and these are the basis of the *Cambridge Structural Database* (CSD) or the *Crystallography Open Database* (COD) [54], [55]. Hence, these databases can be used to identify crystal structures of the substances caffeine, oxalic acid, their salts and hydrates and the cocrystal of these two components. The reference spectra are presented in Appendix in chapter A.3.4 PXRD Analysis of Solid Phases.

This analytical method is used to examine the solid phase of the pH-dependent solubility experiments. In this work, the reference spectra from the CSD for caffeine, oxalic acid and the cocrystal are used to identify the corresponding solid phase. Additionally, the solid phase can be analyzed easily due to the stability of the hydrate forms and cocrystal in exposure to humid air [56]. For the analysis, the X-ray apparatus *MiniFlex600* (by *Rigaku*) with a tube voltage of 40 kV and a power of 15 mA is used. Based on the heat development, the thermostat *Kühlmobil 010-B400-1-4* (by *Van der Heijden Labortechnik GmbH*) is used to temper the apparatus to 20 °C. For the analysis of each sample, an angle range 2° to 50° is used with a scanning rate of 5° min^{-1} and an angle step size of 0.02°.

4. Results and Discussion

This chapter focuses on the results of this master thesis. At first, the temperature-dependent solubility of oxalic acid in organic solvents is presented (4.1). Additionally, the temperature-dependent solubility of oxalic acid dihydrate and caffeine hydrate (1:0.8) are presented within chapter 4.1. The hydration of oxalic acid in the climate chamber which was introduced in chapter 3.3.2.1 is explained in detail in Appendix in chapter A.2.3. In chapter 4.2, the experimental pH-dependent solubility and the modeling of oxalic acid and caffeine in water at 298.15 K and ambient pressure are presented. In the last chapter, the pH-dependent cocrystal and hydrate solubilities of oxalic acid and caffeine are presented (4.3). The experimental values, modeling parameters and data are attached in the Appendix (A.3 Results and A.4 Modeling).

4.1. Temperature-Dependent Solubility Experiments

In this chapter, the temperature-dependent solubility of oxalic acid in organic solvents is presented. At first, the experimental results are presented for oxalic acid in alcohols and acetonitrile (4.1.1). Afterwards, the modeling of the temperature-dependent solubility is shown (4.1.2). Furthermore, the modeling of mixture densities of oxalic acid in water based on literature data is presented (4.1.3). At last, the binary phase diagrams of anhydrous oxalic acid and oxalic acid dihydrate in water and anhydrous caffeine and caffeine hydrate (1:0.8) in water are presented (4.1.4). The aim of this chapter is the determination of PC-SAFT pure component parameters for oxalic acid and binary interaction parameter between oxalic acid and caffeine with water, respectively. PC-SAFT pure component parameter for caffeine already exist as shown in chapter 2.4.

4.1.1. Oxalic Acid in Organic Solvents

This section focuses on the determination of experimental data of oxalic acid in organic solvents. Therefore, solubility screening of oxalic acid in butanol and other alcohols is presented in chapter 4.1.1.1. Afterwards, the oxalic acid solubility in acetonitrile is shown (4.1.1.2). The focus of this chapter is set on the challenging determination of experimental solubility data for oxalic acid in organic solvents. The experimental results for these experiments as well as the DSC analysis for each solvent are presented in the Appendix in A.3.1.1 to A.3.1.3.

4.1.1.1. Solubility Screening in Butanol and Various Alcohols

As described before in chapter 3.3, the liquid phase was investigated with the *Karl-Fischer-Titration* (KF-T) and the UV/VIS spectroscopy and the solid phase was investigated via DSC analysis. In the first section of this chapter, the analysis of oxalic acid in butanol at 318.15 K and ambient pressure is presented. Afterwards, the results of oxalic acid in various alcohols are discussed.

At first, the solid phase of the solubility experiment of oxalic acid in butanol is examined. Therefore, the DSC analysis of a suspension of oxalic acid and butanol is shown in Figure 4-1. As described in chapter 3.3.2.1, the suspension is taken from the solubility vessel and analyzed without drying of the solid due to the fast hydration of oxalic acid. The diagram shows that the suspension sample at 318.15 K (light grey solid line) is close to identical in comparison to the reference curve of anhydrous oxalic acid in butanol (black solid line). For an existence of oxalic acid dihydrate, the sample curve would show a similar trend as the reference curve of oxalic acid dihydrate in butanol (black dashed line). This endothermal peak was not detected and therefore oxalic acid was not hydrated during the solubility experiment and sample preparation for the DSC. This insight is important because the PC-SAFT parameters are adjusted to temperature-dependent solubility data on the basis of equation (2-8). This equation is based on the equilibrium of one single component in the solid and liquid phase. This condition is not fulfilled in the presence of oxalic acid dihydrate.

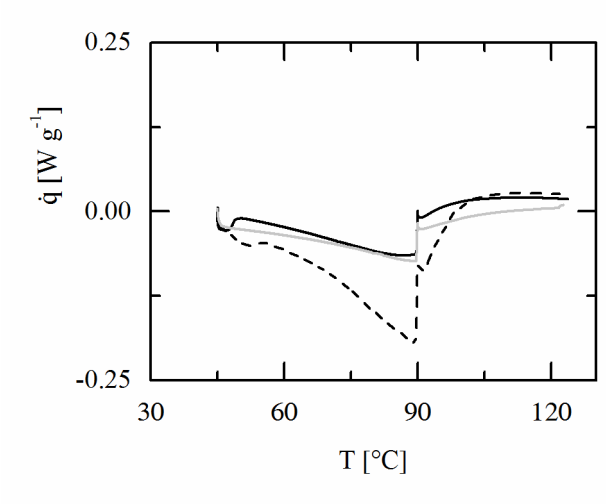

Figure 4-1: Mass specified heat flow $\dot{q}$ of the references anhydrous oxalic acid in butanol (black solid line) and oxalic acid dihydrate in butanol (black dashed line) depending on the temperature T. DSC analysis of a suspension of oxalic acid and butanol at 318.15 K (light grey solid line)

Afterwards, the analysis of the liquid phase is discussed. Therefore, the liquid phase of the solubility experiment is analyzed with KF-T. The results of this analysis are presented in Figure 4-2. The diagram shows that the water content of the saturated oxalic acid in butanol mixture has significantly increased from a water content of pure butanol of 0.026 wt.% (black star) to 3.80 wt.% after three days (light grey star).

As described above, the condition of water absence has to be fulfilled to determine PC-SAFT parameters. Therefore, additional studies were performed with unsaturated mixtures of oxalic acid in butanol (grey stars) to determine if the water content increases even without saturation of the solvent. These studies were carried out at ambient conditions (298.15 K and 1 bar) in inert atmosphere. The results present that even without a saturated solution and high temperatures, the water content of these mixtures is increased up to 1.93 wt.% over 7 days.

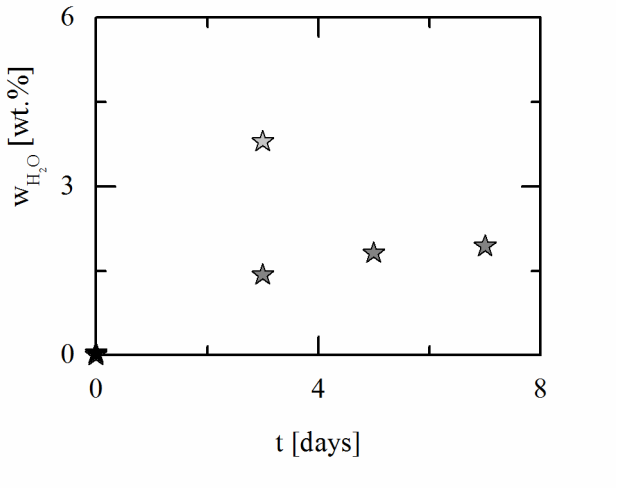

Figure 4-2: Water content w_{H_2O} of pure butanol (black star), unsaturated solution of oxalic acid in butanol (grey stars) at 298.15 K and saturated solution of oxalic acid in butanol at 318.15 K (light grey star) depending on time t in days

Due to this phenomenon, the conclusion can be drawn that an esterification of oxalic acid and butanol occurred and dibutyl oxalate is formed under the release of two water molecules. The reversible reaction of oxalic acid with two alcohols is presented in Figure 4-3. Due to the reversible reaction, the reaction equilibrium can be influenced by the temperature and therefore the water content at 298.15 K is lower than at 318.15 K.

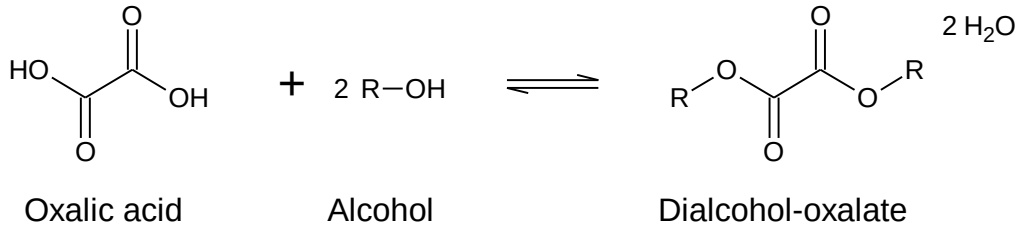

Figure 4-3: Esterification of oxalic acid with two alcohol molecules

To verify the conclusion of the esterification, additional solubility experiments with the alcohols ethanol and isopropanol were carried out for long term studies. These experiments are unsaturated solutions of oxalic acid within these solvents at 298.15 K and ambient pressure with exclusion of humidity. Additionally, the same study was performed with ethyl acetate. The results of these studies are shown in Figure 4-4.

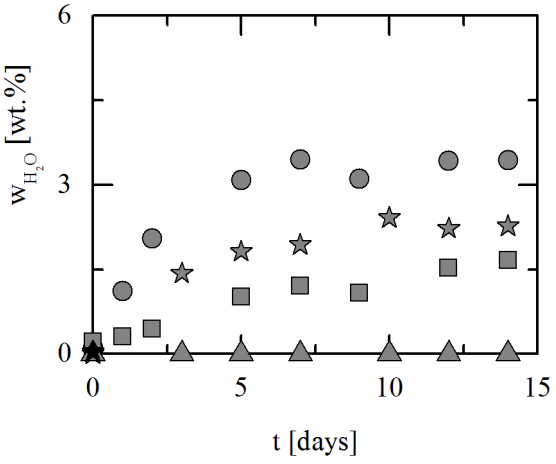

Figure 4-4: Water content w_{H_2O} of unsaturated solutions of oxalic acid in ethanol (grey circles), in isopropanol (grey squares), in butanol (grey stars) and in ethyl acetate (grey triangles) at ambient conditions over time. The black symbols correspond to the water content of their pure solvents

In Figure 4-4 it is shown that the water content of all unsaturated alcohol solutions are increasing over time and equilibria are reached after two weeks. In comparison to this phenomenon, the water content of oxalic acid in ethyl acetate is not increasing. This phenomenon can also be confirmed by *Bader* who submitted a US patent for the preparation of oxalic acid ester [57]. Usually, higher temperatures can enhance the ester production but a reaction can also carried out at room temperature with a long reaction time [57]. This can be confirmed by the presented results. Additionally, other patents and papers confirm either the production of diethyl oxalate [48] or methyl oxalate [58] with sulfuric acid as a catalyst and temperatures of 80 °C. However, no catalyst was used for the experiments of this work.

At last, the composition of the liquid phase is calculated based on a mass balance. Therefore, a calibration curve of oxalic acid in butanol is used (Appendix A.2.1). A detailed description of the mass balance is shown in (Appendix A. 3.1.2). This calculation presents that a significant amount of dibutyl oxalate was formed and the measured water content of 3.8 wt.% is in good agreement with the measured absorbance of the "oxalic acid and dibutyl oxalate" measured in butanol. Based on these results, the alcohols ethanol, isopropanol and butanol are not suited for temperature-dependent solubility experiments with oxalic acid and therefore are not used within this work.

4.1.1.2. Oxalic Acid Solubility in Selected Solvents

In this section, the solubility experiments for the determination of the PC-SAFT parameters are presented. The solvents, that fulfill the criteria mentioned in 3.1.4 and do not react with oxalic acid, are acetonitrile, ethyl acetate and butyl acetate. The focus in this section is set on the analysis of the temperature-dependent solubility of oxalic acid in acetonitrile. Therefore, the solid and the liquid phase is examined. The results of the remaining solubility experiments are presented in the Appendix in A.3.1 and are only discussed briefly in this section.

As presented in the previous section, the solid phase is examined by DSC analysis. Therefore, the suspension of oxalic acid and acetonitrile is presented for five temperatures (Figure 4-5). The analysis in diagram a) shows that all three samples (293.15 K – 303.15 K) only showing one endothermal peak below 348.15 K. Based on the analysis method presented in chapter 3.3.2.1, this indicates that only anhydrous oxalic acid was present in the suspensions. Otherwise the second endothermal peak would be present as well. The same result can be applied for diagram b) where the samples at 310.15 K and 318.15 K are presented. The fluctuations between the samples can be explained by the difficult preparation of the DSC pans with the suspension and the varying mass of the samples and the pans themselves. A higher sample mass would result in a broader peak in the first section below 348.15 K as it is shown by sample 303.15 K and 293.15 K. Furthermore, the ratio of solid to liquid phase has an influence on the results. For a high solid to liquid ratio, the curve is closer to the zero line due to the higher reference mass and vice versa. The DSC analysis of oxalic acid in ethyl acetate, butyl acetate and the mixture of acetonitrile and ethyl acetate for a 1:1 mass ratio are presented in the Appendix in chapter A.3.1.3.

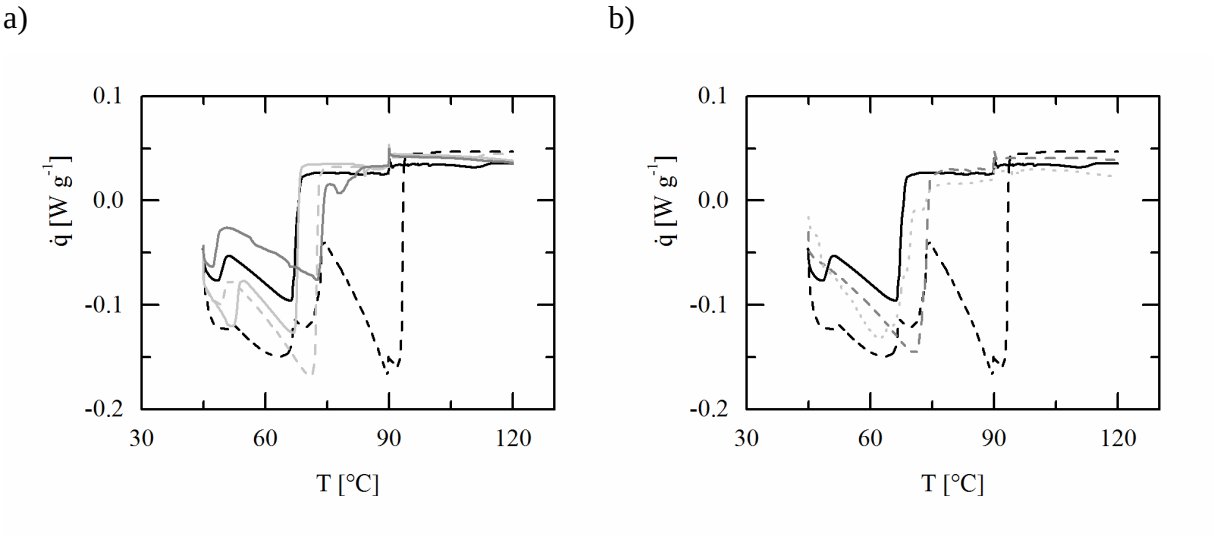

Figure 4-5: Mass specified heat flow $\dot{q}$ of the references oxalic acid in acetonitrile (black solid line) and oxalic acid dihydrate in acetonitrile (black dashed line) depending on the temperature T. a) DSC analysis of a suspension of oxalic acid and acetonitrile at 293.15 K (light grey solid line), 298.15 K (light grey dashed line), 303.15 K (grey solid line). b) DSC analysis of a suspension of oxalic acid and acetonitrile at 310.15 K (grey dashed line) and 318.15 K (light grey dotted line)

The second analysis is performed via *Karl-Fischer-Titration* (KF-T). Therefore, the water content of the liquid phase is examined. The water content of saturated oxalic acid acetonitrile mixtures is presented in Figure 4-6. The water content is illustrated over the time of the solubility experiment. Additionally, the temperature of each measured solubility point is presented within this diagram.

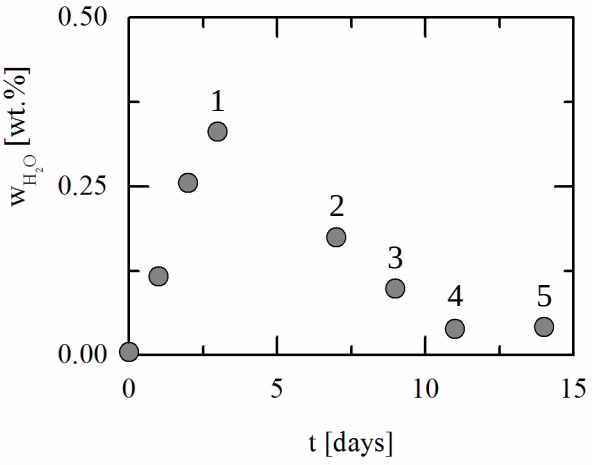

Figure 4-6: Water content w_{H_2O} of saturated oxalic acid acetonitrile mixtures at 318.15 K (1), 310.15 K (2), 303.15 K (3), 298.15 K (4) and 293.15 K (5) and ambient pressure over time t

It is shown that the water content was slightly increased until the analysis at 318.15 K was performed (1). A reason can be that during the sample taking, water was dissolved from air or

that the capacity of *silica gel orange*® at high temperatures is lower and therefore more water was dissolved in the solution. However, the water content reduces over time with the temperature. This can be explained by the increasing capacity of *silica gel orange*® for temperature reduction. Due to a water content below 0.5 wt.% it is assumed that this small amount can be neglected for the solubility experiments. The water content of the remaining solvents ethyl acetate and butyl acetate as well as the analysis of the mixture of acetonitrile and ethyl acetate with a mass ratio of 1:1, are presented in the Appendix in A.3.1.1. In all cases, the water content is below 0.5 wt.% or not detectable. Therefore, the determination of the PC-SAFT parameter can be performed with these solubility experiments.

The analysis of the liquid phase via UV/VIS spectroscopy is presented in Figure 4-7. It is shown that the temperature-dependency of oxalic acid in acetonitrile is high because the solubility with a mole fraction of $9.18 \cdot 10^{-2}$ for 318.15 K is significantly higher in comparison to the solubility at 293.15 K with a mole fraction of $5.81 \cdot 10^{-2}$. The experimental data for all solubility points are listed in the Appendix in chapter A.3.1.4 and illustrated in chapter 4.1.2.

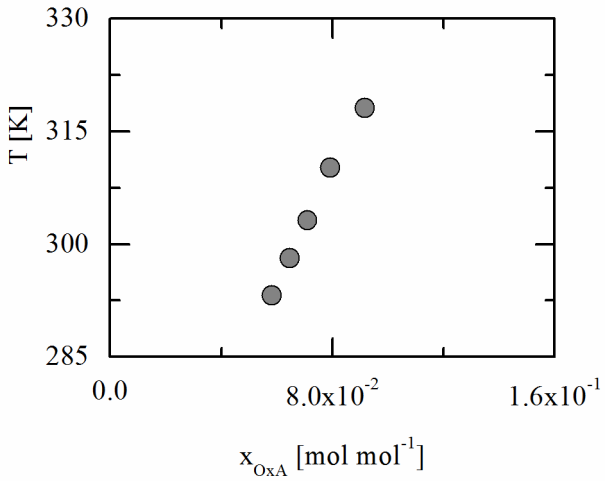

Figure 4-7: Temperature dependent experimental solubility of oxalic acid in acetonitrile

4.1.2. Modeling of Temperature-Dependent Solubility of Oxalic Acid

This chapter is focused on the temperature-dependent solubility of oxalic acid within organic solvents. The aim of this chapter is the determination of PC-SAFT parameters for the modeling of the temperature- and pH-dependent solubility. Therefore, the parameters (segment number $m_{seg,i}$, segment diameter σ_{ii}, the dispersion energy u_{ii}, the association energy ε^{AiBi} and association volume κ^{AiBi}) are adjusted to the experimental solubility data of oxalic acid in acetonitrile, ethyl acetate, butyl acetate and the mixture of acetonitrile and ethyl acetate with a

1:1 mass ratio. Furthermore, temperature-dependent binary interaction parameter between oxalic acid and the solvents are determined. All the mentioned modeling parameter are listed in the Appendix in chapter A.4.1 and in chapter 2.4, the modeling results are presented in chapter A.4.2. In this case, the solubility is calculated by the equations mentioned in chapter 2.2.1 and the activity coefficients by the equations shown in chapter 2.3.

The modeling and the experimental data are presented within this chapter in Figure 4-8. The experimental data show that the solubility in ethyl acetate is almost twice as high as in acetonitrile or butyl acetate. The solubility of oxalic acid in the mixture of acetonitrile and ethyl acetate is higher than the solubility of pure acetonitrile but lower as pure ethyl acetate.

Additionally, it is shown that the solubility in the pure solvents acetonitrile and butyl acetate are modeled with a high accuracy. The modeling of the solubility of oxalic acid in ethyl acetate shows small deviations at very low and very high temperatures. A reason for this phenomenon can be inaccuracies during the sample analysis (e.g. dust particles at the surface of the cuvette). The inaccuracies would lead to a higher absorbance and therefore a higher calculated mole fraction.

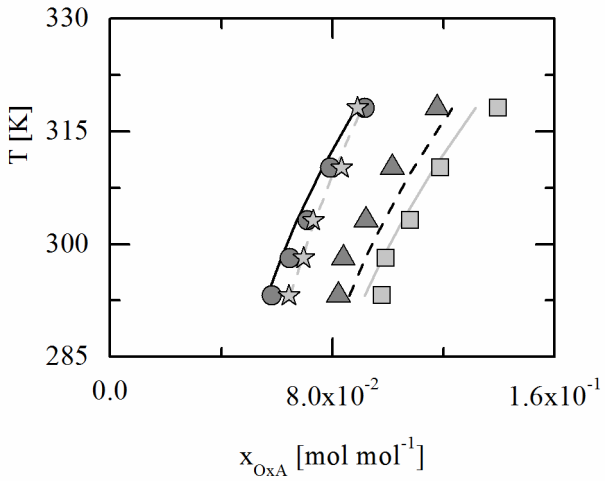

Figure 4-8: Temperature-dependent experimental solubility of oxalic acid in acetonitrile (grey circles), ethyl acetate (light grey squares), butyl acetate (light grey stars) and the mixture of acetonitrile and ethyl acetate with a mass ratio of 1:1 (grey triangles). Modeling of the temperature-dependent solubility of oxalic acid in acetonitrile (black solid line), ethyl acetate (light grey solid line), butyl acetate (light grey dashed line) and the mixture of acetonitrile and ethyl acetate (black dashed line)

Furthermore, modeling of the solubility of oxalic acid in the solvent mixture of acetonitrile and ethyl acetate shows a deviation across the complete solubility points. These deviations can be minimized by the application of a binary interaction parameter between aceotonitrile and ethyl

acetate. However, this was not modeled within this work. Afterwards, these parameters are used in the following chapter to validate the experimental densities by *Dischlov* [26] of oxalic acid water mixtures to achieve robust parameters.

4.1.3. Modeling of Mixture Densities of Oxalic Acid in Water

This chapter is focused on the validation of the modeling parameters with experimental densities measured in a previous work by *Dischlov* [26]. These experimental data are presented in the Appendix in chapter A.3.1.5 and these data are also illustrated in this chapter in Figure 4-9. The density was measured for 5 mixtures at the temperatures 283.15 K, 293.15 K, 303.15 K, 313.15 K and 323.15 K. It is shown that the density increases with increasing amount of oxalic acid.

Before adjusting the model parameters for oxalic acid to the densities of oxalic acid and water mixtures, the densities of the mixtures are predicted with the current parameters. The prediction is performed via PC-SAFT. For strong deviations between the prediction and the experimental values, the PC-SAFT parameters have to be adjusted to the densities as well. The results of the prediction are shown in Figure 4-9. The diagram presents that the densities of oxalic acid and water mixtures can be predicted with high accuracy.

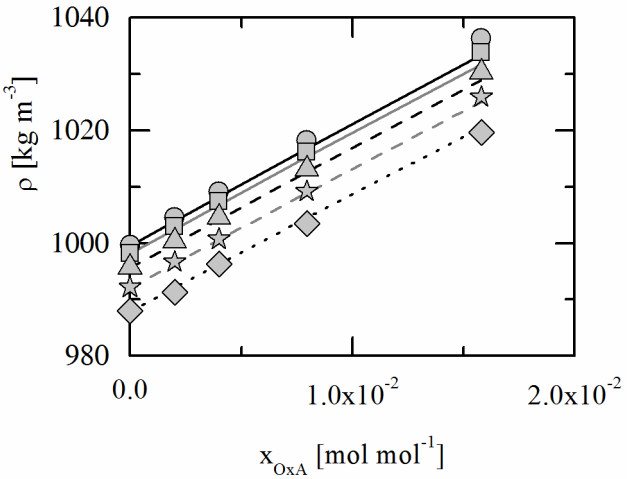

Figure 4-9: Experimental densities of unsaturated oxalic acid and water mixtures of 283.15 K (grey circles), 293.15 K (grey squares), 303.15 K (grey triangles), 313.15 K (grey stars) and 323.15 K (grey diamonds) from previous work [26]. Prediction of experimental densities for 283.15 K (black solid line), 293.15 K (grey solid line), 303.15 K (black dashed line), 313.15 K (grey dashed line) and 323.15 K (black dotted line) within this work

The prediction shows the highest accuracy at the highest temperature of 323.15 K. The lowest accuracy is shown for a temperature of 283.15 K. By adjusting the segment diameter to the

densities of oxalic acid and water mixtures, the deviation of the modeling can be reduced slightly but the application of the new segment diameter has a high influence on the solubility modeling of oxalic acid in organic solvents. Therefore, the parameter remain unchanged because the prediction is already in good agreement with the experimental results of *Dischlov* [26]. Hence, PC-SAFT parameters were determined which can model the temperature-dependent solubility of oxalic acid within organic solvents and additionally predict the temperature-dependent densities of oxalic acid and water mixtures. The prediction of the densities are presented in the Appendix in chapter A.4.2.

4.1.4. Binary Phase Diagrams of Oxalic Acid and Caffeine with Water

This chapter focuses on modeling the binary phase diagrams of oxalic acid, caffeine and their hydrates in water. For this purpose, binary interaction parameter k_{ij} between the solutes oxalic acid and caffeine with the solvent water are introduced. These interaction parameters are required to model the temperature-dependent solubility and are considered in the pH-dependent solubility of oxalic acid and caffeine in water with the presence of ions. The literature data which are used for modeling anhydrous oxalic acid, oxalic acid dihydrate, anhydrous caffeine and caffeine hydrate (1:0.8) are listed in Appendix in A.3.1.6. The modeling data are listed in the Appendix in A.4.2 and the binary interaction parameter that are fitted to model the solubility of these components are presented in the Appendix in A.4.1.

4.1.4.1. Binary Phase Diagram of Oxalic Acid

At first, the modeling of oxalic acid dihydrate and anhydrous oxalic acid solubility is presented. The anhydrous form of oxalic acid is modeled with the equations shown in 2.2.1. The modeling of oxalic acid dihydrate is performed with the equations mentioned in chapter 2.2.3. For this purpose, the solubility product $K_{s,H_2C_2O_4\cdot 2H_2O}$ for oxalic acid dihydrate has to be determined which is presented in equation (4-1) and (4-2).

$$H_2C_2O_4 \cdot 2\,H_2O \overset{K_{s,H_2C_2O_4\cdot 2H_2O}}{\longleftrightarrow} H_2C_2O_4 + 2\,H_2O \qquad \textbf{(4-1)}$$

$$K_{s,H_2C_2O_4\cdot 2H_2O} = a_{H_2C_2O_4} \cdot a_{H_2O}^2 \qquad \textbf{(4-2)}$$

Based on equation (4-2), the reference solubility product $K^{ref}_{S,H_2C_2O_4\cdot 2H_2O}$ can be determined for one literature data point with its reference temperature (313.15 K). By determination of another $K_{S,H_2C_2O_4\cdot 2H_2O}$ at 338.15 K, equation (2-22) is used to determine the reference enthalpy Δh^{ref}_{OxA} according to *Lange* [10]. However, the solubility of oxalic acid dihydrate and anhydrous oxalic acid cannot be modeled properly with this approach alone. Therefore, binary interaction parameter between oxalic acid and water are introduced to adjust the model to the experimental data. Based on the binary interaction parameter of -0.0256, the reference enthalpy is determined to 15300 J mol^{-1} and $K^{ref}_{S,H_2C_2O_4\cdot 2H_2O}$ is set to 0.128. These parameters are also listed in the Appendix in A.4.1. The results of the modeling and the literature data are presented in Figure 4-10.

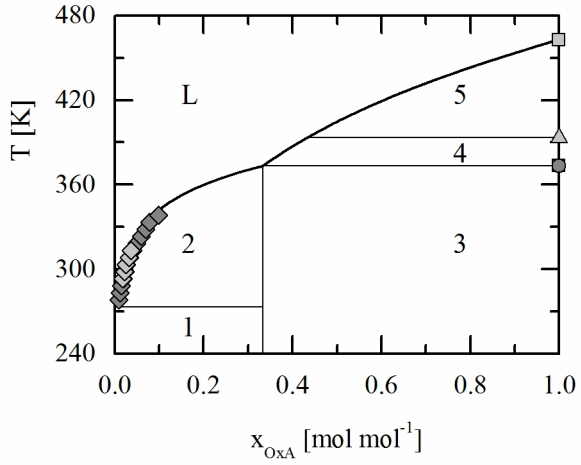

Figure 4-10: Binary temperature-dependent phase diagram of oxalic acid in water with experimental data (grey diamonds [27], light grey diamonds [26], light grey squares [25], light grey triangle [39] and grey circle [this work]). Modeling of the hydrate and anhydrous oxalic acid is performed via PC-SAFT (bold black solid line). L represents the liquid phase, (1) the equilibrium between solid water and solid oxalic acid dihydrate, (2) the equilibrium between the liquid phase and oxalic acid dihydrate, (3) equilibrium between oxalic acid dihydrate and anhydrous β-oxalic acid, (4) equilibrium between the liquid phase and β-oxalic acid and (5) equilibrium between the liquid phase and α-oxalic acid

The diagram shows the complete binary phase diagram of oxalic acid and water in its anhydrous and dihydrate form. The bold black lines correspond to the solubility calculations and the thin black lines to the separation of the diverse equilibria. In this diagram, area (2) that represents the equilibrium of the liquid phase L and the composition of oxalic acid dihydrate (vertical thin black solid line) is of major interest. It is shown that oxalic acid is most stable in its hydrate form because its solubility is increased until the melting point of oxalic acid dihydrate at 373.15 K is reached. Afterwards, the solubilities of the anhydrous forms are determined.

Anhydrous oxalic acid can be present in 2 polymorphic forms, the β-oxalic acid and α-oxalic acid. These forms were already introduced in chapter 3.1.2 and are presented in this diagram with area (4) for β-oxalic acid and the liquid phase and (5) for α-oxalic acid and the liquid phase. In addition, the solubility line of both polymorphic forms should have different slopes, due to different melting properties (Δh_{0i}^{sl}, $\Delta c_{p,i}$ and $T_{m,i}$). However, no melting properties for both polymorphs and literature data within this section are available and therefore, the solubility of the anhydrous oxalic acid form is determined by the melting properties of α-oxalic acid. The temperature-dependent solubility of the anhydrous form is modeled with the binary interaction parameter between oxalic acid and water until the theoretical melting point of 462.65 K is reached [37]. This temperature is just a theoretical melting point because it is actually a decomposition temperature [37]. In this case, the assumption is made that before the decomposition of the component, a liquid phase is formed.

4.1.4.2. Binary Phase Diagram of Caffeine

In the second part of this chapter, the solubility of caffeine and its hydrate in water is modeled. For the modeling of the hydrate solubility, the equations in chapter 2.2.3 are applied. The solubility product for caffeine hydrate (1:0.8) can be determined by the following equations:

$$Caffeine \cdot 0.8\, H_2O \overset{K_{s,C\,hydrate}}{\longleftrightarrow} Caffeine + 0.8\, H_2O \qquad \textbf{(4-3)}$$

$$K_{s,C\,hydrate} = a_{caffeine} \cdot a_{H_2O}^{0.8} \qquad \textbf{(4-4)}$$

Afterwards, the same procedure can be applied as for oxalic acid dihydrate. Therefore, the reference solubility product $K_{s,C\,hydrate}^{ref}$ with its reference temperature T^{ref} at 313.15 K is determined. Then the binary interaction parameter between anhydrous caffeine and water is introduced. Furthermore, the reference enthalpy Δh^{ref} is determined for an average temperature of 345.8 K of two literature data points of *Suzuki et al.* [28] with equation (2-22) to 73000 J mol^{-1}. By the introduction of a binary interaction parameter k_{ij} of -0.0395 and $K_{s,C\,hydrate}^{ref}$ of 0.01011, the modeling of the temperature-dependent solubility of caffeine hydrate and the literature data are presented in Figure 4-11. Furthermore, the modeling of anhydrous caffeine, modeled with equation (2-8) mentioned in chapter 2.2.1, is presented within this diagram. In this case, anhydrous caffeine is also modeled with the melting properties of α-caffeine because no melting properties for β-caffeine are available in literature. In this diagram,

(1) corresponds to an equilibrium of water and caffeine hydrate (1:0.8), while (2) corresponds to the equilibrium of caffeine hydrate (1:0.8) and the liquid phase. The equilibria of β-caffeine (4) and α-caffeine in (5) with the liquid phase are presented as well. It is shown that even without the application of divers melting properties for α- and β-caffeine, the literature data can be modeled with high accuracy. Therefore, a sufficient binary interaction parameter between caffeine and the solvent water was introduced. The binary interaction parameters that were determined within this chapter, are used in the following chapter to model the pH-dependent solubility of both oxalic acid in water and caffeine in water.

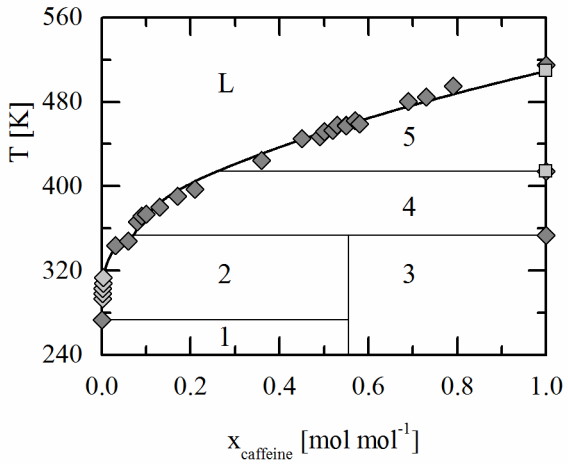

Figure 4-11: Binary temperature-dependent phase diagram of caffeine in water with experimental data (grey diamonds [28], light grey diamonds [26], light grey square [24]). Modeling of caffeine hydrate (1:0.8) and anhydrous caffeine is performed with PC-SAFT model (bold black solid line). L represents the liquid phase, (1) the equilibrium between solid water and solid caffeine hydrate (1:0.8), (2) the equilibrium between the liquid phase and caffeine hydrate (1:0.8), (3) equilibrium between caffeine hydrate (1:0.8) and anhydrous β-caffeine, (4) equilibrium between the liquid phase and β-caffeine and (5) equilibrium between the liquid phase and α-caffeine

4.2. pH-Dependent Solubility of Oxalic Acid and Caffeine

This chapter is focused on the pH-dependent solubility of oxalic acid and caffeine. At first, the pH-dependent solubility of oxalic acid in water is presented (4.2.1). Afterwards, the pH-dependent solubility of caffeine in water is shown (4.2.2). The presentation of the results includes the experimental data measured within this work and the experimental data measured by *Rela* [29]. The aim of this chapter is the determination of dissociation constants between the neutral species of oxalic acid and its ions and the dissociation constants of caffeine and its ions. Furthermore, the salt solubility products of oxalic acid and caffeine are determined.

4.2.1. pH-Dependent Solubility of Oxalic Acid

This chapter focuses on the pH-dependent solubility of oxalic acid in water. For this purpose, the modeling of the dissociation constants of oxalic acid and the salt solubility products are required. For a better insight, the required equilibria are presented in the first part of this chapter. Afterwards, the modeling in comparison to the experimental data is discussed.

At first, the dissociation steps of oxalic acid are presented in equation (4-5).

$$H_2C_2O_4 \overset{K_{a1,OxA}}{\longleftrightarrow} HC_2O_4^- + H^+ \overset{K_{a2,OxA}}{\longleftrightarrow} {C_2O_4}^{2-} + 2\,H^+ \qquad \textbf{(4-5)}$$

It is shown that two dissociation constants for oxalic acid have to be considered. Based on equation (4-5), the dissociation constants $K_{ai,OxA}$ can be determined by the following equations:

$$K_{a1,OxA} = \frac{a_{HC_2O_4^-} \cdot a_{H^+}}{a_{H_2C_2O_4}} \quad \text{and} \quad K_{a2,OxA} = \frac{a_{{C_2O_4}^{2-}} \cdot a_{H^+}}{a_{HC_2O_4^-}} \qquad \textbf{(4-6)}$$

In this case, $K_{a1,OxA}$ corresponds to the dissociation of non-dissociated oxalic acid ($H_2C_2O_4$) to hydrogen oxalate ($HC_2O_4^-$). The second dissociation constant is determined with the activity of hydrogen oxalate $a_{HC_2O_4^-}$ and the activity of oxalate $a_{{C_2O_4}^{2-}}$. In addition to the dissociation constants, salt solubility products have to be considered. The concentration range, in which the salt solubility product of each salt can be applied, is of major interest. Therefore, the following three salt equilibria are shown.

The first equation presents the solubility product of oxalic acid dihydrate (4-7). The solid phase of this component is only present at a pH value below the $pK_{a,1}$ value of 1.27 [40]. This solubility product is based on neutral species which was explained in chapter 2.2.3. The determination of the solubility products can be performed analogously as shown above. In case of solubility products, one has to consider that the salt presented on the left side of the equilibria for equations (4-7) to (4-9) is a solid and therefore the assumption is made that its activity is equal to one.

$$H_2C_2O_4 \cdot 2\,H_2O \overset{K_{S,H_2C_2O_4 \cdot 2H_2O}}{\longleftrightarrow} H_2C_2O_4 + 2\,H_2O \qquad \textbf{(4-7)}$$

As an initial approach, it can be assumed that sodium hydrogen oxalate monohydrate is formed at pH values above $pK_{a,1}$. The exact pH range is determined by modeling in a next step. The equilibrium with the solubility product for this component is shown in (4-8). The equations for the determination of salt solubility products were introduced in chapter 2.2.2 in equation (2-10).

$$NaHC_2O_4 \cdot H_2O \overset{K_{S,NaHC_2O_4 \cdot H_2O}}{\longleftrightarrow} HC_2O_4^- + Na^+ + H_2O \quad \textbf{(4-8)}$$

If the pH value is increased above the $pK_{a,2}$ value of 4.2 [40], disodium oxalate $Na_2C_2O_4$ is in equilibrium with the liquid phase.

$$Na_2C_2O_4 \overset{K_{S,Na_2C_2O_4}}{\longleftrightarrow} {C_2O_4}^{2-} + 2\,Na^+ \quad \textbf{(4-9)}$$

After the introduction of all required dissociation constants and solubility products, the experimental data and modeling results are presented in Figure 4-12. Additionally, all modeling parameters are listed in the Appendix in A.4.1. The experimental data of this section are listed in A.3.2 and the modeling of these data are listed in A.4.3. The diagram shows the experimental data by *Rela* [29] and experimental data measured within this work. Furthermore, the pK_a values are presented in black dashed lines [40]. The vertical black solid lines are phase boundaries between the three equilibria. The black solid line shows the modeling of the three phases.

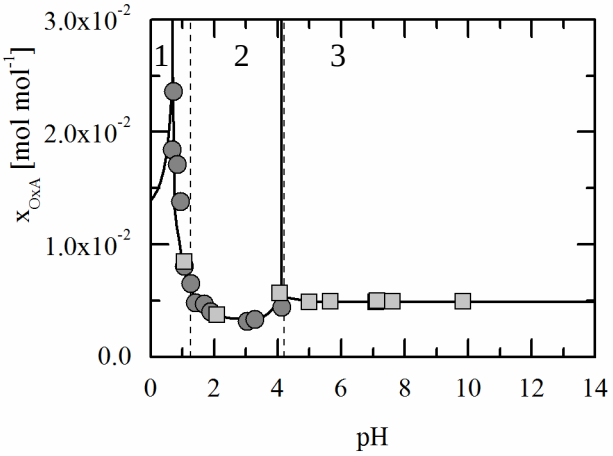

Figure 4-12: pH-dependent solubility of oxalic acid in water with experimental data (grey circles [29] and light grey squares [this work]), the pK_a values for oxalic acid at 1.27 and 4.2 [40] (black dashed lines) and the modeling of the pH-dependent solubility with black solid lines at 298.15 K and ambient pressure are shown. Furthermore, the equilibria between the liquid phase and oxalic acid dihydrate (1), the liquid phase and sodium hydrogen oxalate dihydrate (2) and the liquid phase and disodium oxalate (3) are presented

Modeling of the pH-dependent solubility of oxalic acid is a challenging task because all species are present in all three concentration ranges shown above. Therefore, modeling of the solubility has to start in one concentration range with starting values for the model parameters $K_{a1,OxA}$, $K_{a2,OxA}$ and the intrinsic solubility of non-dissociated oxalic acid. In this case, the modeling is started in concentration range (1) and afterwards range (2) and (3) are modeled. If the complete

pH-dependent solubility is modeled, all concentration ranges have to be modeled with the same parameters to achieve consistency between the concentration ranges.

Due to the fact that the presence of oxalate ions ($C_2O_4^{2-}$) as the two times dissociated species is small in the first concentration range, the adjustment of $K_{a2,OxA}$ is performed in the second range. The concentration range (1) is modeled by varying the intrinsic concentration of non-dissociated oxalic acid to model the experimental value at pH 0.68 with mole fraction of $2.36 \cdot 10^{-2}$. However, this mole fraction represents the total mole fraction of all oxalic acid species and therefore, this concentration cannot be equated with the intrinsic oxalic acid concentration. By an adjustment of the dissociation constant $K_{a1,OxA}$ to 0.7 and the binary interaction parameter k_{ij} between water and hydrogen oxalate $HC_2O_4^-$ to 0.05, the intrinsic solubility of oxalic acid is adjusted to a mole fraction of $1.38 \cdot 10^{-2}$. Then the solubility product of the hydrate $K_{s,H_2C_2O_4 \cdot 2H_2O}$ can be determined to $5.64 \cdot 10^{-2}$. Based on the modeling and the experimental data, the first concentration range is modeled until a pH value of 0.7 is reached. Due to the experimental data, the solubility of oxalic acid and its dissociated species is strongly reduced for higher pH values. In addition, the solid phases of the experimental data are identified as sodium hydrogen oxalate monohydrate. Therefore, the liquid phase is in equilibrium with sodium hydrogen oxalate monohydrate which is modeled in the next concentration range.

In concentration range (2), the dissociation constant $K_{a2,OxA}$ between hydrogen oxalate and two times dissociated oxalic acid is adjusted to the experimental data point at pH 2.09 with a total mole fraction ($H_2C_2O_4$, $HC_2O_4^-$, $C_2O_4^{2-}$) of $3.71 \cdot 10^{-3}$. The dissociation constant $K_{a2,OxA}$ is adjusted to $2.00 \cdot 10^{-4}$. Based on this dissociation constant, the solubility product of sodium hydrogen oxalate monohydrate $K_{s,NaHC_2O_4 \cdot H_2O}$ is determined to $1.67 \cdot 10^{-1}$ (4-8). This concentration range is modeled until a pH value of 4.1 is reached. Between a pH of 4.1 and 4.2 the concentration range shifts from the salt equilibrium of sodium hydrogen oxalate monohydrate to disodium oxalate which is indicated by the $pK_{a,2}$ at 4.2 [40]. In the last concentration range (3), the salt solubility product of disodium oxalate $K_{s,Na_2C_2O_4}$ is adjusted to the experimental value at pH 5.67 and a mole fraction of $4.89 \cdot 10^{-3}$.

Finally, the complete pH-dependent solubility of oxalic acid and its species is modeled. The modeling was achieved by the determination of the two dissociation constants $K_{a1,OxA}$ and $K_{a2,OxA}$, the application of the binary interaction parameter between hydrogen oxalate and water. Additionally, the intrinsic solubility of non-dissociated oxalic acid is adjusted in the first

concentration range. These parameters are adjusted to three experimental values at pH 0.68, 2.09 and 5.67, one for each concentration range. In Figure 4-12 it shown that with the adjusted parameters, the modeling has a high accuracy across the complete pH range. The determined parameters within this section are necessary for modeling the pH-dependent solubility of the cocrystal of caffeine and oxalic acid.

4.2.2. pH-Dependent Solubility of Caffeine

This chapter focuses on the pH-dependent solubility of caffeine in water. At first, the experimental results of the pH-dependent solubility are presented in Figure 4-13. It is shown that the solubility of caffeine remains constant from pH 3 to pH 11. Additionally, the pK_a value at 1 is shown by black dashed lines [45]. The second pK_a value at 14 corresponds to the frame of the diagram. Furthermore, the results show that the solubility of caffeine at low pH values and at high pH values increases. These phenomena indicate that at low pH values caffeine acts as a base and is protonated. At pH values above pH 8, caffeine acts as an acid. This amphoteric characteristic can also by observed by other substances (e.g. carboxylic acid amides) [40]. After the short introduction, the modeling of the pH-dependent solubility of caffeine is presented.

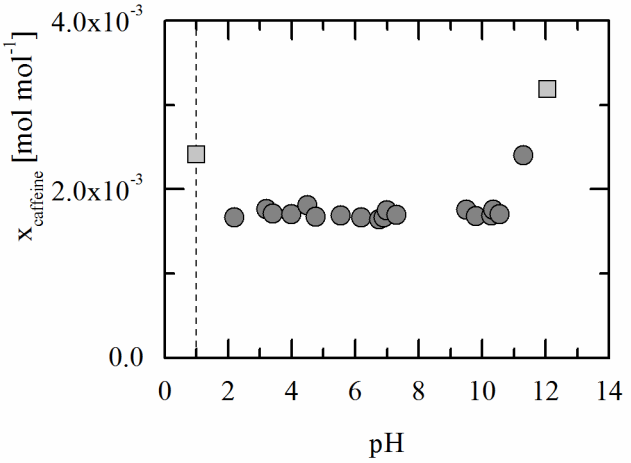

Figure 4-13: pH-dependent solubility of caffeine in water with experimental data (grey circles [29] and light grey squares [this work]) and pK_a values for caffeine at 1 (black dashed line) and 14 (frame) [45] at 298.15 K and ambient pressure are presented

After the short introduction, the modeling of the pH-dependent solubility of caffeine is presented. For this purpose, the modeling of the dissociation constants of caffeine and the hydrate solubility product of caffeine hydrate (1:0.8) are required. For a better insight, the

required equilibria are presented in the first part of this chapter. Afterwards, the modeling in comparison to the experimental data is discussed.

At first, the dissociation steps of caffeine are presented in (4-10).

$$Caffeine^{+} \overset{K_{a1,C}}{\longleftrightarrow} Caffeine + H^{+} \overset{K_{a2,C}}{\longleftrightarrow} Caffeine^{-} + 2\,H^{+} \qquad \textbf{(4-10)}$$

It is shown that two dissociation constants for caffeine have to be considered. Based on equation (4-10), the dissociation equilibrium constants $K_{ai,C}$ can be determined by the following equations:

$$K_{a1,C} = \frac{a_{caffeine} \cdot a_{H^+}}{a_{caffeine^+}} \quad \text{and} \quad K_{a2,C} = \frac{a_{caffeine^-} \cdot a_{H^+}}{a_{caffeine}} \qquad \textbf{(4-11)}$$

In this case, $K_{a1,C}$ corresponds to the dissociation of non-dissociated caffeine to the protonated caffeine. The second dissociation constant is determined with the activity of negative charged caffeine $a_{caffeine^-}$ and the activity of the non-dissociated caffeine $a_{caffeine}$. Due to the fact that caffeine hydrate (1:0.8) is the only measured solid substance, the hydrate solubility product of caffeine has to be considered. The equation (4-12) is based on the equations presented in chapter 2.2.3 and the solubility product was already presented in chapter 4.1.4.2. Therefore, only the equilibrium between the hydrate and its non-dissociated species is presented within this chapter.

$$Caffeine \cdot 0.8\,H_2O \overset{K_{s,C\,hydrate}}{\longleftrightarrow} Caffeine + 0.8\,H_2O \qquad \textbf{(4-12)}$$

After this short introduction of the constants of the caffeine species, the modeling of the pH-dependent solubility is described. The modeling of the solubility is divided in two concentration ranges, the basic and the acidic approach. The basic approach is modeled with $K_{a1,C}$ from pH 0 to pH 7. The second concentration range is modeled with the acidic approach of caffeine from pH 7 to pH 14. The acidic approach only considers the dissociation constant $K_{a2,C}$ while $K_{a1,C}$ is neglected within this concentration range. Because of the constant solubility from pH 3 to 11, the ions do not influence themselves and therefore this separation is valid. Furthermore, only the basic approach is required for the modeling of the cocrystal solubility because the examined pH values reach from 1 to 7. Therefore, the equation system can be simplified by the neglect of the second dissociation constant $K_{a2,C}$ for the basic approach.

For the first concentration range, the dissociation constant $K_{a1,C}$ is adjusted to the mole fraction of $1.73 \cdot 10^{-3}$ at 298.15 K and pH 7. The dissociation constant $K_{a1,C}$ is determined to

$1.0234 \cdot 10^{-5}$. Based on these result, the hydrate solubility product for 298.15 K is determined to $5.49825 \cdot 10^{-3}$ and the first concentration range from pH 1 to pH 7 is modeled. The modeling results with the experimental values are presented in Figure 4-14. Additionally, the experimental values, the modeling parameters and the modeling results are listed in the Appendix in chapter A.3.2, A.4.1 and A.4.3.

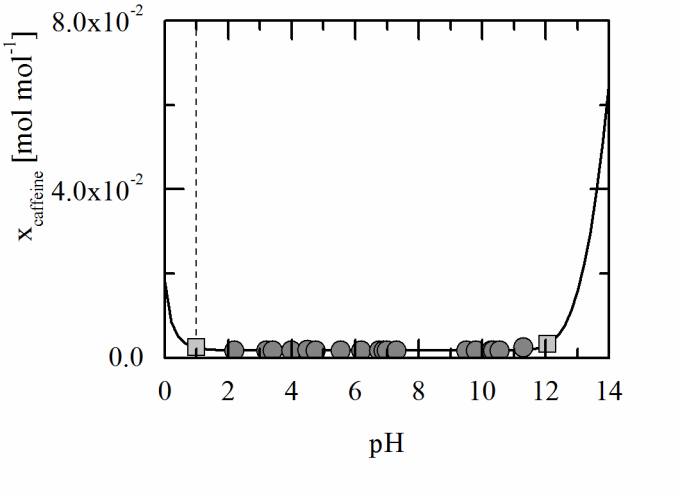

Figure 4-14: pH-dependent solubility of caffeine in water with experimental data (grey circles [29] and light grey squares [this work]), the pK_a values for caffeine at 1 (black dashed lines) and 14 (frame) [45] and the modeling of pH-dependent caffeine hydrate (1:0.8) solubility are presented (black solid line) at 298.15 K and ambient pressure

The second concentration range from pH 7 to pH 14 is modeled with the acidic approach. Therefore, only $K_{a2,C}$ is considered and $K_{a1,C}$ is neglected. By adjusting $K_{a2,C}$ to the same experimental value as for the previous approach, a binary interaction parameter k_{ij} between the negative charged caffeine and water has to be introduced. The interaction parameter is set to -0.08 and then the dissociation constant $K_{a2,C}$ is determined with $4.3521 \cdot 10^{-16}$, while the hydrate solubility remains unchanged over the complete pH range.

In this chapter, the pH-dependent solubility of caffeine was modeled successfully with a high accuracy. Additionally, the amphoteric characteristic of caffeine was presented and sufficient modeling parameters were achieved. The dissociation constant $K_{a1,C}$ is used in the following chapter to model the hydrate solubility in presence of oxalic acid and the solubility of the cocrystal of caffeine and oxalic acid.

4.3. pH-Dependent Cocrystal Solubility

This chapter focuses on the pH-dependent solubility of the cocrystal of caffeine and oxalic acid (2:1) in water at 298.15 K. The aim of this chapter is the complete determination of the ternary system of the aforementioned components. At first, the ternary phase diagram at the pH value 1 (4.3.1) and the pH value 2 (4.3.2) are examined. Afterwards, the prediction of the cocrystal solubility is performed for the pH value 2.6 (4.3.3). Then the analysis of the pH values 4, 5 and 7 are presented (4.3.4). The experimental data that are presented in this chapter are also listed in the Appendix in chapter A.3.3 and a PXRD analysis for every relevant solid phase is illustrated in chapter A.3.4. Additionally, the model parameters that are applied are listed in the Appendix in A.4.1 and the modeling results are presented in A.4.4.

4.3.1. Cocrystal Solubility at pH 1

The first chapter starts with a short introduction to the cocrystal solubility. As described in 3.1.1, the anhydrous cocrystal of caffeine and oxalic acid has a 2:1 stoichiometry [31]. Based on this knowledge and with equation (2-17) in chapter 2.2.3, the cocrystal solubility product can be determined by the following equilibrium:

$$Caffeine_2 \cdot OxA \overset{K_{s,CC}}{\longleftrightarrow} 2\,Caffeine + OxA \qquad \textbf{(4-13)}$$

The cocrystal solubility product $K_{s,CC}$ of caffeine and oxalic acid is shown in equation (4-14).

$$K_{s,CC} = a_{caffeine}^2 \cdot a_{OxA} \qquad \textbf{(4-14)}$$

Due to the stoichiometry, the activity of caffeine $a_{caffeine}$ is powered by the factor two in comparison to the activity of oxalic acid a_{OxA}. As described in chapter 2.2.3, the cocrystal solubility product is determined by the non-dissociated species of oxalic acid and caffeine. For the determination of the neutral species, the dissociation constants of oxalic acid $K_{a1,OxA}$ and $K_{a2,OxA}$, the dissociation constant of caffeine for the basic approach $K_{a1,C}$ are required.

In the following section, the modeling procedure for the cocrystal modeling is presented. As already described in chapter 2.2.3, one experimental cocrystal solubility point is required to model each pH value at the same temperature. In this case, the experimental value is a cocrystal solubility point at pH 2 and 298.15 K. Based on this experimental point, the neutral cocrystal line is calculated with the dissociation constants of oxalic acid and caffeine as shown in chapter 2.2.2 with equation (2-10) and (2-13). This allows the calculation of the ion species and the

determination of the non-dissociated components. With the neutral solubility line, every desired pH value can be calculated in the next step.

In this section, the prediction of the hydrate and salt solubility lines are explained. These solubility lines are basically calculated as described in chapter 4.2 but in the ternary system, the salt and hydrate solubility are calculated in the presence of the third component. As an example, the pH-dependent caffeine hydrate (1:0.8) solubility is calculated in the presence of oxalic acid and the sodium hydrogen oxalate monohydrate solubility is calculated in the presence of caffeine.

For a better insight, the prediction and the diverse equilibria of cocrystals, hydrates and salts are presented in Figure 4-15 for pH 1 and 298.15 K. The diagram shows the liquid phase (L) below the measured solubility points. The experimental values on the axes are the pure component pH-dependent solubility that were presented in the previous chapter (4.2) for oxalic acid and caffeine. The bold black solid curved line represents the cocrystal solubility line and the straight bold black solid line represents the salt solubility line of sodium hydrogen oxalate monohydrate for a pH of 1.

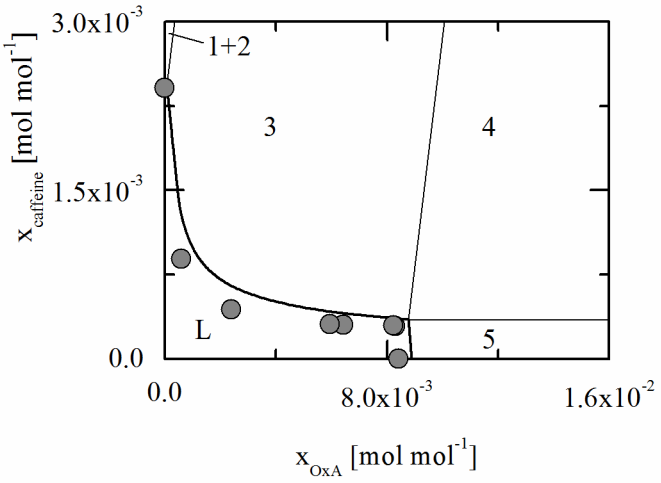

Figure 4-15: Experimental solubility data of the cocrystal of caffeine and oxalic acid (2:1) at 298.15 K, ambient pressure and pH 1. The solubility points on the axes correspond to the binary solubility of caffeine hydrate (1:0.8) and sodium hydrogen oxalate monohydrate in water at pH 1. Prediction of the cocrystal and salt solubility is presented by bold black solid lines. The thin black solid lines represent the phase boundaries between two solid phases. The liquid phase L is in equilibrium with caffeine hydrate (1:0.8) (1), a mixture of caffeine hydrate (1:0.8) and cocrystal (2), pure cocrystal formation (3), a mixture of cocrystal formation and sodium hydrogen oxalate monohydrate (4) and with pure sodium hydrogen oxalate monohydrate (5)

The concentration range (1+2) represents the equilibrium of caffeine hydrate (1:0.8), cocrystal and the liquid phase. Concentration range (3) represent the equilibrium between the liquid phase and pure cocrystal formation. Concentration range (4) represent the equilibrium between the liquid phase, cocrystal formation and sodium hydrogen oxalate monohydrate formation and the last concentration range (5) stands for pure sodium hydrogen oxalate monohydrate formation.

It is shown that the cocrystal concentration range is large and therefore cocrystal formation can be achieved quite easily. The modeling shows a high accuracy for high oxalic acid concentrations. For the prediction of oxalic acid concentration below mole fractions of $2 \cdot 10^{-3}$, a lower accuracy can be achieved in comparison to higher oxalic acid concentrations. A reason for this behavior could be that the analysis method which was introduced in 3.3.1.1 and is described in detail in chapter A.2.2 is more accurate for higher oxalic acid concentrations. Therefore, the experimental values with oxalic acid concentrations below $2 \cdot 10^{-3}$ have higher standard deviations ($2.93 \cdot 10^{-4}$) in comparison to the remaining experimental values ($1.18 \cdot 10^{-4}$). Although the difference is not great, the standard deviation has a greater influence for solubility points with oxalic acid concentrations below mole fractions of $2 \cdot 10^{-3}$. As a result, the analysis method for the liquid phase could be optimized to smaller mass ratios. Furthermore, the cocrystal solubility and the neutral cocrystal line was determined by a solubility point at pH 2. Nevertheless, the prediction of the salt solubility and the cocrystal solubility are in good agreement to the experimental values. Due to the fact that no additional binary interaction parameters between oxalic acid and caffeine species are applied, these are remarkable results.

4.3.2. Cocrystal Solubility at pH 2

This chapter focuses on the analysis of the cocrystal solubility at pH 2. The cocrystal and hydrate solubility is calculated with the same procedure as described in the previous section. As mentioned in chapter 4.3.1, the experimental value that is applied for modeling the cocrystal solubility was measured at pH 2. The modeling results for the cocrystal solubility and the prediction for the hydrate solubility for pH 2 are presented in Figure 4-16. In this diagram, concentration range (1), the caffeine hydrate (1:0.8) solubility, and concentration range (2), the solubility of a mixture of caffeine hydrate (1:0.8) and cocrystal, are increasing in comparison to the salt and hydrate solubility at pH 1. Furthermore, concentration range (5) with pure sodium hydrogen oxalate monohydrate in equilibrium with the liquid phase and concentration range (4) with sodium hydrogen oxalate monohydrate and cocrystal in equilibrium with the liquid phase are increasing as well in comparison to pH 1. Only concentration range (3) the pure cocrystal

formation in equilibrium with the liquid phase is reduced. The reason is that for increasing pH value, the concentration of non-dissociated oxalic acid reduces while the concentration of non-dissociated caffeine remains constant. Hence, pure cocrystal formation can only be achieved within a smaller concentration range.

The prediction for pH 2 shows that the salt solubility of sodium hydrogen oxalate monohydrate (bold black solid line (5)) and the caffeine hydrate (1:0.8) solubility line (bold black solid line (1)) have a high accuracy. Additionally, the cocrystal solubility can be modeled with high accuracy (bold black solid line (3)). The results indicate that the salt and hydrate solubility are thermodynamically ideal because the solubility lines are parallel to the axes [9]. Interestingly, the experimental value (light grey circle) at the intersection of concentration ranges (3), (4) and (5) was identified as a eutectic formation of sodium hydrogen oxalate monohydrate and cocrystal. The other experimental value shows pure sodium hydrogen oxalate monohydrate formation (light grey triangle). This phenomenon shows that the identification of solubility points especially at the intersection point is a challenging task.

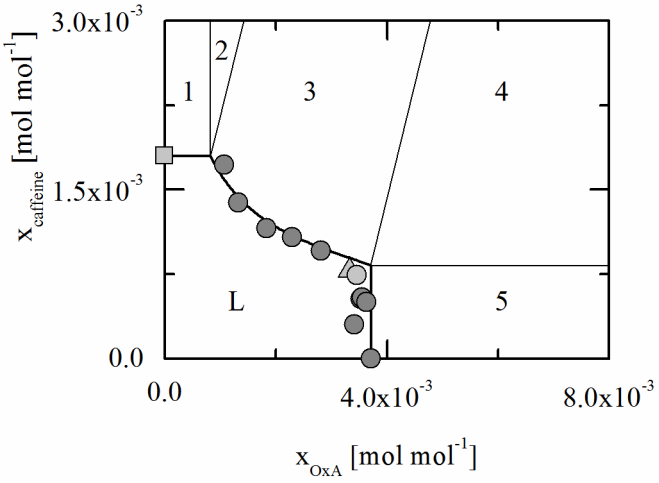

Figure 4-16: Experimental solubility (grey circles [this work], light grey circle and triangle [this work], light grey squares [29]) of the cocrystal of caffeine and oxalic acid (2:1) and their salts and hydrates at 298.15 K, ambient pressure and pH 2. The solubility points on the axes correspond to the binary solubility of caffeine hydrate (1:0.8) and sodium hydrogen oxalate monohydrate in water at pH 2. Modeling of the cocrystal solubility and the prediction of the salt and hydrate solubility are presented by bold black solid lines. The thin black solid lines represent the phase boundaries between two solid phases. The liquid phase is in equilibrium with solid caffeine hydrate (1:0.8) (1), with a mixture of caffeine hydrate (1:0.8) and cocrystal (2), with pure cocrystal formation (3), a mixture of cocrystal formation and sodium hydrogen oxalate monohydrate (4) and with pure sodium hydrogen oxalate monohydrate (5)

4.3.3. Prediction of pH-Dependent Cocrystal Solubility

After modeling the cocrystal solubility for pH 2 and predict the cocrystal solubility for pH 1 and the salt and hydrate solubility at pH 1 and 2, a prediction for the cocrystal solubility for pH 2.6 is performed. The aim of this chapter is the illustration of the reduction of the concentration range of pure cocrystal formation which depends on the pH value. The alteration of the cocrystal solubility is shown in Figure 4-17. The diagram shows that with increasing pH value from 1 to 2 the pure cocrystal formation is reduced strongly (grey solid lines to light grey solid lines). If the pH value is increased further, the cocrystal concentration range is reduced to a minimum as indicated by the black solid and dashed lines. The pH value of 2.6 corresponds to the turning point of pure cocrystal formation. Based on these results, no cocrystal formation should be observed for higher pH values that are presented in the following chapters.

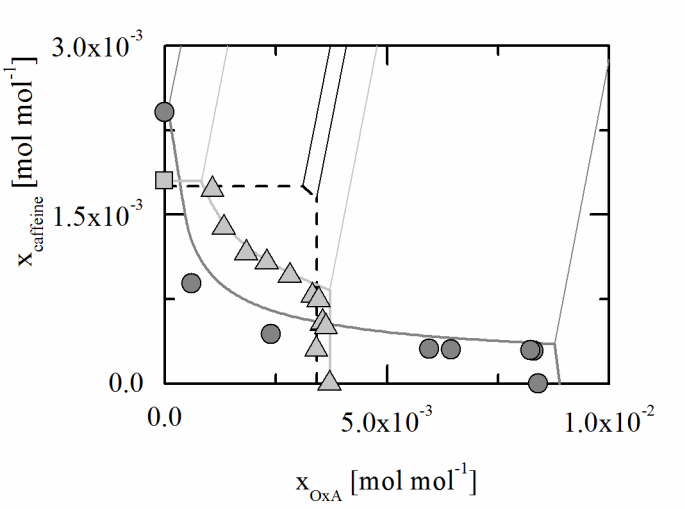

Figure 4-17: Experimental solubility (grey circles [this work at pH 1], light grey squares [29] at pH 2, light grey triangles [this work at pH 2]) of the cocrystal of caffeine and oxalic acid (2:1) and their salts and hydrates at 298.15 K and ambient pressure. The solubility points on the axes correspond to the binary solubility of caffeine hydrate (1:0.8) and sodium hydrogen oxalate monohydrate in water at pH 1 and pH 2. Prediction of cocrystal and salt solubility at pH 1 (grey solid line), modeling of cocrystal solubility and prediction of salt and hydrate solubility at pH 2 (light grey solid line) and the prediction for pH 2.6 (black dashed line). The thin solid lines show the phase boundaries of the pure cocrystal solubility and therefore pure cocrystal formation from pH 1 to pH 2.6

4.3.4. Cocrystal Solubility at pH 4, 5 and 7

This chapter focuses on the results of cocrystal, salt and hydrate solubility of oxalic acid and caffeine at pH value 4, 5 and 7 at 298.15 K. The results of the experimental data and the predictions are presented in Figure 4-18. In this diagram, the first concentration range (1) corresponds to the equilibrium between the liquid phase and caffeine hydrate (1:0.8). For pH 4, concentration range (5) corresponds to the equilibrium between pure sodium hydrogen oxalate monohydrate and the liquid phase and concentration range (2) corresponds to the equilibrium between the liquid phase and a solid mixture of caffeine hydrate (1:0.8) and sodium hydrogen oxalate monohydrate. In case of pH 5 and 7, concentration range (5) corresponds to the equilibrium between pure disodium oxalate formation and the liquid and concentration range (2) to the equilibrium between the liquid phase and a solid mixture of disodium oxalate and caffeine hydrate (1:0.8). As predicted in chapter 4.3.3, no cocrystal solubility point could be determined for pH value 4, 5 and 7.

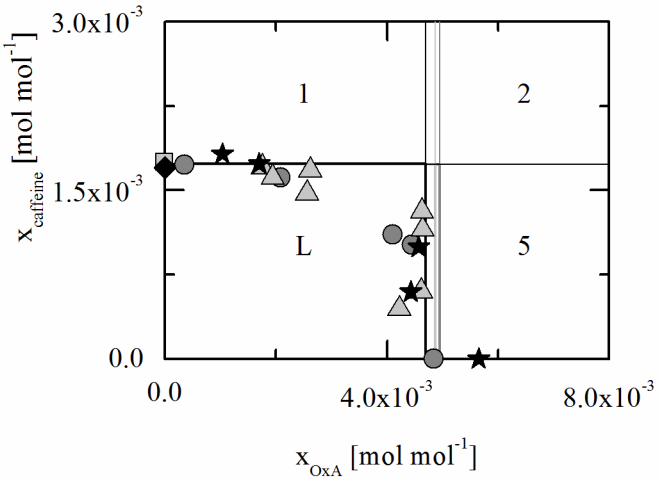

Figure 4-18: Experimental solubility for pH 4 (black stars [this work], black diamond [29]) of caffeine hydrate (1:0.8) and sodium hydrogen oxalate monohydrate, pH 5 (grey circles [this work]) and pH 7 (light grey triangles [this work], light grey square [29]) of caffeine hydrate (1:0.8) and disodium oxalate at 298.15 K and ambient pressure. The solubility points on the axes correspond to the binary solubility of caffeine hydrate (1:0.8), sodium hydrogen oxalate monohydrate and disodium oxalate in water. The prediction of the salt and hydrate solubility of caffeine hydrate (1:0.8) and sodium hydrogen oxalate monohydrate at pH 4 (bold black solid lines), the prediction of the solubility of caffeine hydrate (1:0.8) and disodium oxalate at pH 5 (bold grey solid lines) and the prediction of the solubility of caffeine hydrate (1:0.8) and disodium oxalate at pH 7 (bold light grey solid lines) are shown. The thin lines represent the phase boundaries between two solid phases. The liquid phase L is in equilibrium with caffeine hydrate (1:0.8) (1), with a mixture of caffeine hydrate (1:0.8) with sodium hydrogen oxalate monohydrate for pH 4 and a mixture with disodium oxalate for pH 5 and 7 (2). The concentration range (5) corresponds to the equilibrium between the liquid phase and sodium hydrogen oxalate monohydrate for pH 4 and disodium oxalate for pH 5 and 7.

The first section is focused on the experimental results and the prediction for pH 4 (black symbols and black lines). It is shown that the solubility of caffeine hydrate (1:0.8) in presence of oxalic acid and without oxalic acid is predicted with high accuracy and in comparison to pH 5 and 7 the solubility does not change significantly. In addition, the prediction of sodium hydrogen oxalate monohydrate solubility is in a good agreement to the experimental data. The deviation between the prediction of the salt solubility of oxalic acid and the binary experimental value on the axis is due to its pH value of 4.08. As presented in chapter 4.2.1, the oxalic acid solubility in the binary pH-dependency is increasing at the end of the concentration range of sodium hydrogen oxalate monohydrate and therefore the measured solubility is higher as the predicted one at pH 4.

The second section focuses on the experimental results and the prediction for pH 5 (grey symbols and grey lines). For pH 5, a trend for decreasing caffeine hydrate (1:0.8) solubility can be detected but this could also be explained by variation due to the standard deviation of the sample. In comparison to this phenomenon, the solubility of disodium oxalate starts to decrease with increasing amount of caffeine in the liquid phase as well. The reason is that the prediction of the eutectic point of concentration ranges (1), (2) and (5) is a challenging task and therefore the deviation between the prediction and the experimental results occur.

The last section focuses on the experimental results and the prediction for pH 7 (light grey symbols and light grey lines). It is shown that the solubility for disodium oxalate is predicted with high accuracy. The deviation of the lowest solubility point can be explained by inaccuracies due to the sample analysis. In comparison to the prediction of disodium oxalate, caffeine hydrate (1:0.8) is predicted with lower accuracy. The emerging trend that was observed for pH 5 is increasing with increasing pH value. Hence, the caffeine hydrate solubility is reduced by increasing amount of oxalic acid in the liquid phase. This trend can be confirmed by the experimental data because the highest solubility point along the solubility line of disodium oxalate is actually caffeine hydrate (1:0.8). Based on these results, the decreasing solubility of caffeine hydrate (1:0.8) can be confirmed. Unfortunately, this trend is not predicted by PC-SAFT. However, the caffeine hydrate (1:0.8) solubility can be modeled by an application of a binary interaction parameter between caffeine and disodium oxalate for pH 5 and 7 to increase the accuracy. Additionally, these trends were not observed for the sodium hydrogen oxalate monohydrate systems from pH 1 to pH 4. Therefore, it can be concluded that only disodium oxalate interacts with caffeine and not the other oxalic acid species.

5. Conclusion and Outlook

The aim of this work was the investigation of oxalic acid as a hydrate and cocrystal forming component. This investigation included the experimental analysis and modeling of the results with perturbed-chain statistical associating fluid theory (PC-SAFT). The investigated cocrystal consists of caffeine and oxalic acid in a 2:1 stoichiometry. In the first step, PC-SAFT pure component parameters for oxalic acid were adjusted to solubility data of oxalic acid in organic solvents. In the second step, the temperature-dependent solubilities of oxalic acid dihydrate, caffeine hydrate (1:0.8) and their anhydrous polymorphs α- and β-oxalic acid and α- and β-caffeine in water were modeled based on experimental and literature data. In the third step, the binary pH-dependent solubilities of oxalic acid and caffeine within water were investigated. At last, the cocrystal, salt and hydrate solubility of the system caffeine, oxalic acid and water was examined for various pH values.

In the first step, PC-SAFT pure component parameters for oxalic acid were adjusted to solubility data of oxalic acid in organic solvents. This is a challenging task due to oxalic acid dihydrate formation in organic solvents. Therefore, the solvents were selected by the water content of the solvents themselves and the reactivity with oxalic acid. Based on these selection criteria, the organic solvents acetonitrile, ethyl acetate and butyl acetate were selected and the temperature-dependent solubility of oxalic acid within these solvents was investigated. Afterwards, PC-SAFT pure component parameters were determined. The modeling shows a high accuracy with the experimental data (average relative deviation (ARD) of 3.05%). Only the modeling of oxalic acid's solubility within the mixture of acetonitrile and ethyl acetate shows a lower accuracy (ARD of 6.60%). To improve the modeling of the solvent mixture, binary interaction parameter between acetonitrile and ethyl acetate can be applied that were not adjusted within this work.

In the second part, the temperature-dependent solubility of oxalic acid and caffeine within water was modeled based on experimental and literature data. Therefore, the binary phase diagram was determined by modeling the hydrate solubility of the solutes oxalic acid and caffeine separately from the anhydrous solubility of these components. The modeling of the temperature-dependent hydrate solubility by Gibbs-Helmholtz, one reference solubility product K_a^{ref} and adjusting of the reference enthalpy Δh^{ref} is in good agreement with the experimental data. The anhydrous polymorphs of both components are modeled by standard solubility calculations. Unfortunately, no melting properties for the metastable polymorphs β-caffeine and β-oxalic acid were available and therefore these concentration ranges were modeled on the basis

of the α-polymorphs. Even though this is not quite accurate, the modeling for anhydrous caffeine polymorphs showed a high accuracy in comparison to the experimental data. In case of oxalic acid, the results cannot be confirmed due to the lack of experimental solubility data for anhydrous oxalic acid polymorphs.

In the third part, the pH-dependent solubility for oxalic acid and caffeine within water at 298.15 K was examined. For this purpose, experiments were performed and experimental data from previous work were taken into account. In this case, the solubility is modeled using dissociation constants between the non-dissociated oxalic acid, its dissociated species and salt solubility products. By their application, each equilibrium of oxalic acid species was modeled with high accuracy. Additionally, the three equilibria of oxalic acid species are in good agreement with the pK_a values from literature. The same procedure can be applied for the pH-dependency of caffeine. The modeling of caffeine's pH-dependency is also quite accurate. In addition, the amphoteric behavior of caffeine was presented by the modeling and the experimental results.

In the last step, the cocrystal system consisting of caffeine, oxalic acid and water was investigated at 298.15 K for pH 1, 2, 4, 5 and 7. Based on the adjustment of $K_{a,CC}$ to one experimental value at pH 2, the cocrystal solubility line was modeled for pH 2 and predicted for pH 1 quite successfully. In addition, it was possible to predict the turning point of cocrystal formation at pH 2.6. Furthermore, it was confirmed by the prediction of the pH values at 4, 5 and 7 that no cocrystal was formed at these pH values and therefore only hydrates and salts could be determined. The hydrate and salt solubility in the ternary phase diagrams were predicted with high accuracy as well to present the complete ternary phase diagram for each pH value.

In future work, the temperature-dependent solubility of this system could be investigated. In addition, the stability of oxalic acid and caffeine cocrystals can be analyzed in a next step. Based on the determined pure component parameters for oxalic acid, new cocrystal systems with oxalic acid as the coformer can be examined as well. In addition, the reduction of the cocrystal formation can be investigated with other active pharmaceutical ingredients. These studies could validate if the reduction occurs due to the application of oxalic acid as a coformer or the component system itself.

6. Bibliography

[1] Babu, N. J.; Nangia, A.: Solubility Advantage of Amorphous Drugs and Pharmaceutical Cocrystals. *Crystal Growth & Design* 11: (2011) 7, p. 2662–2679.

[2] Jones, W.; Motherwell, W. D. S.; Trask, A. V.: Pharmaceutical Cocrystals: An Emerging Approach to Physical Property Enhancement. *MRS Bulletin* 31: (2006) 11, p. 875–879.

[3] Trask, A. V.: An Overview of Pharmaceutical Cocrystals as Intellectual Property. *Mol. Pharmaceutics* 4: (2007) 3, p. 301–309.

[4] Serajuddin, A. T.: Salt Formation to Improve Drug Solubility. *Advanced Drug Delivery Reviews* 59: (2007) 7, p. 603–616.

[5] Miroshnyk, I.; Mirza, S.; Sandler, N.: Pharmaceutical Co-Crystals – an Opportunity for Drug Product Enhancement. *Expert Opinion on Drug Delivery* 6: (2009) 4, p. 333–341.

[6] Good, D. J.; Rodríguez-Hornedo, N.: Solubility Advantage of Pharmaceutical Cocrystals. *Crystal Growth & Design* 9: (2009) 5, p. 2252–2264.

[7] Sekhon, B. S.: Pharmaceutical Co-Crystals - a Review. *Ars Pharm.* 50: (2009) 2, p. 99–117.

[8] Friščić, T.; Jones, W.: Recent Advances in Understanding the Mechanism of Cocrystal Formation via Grinding. *Crystal Growth & Design* 9: (2009) 3, p. 1621–1637.

[9] Lange, L.; Sadowski, G.: Thermodynamic Modeling for Efficient Cocrystal Formation. *Crystal Growth & Design* 15: (2015) 9, p. 4406–4416.

[10] Sadowski, G.: Biothermodynamics - Script, TU Dortmund, Department of Biochemical and Chemical Engineering. Laboratory of Thermodynamics. 2015.

[11] Sadowski, G.: Thermodynamics II - Script, TU Dortmund, Department of Biochemical and Chemical Engineering. Laboratory of Thermodynamics. 2012.

[12] Gmehling, J.; Kolbe, B.; Kleiber, M., *et al.:* Chemical Thermodynamics for Process Simulation, Wiley-VCH-Verl., Weinheim, 2012.

[13] Hansen, N. T.; Kouskoumvekaki, I.; Jørgensen, F. S., *et al.:* Prediction of pH-Dependent Aqueous Solubility of Druglike Molecules. *J. Chem. Inf. Model.* 46: (2006) 6, p. 2601–2609.

[14] Johnson, S. R.; Chen, X.-Q.; Murphy, D., *et al.:* A Computational Model for the Prediction of Aqueous Solubility That Includes Crystal Packing, Intrinsic Solubility, and Ionization Effects. *Molecular Pharmaceutics* 4: (2007) 4, p. 513–523.

[15] Bethune, S. J.; Huang, N.; Jayasankar, A., *et al.:* Understanding and Prediciting the Effect of Cocrystal Components and pH on Cocrystal Solubility. *Crystal Growth & Design* 9: (2009) 9, p. 3976–3988.

[16] Lange, L.; Lehmkemper, K.; Sadowski, G.: Predicting the Aqueous Solubility of Pharmaceutical Cocrystals as Function of pH. submitted 2016.

[17] Gross, J.; Sadowski, G.: Perturbed-Chain SAFT: An Equation of State Based on a Perturbation Theory for Chain Molecules. *Ind. Eng. Chem. Res.* 40: (2001) 4, p. 1244–1260.

[18] Ruether, F.; Sadowski, G.: Modeling the Solubility of Pharmaceuticals in Pure Solvents and Solvent Mixtures for Drug Process Design. *Journal of Pharmaceutical Sciences* 98: (2009) 11, p. 4205–4215.

[19] Tumakaka, F.; Prikhodko, I. V.; Sadowski, G.: Modeling of Solid-Liquid Equilibria for Systems with Solid-Complex Phase Formation. *Fluid Phase Equilibria* 260: (2007) 1, p. 98–104.

[20] Fuchs, D.; Fischer, J.; Tumakaka, F., *et al.:* Solubility of Amino Acids. *Ind. Eng. Chem. Res.* 45: (2006) 19, p. 6578–6584.

[21] Kolská, Z.; Kukal, J.; Zábranský, M., *et al.:* Estimation of the Heat Capacity of Organic Liquids as a Function of Temperature by a Three-Level Group Contribution Method. *Ind. Eng. Chem. Res.* 47: (2008) 6, p. 2075–2085.

[22] Lange, L.: Melting Properties of Oxalic Acid. 04.01.2016, Dortmund.

[23] Cesaro, A.; Starec, G.: Thermodynamic Properties of Caffeine Crystal Forms. *J. Phys. Chem.* 84: (1980), p. 1345–1346.

[24] Bothe, H.; Cammenga, H. K.: Phase Transitions and Thermodynamic Properties of Anhydrous Caffeine. *J. Therm. Anal.* 16: (1979), p. 267–275.

[25] Budavari, Susan: The Merck-index: An Encyclopedia of Chemicals, Drugs, and Biologicals. 11. ed., 3. print., centennial ed., Rahway, NJ, 1991.

[26] Dischlov, E.: Messung und Modellierung des Löslichkeits- und Freisetzungsverhaltens pharamzeutischer Co-Kristalle. Master Thesis. October 2013, Department of Biochemical and Chemical Engineering.

[27] Apelblat, A.; Manzurola, E.: Solubility of Oxalic, Malonic, Succinic, Adipic, Maleic, Malic, Citric, and Tartaric Acids in Water from 278.15 to 338.15 K. *J.Chem. Thermodynamics* 19: (1987) 3, p. 317–320.

[28] Suzuki, E.; Shirotani, K.-I.; Tsuda, Y., *et al.:* Water Content and Dehydration Behavior of Crystalline Caffeine Hydrate. *Chem. Pharm. Bull.* 33: (1985) 11, p. 5028–5035.

[29] Rela, G.: Solubility of Pharmaceutical Co-Crystals and Hydrates as Function of pH. Master Thesis. March 2015, Department of Biochemical and Chemical Engineering.

[30] Eddleston, M. D.; Madusanka, N.; Jones, W.: Cocrystal Dissociation in the Presence of Water: A General Approach for Identifying Stable Cocrystal Forms. *Journal of Pharmaceutical Sciences* 103: (2014) 9, p. 2865–2870.

[31] Aher, S.; Dhumal, R.; Mahadik, K., *et al.:* Effect of Cocrystallization Techniques on Compressional Properties of Caffeine/Oxalic Acid 2:1 Cocrystal. *Pharamceutical Development and Technology* 18: (2013) 1, p. 55–60.

[32] Trask, A. V.; Motherwell, W. D. S.; Jones, W.: Physical Stability Enhancement of Theophylline via Cocrystallization. *International Journal of Pharmaceutics* 320: (2006) 1-2, p. 114–123.

[33] Karki, S.; Friščić, T. and Jones, W.: Control and Interconversion of Cocrystal Stoichiometry in Grinding: Stepwise Mechanism for the Formation of a Hydrogen-Bonded Cocrystal. *CrystEngComm* 11: (2009) 3, p. 470–481.

[34] Hathwar, V. R.; Pal, R.; Guru Row, T. N.: Charge Density Analysis of Crystals of Nicotinamide with Salicylic Acid and Oxalic Acid: An Insight into the Salt to Cocrystal Continuum. *Crystal Growth & Design* 10: (2010) 8, p. 3306–3310.

[35] Heisel, S.: Formation of Pharmaceutical Cocrystals from Solvent Mixtures. Master Thesis. November 2015, Department of Biochemical and Chemical Engineering.

[36] Trask, A. V.; Motherwell, W. D. S.; Jones, W.: Pharmaceutical Cocrystallizaton: Engineering a Remedy for Caffeine Hydration. *Crystal Growth & Design* 5: (2004) 3, p. 1013–1021.

[37] National Center for Biotechnology Information: Oxalic Acid Properties, PubChem Open Chemistry Database, last check: 10.01.2016. https://pubchem.ncbi.nlm.nih.gov/compound/971.

[38] International Programme on Chemical Safety and the European Commission (IPCS): International Chemical Safety Cards (ICSC) of Oxalic Acid Dihydrate, last check: 18.03.2016. http://www.ilo.org/dyn/icsc/.

[39] Petropavlov, N. N.; Tsygankova, I.; Teslenk, L. A.: Microcalorimetric Investigation of Polymorphic Transitions in Organic Crystals. *Sov. Phys. Crystallogr.* 33: (1988) 6, p. 853–855.

[40] Buddrus, J.: Grundlagen der Organischen Chemie. 4., überarb. u. aktualisierte Aufl., de Gruyter, Berlin, 2011.

[41] Ma, Q.; He, H.; Liu, C.: Hygroscopic Properties of Oxalic Acid and Atmospherically relevant Oxalates. *Atmospheric Enviroment* 69: (2013), p. 281–288.

[42] Encyclopaedia Britannica: Oxalic Acid Properties, Encyclopaedia Britannica Online, last check: 10.01.2016. http://www.britannica.com/science/oxalic-acid.

[43] Oliver, R.: Oxalic Acid: Questions, Answers, and More, last check: 10.01.2016. http://scientificbeekeeping.com/oxalic-acid.

[44] Sigma Aldrich: Product Information: Caffeine, last check: 10.01.2016. https://www.sigmaaldrich.com/content/dam/sigma-aldrich/docs/Sigma-Aldrich/Product_Information_Sheet/c0750pis.pdf.

[45] Dews, P. B.: Caffeine, Springer, Berlin, 1984.

[46] Bothe, H.; Cammenga, H. K.: Composition, Properties, Stability and Thermal Dehydration of Crystalline Caffeine Hydrate. *Thermochimica Acta* 40: (1980) 1, p. 29–39.

[47] National Center for Biotechnology Information: Caffeine Properties, last check: 10.01.2016. https://pubchem.ncbi.nlm.nih.gov/compound/2519.

[48] Chen, R.; Yu, Z.; Chen, Y.: Method for Producing Diethyl Oxalate by Ethyl Alchohol Dehydration. CN 1192433 A, China, 1998.

[49] Lehmkemper, K.: Messung und Modellierung der pH-abhängigen Löslichkeit pharmazeutischer Co-Kristalle. Master Thesis. July 2014, Department of Biochemical and Chemical Engineering.

[50] Owen, T.: Fundamentals of UV-Visible Spectroscopy: A Primer, Hewlett-Packard Company, Germany, 1996.

[51] Scholz, E.: Karl-Fischer-Titration: Methoden zur Wasserbestimmung, Springer, Berlin, Heidelberg, 1984.

[52] Höhne, G. W. H.; Hemminger, W. F.; Flammersheim, H.-J.: Differential Scanning Calorimetry. 2nd revised and enlarged edition, Springer, Berlin, Heidelberg, 2003.

[53] Fultz, B.; Howe, J.: Transmission Electron Microscopy and Diffractometry of Materials. 4th ed. 2013, Springer, Berlin, Heidelberg, 2013.

[54] Allen, F. H.: The Cambridge Strucutural: a quarter of a million crystal strucutres and rising. *Acta Cryst.* B58: (2002) 3, p. 380–388.

[55] Chateigner, D.: Crystallography Open Database, last check: 10.01.2016. http://www.crystallography.net/.

[56] Eddleston, M. D.; Patel, B.; Day, G. M., *et al.:* Cocrystallization by Freeze-Drying: Preparation of Novel Multicomponent Crystal Forms. *Crystal Growth & Design* 13: (2013) 10, p. 4599–4606.

[57] Bader, A. R.: Preparation of Esters of Oxalic Acid. US 2693478, USA, 1951.

[58] Bowden, E.: Working with Hazardous Chemicals - Methyl Oxalate. *Organic Syntheses* 2: (1943), p. 414.

[59] Kleiner, M.; Gross, J.: An Equation of State Contribution for Polar Components. *AIChE J.* 52: (2006) 5, p. 1951–1961.

A. Appendix

A.1 Theory

$$\Delta h^{SL} = \Delta h_{0i}^{SL} + \int_{T_{0i}^{SL}}^{T} \Delta c_{p,i}^{SL}\, dT \qquad \textbf{(A-1)}$$

$$\Delta s^{SL} = \frac{\Delta h_{0i}^{SL}}{T_{0i}^{SL}} + \int_{T_{0i}^{SL}}^{T} \frac{\Delta c_{p,i}^{SL}}{T}\, dT \qquad \textbf{(A-2)}$$

A.2 Materials and Methods

Table A-1: Chemical substances used in this work

Chemical	Manufacturer	Purity
2-Propanol	VWR Chemicals	≥ 99.90%
Acetonitrile	VWR Chemicals	≥ 99.90%
Apura® CombiTitrant 5	Merck KGaA	≥ 99.99%
Butanol	VWR Chemicals	≥ 99.80%
Butyl acetate	VWR Chemicals	≥ 96.00%
Caffeine	Alfa Aesar	≥ 99.00%
Dibutyl oxalate	Sigma-Aldrich	≥ 99.00%
Ethanol	Merck KGaA	≥ 99.90%
Ethyl acetate	VWR Chemicals	≥ 99.80%
Hydrochloric acid	Merck KGaA	2 mol L^{-1}
Methanol (dry)	Sigma-Aldrich	≥ 99.99%
Oxalic acid	Sigma-Aldrich	≥ 98.00%
Potassium dihydrogen phosphate	Merck KGaA	≥ 99.50%
Sodium dihydrogen phosphate dihydrate	Merck KGaA	≥ 99.00%
Sodium hydroxide	Bernd Kraft	≥ 98.00%

Table A-2: Equipment used in this work

Equipment	Model	Manufacturer
Analysis scale	Talent TE214S	Sartorius
DSC	Q100	TA Instruments
Humidity Temp. Meter	PCE-313-A	PCE Instruments
Karl-Fischer-Titration	915 KF Ti-Touch	Metrohm
Magnetic plate	RCT basic	IKA Labortechnik
Magnetic plate	RH basic	IKA Labortechnik
pH-Meter	SevenGo pH	Mettler Toledo
pH-Electrode	InLab® 413 SG/2m IP67	Mettler Toledo
Powder X-ray diffraction (PXRD)	MiniFlex 600	Rigaku
Precision scale	Cubis® MSU524P-000-DU	Sartorius
Thermostat	Ecoline Staredition RE304	LAUDA
Thermostat (PXRD)	Kühlmobile 010-B400-1-4	Van der Heijden Labortechnik GmbH
UV/VIS-spectrometer	BioSpectrometer®	eppendorf

A.2.1 Calibration Curves of Oxalic Acid in Organic Solvents

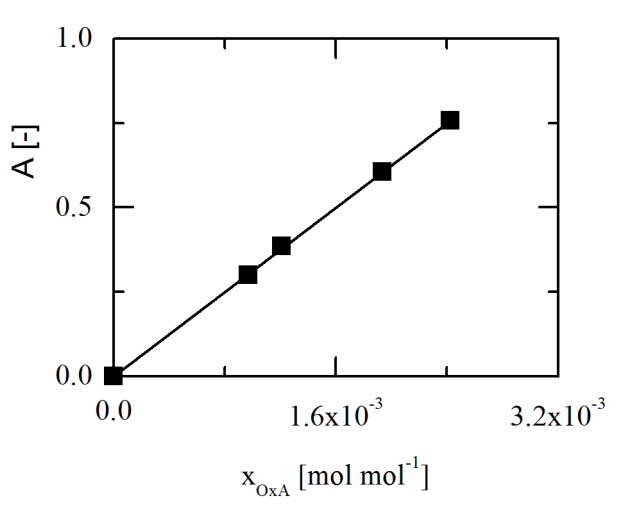

Figure A-1: Calibration curve of oxalic acid in ethyl acetate for four different mole fractions ($2.42 \cdot 10^{-3}$, $1.93 \cdot 10^{-3}$, $1.21 \cdot 10^{-3}$, $9.71 \cdot 10^{-4}$) at λ = 260 nm depending on the mole fraction of oxalic acid with a molar extinction $\varepsilon_{OxA,ethyl\ acetate}$ = 31.23 mm^{-1}

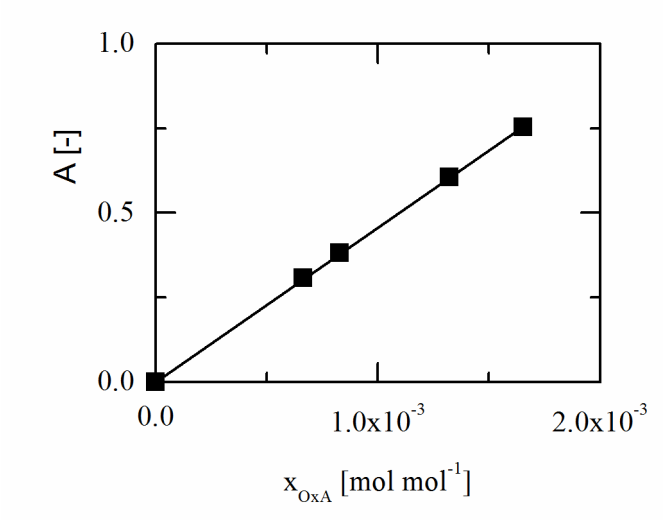

Figure A-2: Calibration curve of oxalic acid in the mixture of acetonitrile and ethyl acetate (ACN/EA) with a mass ratio of 1:1 for four different mole fractions ($1.66 \cdot 10^{-3}$, $1.32 \cdot 10^{-3}$, $8.30 \cdot 10^{-4}$, $6.64 \cdot 10^{-4}$) at λ = 260 nm depending on the mole fraction of oxalic acid with a molar extinction $\varepsilon_{OxA,ACN/EA}$ = 45.64 mm^{-1}

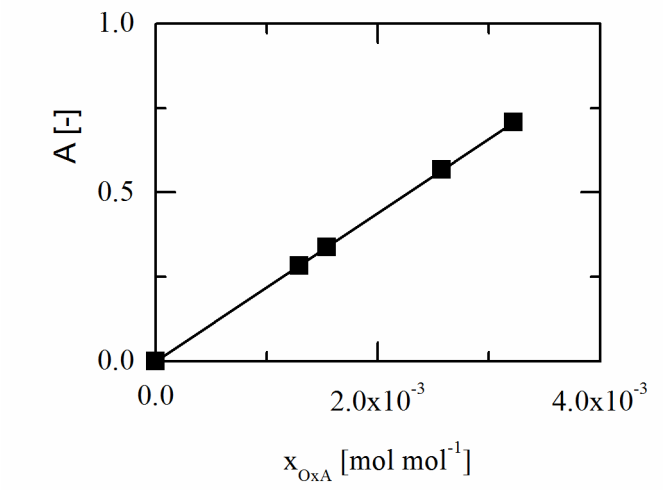

Figure A-3: Calibration curve of oxalic acid in butyl acetate for four different mole fractions ($3.22 \cdot 10^{-3}$, $2.57 \cdot 10^{-3}$, $1.54 \cdot 10^{-3}$, $1.29 \cdot 10^{-3}$) at λ = 260 nm depending on the mole fraction of oxalic acid with a molar extinction $\varepsilon_{OxA,butyl\ acetate}$ = 21.97 mm^{-1}

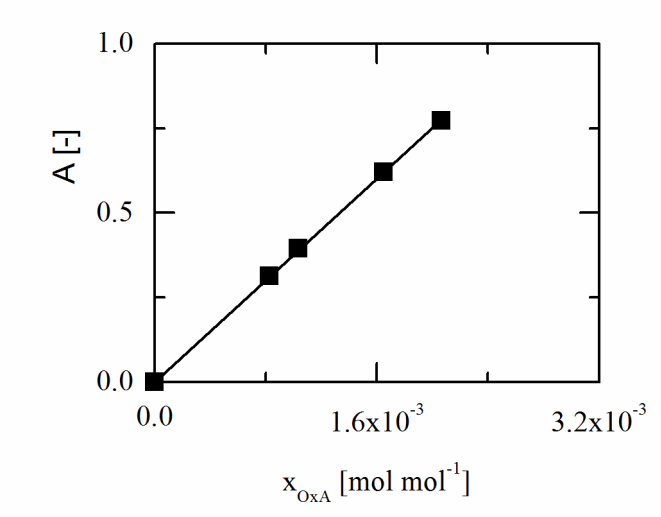

Figure A-4: Calibration curve of oxalic acid in butanol for four different mole fractions ($2.01 \cdot 10^{-3}$, $1.65 \cdot 10^{-3}$, $1.03 \cdot 10^{-3}$, $8.26 \cdot 10^{-4}$) at λ = 260 nm depending on the mole fraction of oxalic acid with a molar extinction $\varepsilon_{OxA,butanol}$ = 37.51 mm^{-1}

A.2.2 Recalibration of the Analysis Method for the Ternary System

This chapter presents the difference with and without a recalibration of the analysis method. In Table A-3 the average relative deviation (ARD) for several mass ratios is shown. It is shown that the ARD for caffeine is 3.70% and for oxalic acid it is 7.42%.

Table A-3: Analysis of the cocrystal system without the usage of a recalibration

Mass ratio [-]	**$A_{208\ Cal}$**	**$A_{273\ Cal}$**	**$ARD_{caffeine}$ [%]**	**ARD_{OxA} [%]**	**ARD_{total} [%]**
5:1	0.0000	0.0000	6.24	2.78	9.02
7:1	0.0000	0.0000	3.01	8.37	11.38
8:1	0.0000	0.0000	0.87	9.42	10.29
10:1	0.0000	0.0000	5.82	4.90	10.72
12:1	0.0000	0.0000	5.28	2.77	8.05
13:1	0.0000	0.0000	2.92	8.40	11.31
13:1	0.0000	0.0000	1.75	15.31	17.06
Overall	0.0000	0.0000	3.70	7.42	11.12

With a recalibration of the equation (3-2) these ARD values can be reduced by the application of the following equation. In this case, the absorbance at 208 nm is reduced by $A_{208\,Cal}$ to improve the analysis.

$$A_{208} \cdot (1 - A_{208\,Cal}) = \sum_{i=1}^{2} d \cdot \varepsilon_{i,solvent} \cdot x_i \qquad \textbf{(A-3)}$$

The improved results for the mass ratios of 5:1 to 15:1 are shown in Table A-4. It can be seen that the overall ARD for caffeine is reduced to 2.61% and for oxalic acid to 6.56%. Therefore, the absorbance at 208 nm is reduced by 2.86%.

Table A-4: Recalibration of the cocrystal system analysis to achieve the lowest average deviation based on the mass ratios of oxalic acid to caffeine

Mass ratio [-]	**$A_{208\,Cal}$**	**$A_{273\,Cal}$**	**$ARD_{caffeine}$ [%]**	**ARD_{OxA} [%]**	**ARD_{total} [%]**
5:1	0.0286	0.0000	4.41	6.10	10.51
7:1	0.0286	0.0000	0.10	4.20	4.30
8:1	0.0286	0.0000	2.08	9.45	11.53
10:1	0.0286	0.0000	3.67	1.97	5.65
12:1	0.0286	0.0000	2.19	2.81	5.00
13:1	0.0286	0.0000	1.51	6.11	7.63
13:1	0.0286	0.0000	4.33	15.30	19.63
Overall	0.0286	0.0000	2.61	6.56	9.18

A.2.3 Hydration of Oxalic Acid in Climate Chamber

In this chapter, the hydration process of oxalic acid is presented. Therefore, oxalic acid is placed in a climate chamber with 25 °C and a relative humidity of 60%. The relative humidity is achieved by a sodium bromide solution. At the temperature of 25 °C an equilibrium between the sodium bromide solution and the air is reached. The equilibrium point has a relative humidity of 60% with small fluctuations. During the opening process of the climate chamber, the relative humidity is reduced to 55.0% relative humidity which was measured with *PCE 313-A* from *PCE Instruments*. After 10 minutes, the relative humidity has increased to 60%. The analysis as described in chapter 3.3.2.1 was performed every hour and therefore it can be assumed that the relative humidity remains constant over the exposure time.

In Figure A-5 the DSC analysis for a few samples are presented. It is shown that the amount of water is increased over time. After 8.2 hours the analysis curve becomes broader and after 24.0 hours the peak of oxalic acid dihydrate is bigger in comparison to the peak of the dihydrate measured after 3 days. A reason can be the formation of oxalic acid dihydrate. In this case, the sample after 3 days (black dashed line) is analyzed after oversaturation of a solution of water with oxalic acid and drying of the particles at room temperature.

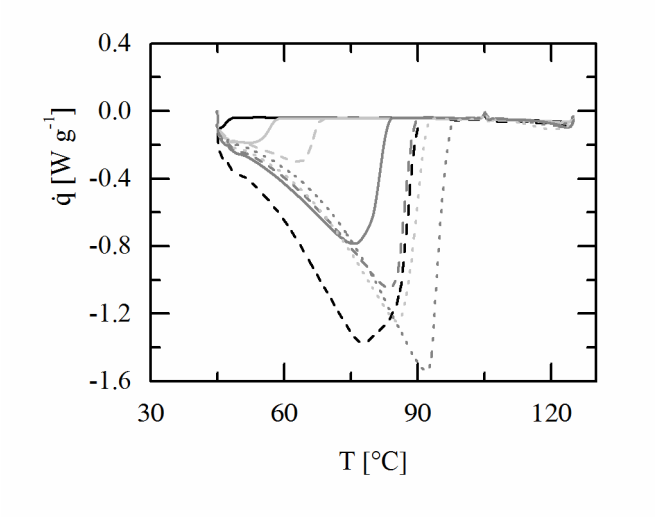

Figure A-5: a) Mass specified heat flow $\dot{q}$ of oxalic acid (black solid line), oxalic acid after 0.5 h (light grey solid line), oxalic acid after 1.5 h (light grey dashed line), oxalic acid after 3.0 h (grey solid line), oxalic acid after 6.5 h (grey dashed line), oxalic acid after 8.2 h (light grey dotted line), oxalic acid after 24.1 h (grey dotted line) and oxalic acid dihydrate after 3 days (black dashed line) of exposition in a climate chamber at 25 °C and 60% relative humidity depending on the temperature T.

The mass fraction of water in the oxalic acid samples is presented in Figure A-6. The diagram shows that the formation of oxalic acid dihydrate is fast and after 3 hours the mass fraction of water is at 17.8 wt.%. By further exposure of oxalic acid particles, the theoretical water content of oxalic acid dihydrate is reached. This is illustrated by the grey solid line in this diagram. Furthermore, the water content can be increased above the theoretical value to 40.8 wt.%. In this case, additional water molecules are bound in the crystal structure of oxalic acid dihydrate via intermolecular forces. This high water content can also be confirmed by *Ma et al.* [41] who has performed studies on oxalic acid water content for various relative humidity values. The experimental values measured within this work are presented in Table A-5. These measurements show that a sole analysis of oxalic acid particles is a challenging task.

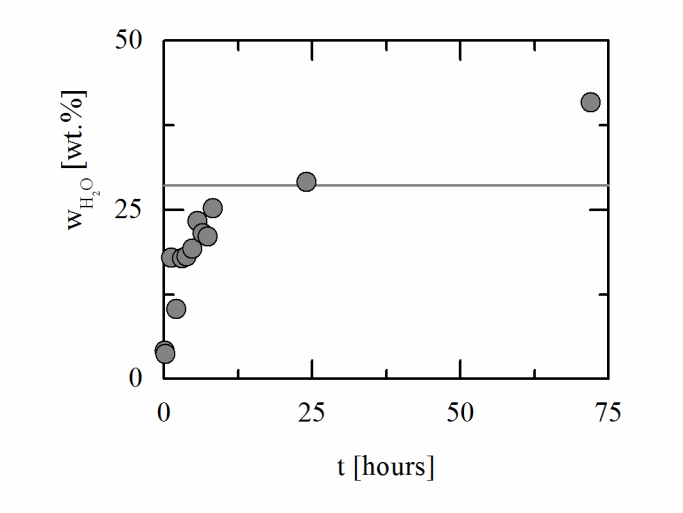

Figure A-6: Mass fraction of water in oxalic acid samples over the exposure time in the climate chamber with 25 °C and 60% relative humidity with the theoretical mass fraction of 28.58% of oxalic acid dihydrate (grey solid line)

Table A-5: Experimental data of the mass fraction of water in oxalic acid samples over the exposure time in the climate chamber at 25 °C and 60% relative humidity

t [hours]	w_{H2O} [wt.%]	t [hours]	w_{H2O} [wt.%]
0.08	4.20	5.60	23.27
0.28	3.67	6.50	21.54
1.18	17.95	7.35	21.08
2.08	10.28	8.22	25.23
3.03	17.86	24.08	29.08
3.83	18.12	72.00	40.83
4.77	19.23		

A.3 Results

A.3.1 Temperature-Dependent Solubility of Oxalic Acid and Caffeine

A.3.1.1 Water Content of Oxalic Acid in Organic Solvents

Table A-6: Water content of unsaturated mixtures of oxalic acid in ethanol, isopropanol, butanol and ethyl acetate over time in days at 298.15 K and ambient pressure with the standard deviation in brackets

t [days]	Solvent			
	Ethanol w_{H_2O} [wt.%]	Isopropanol w_{H_2O} [wt.%]	Butanol w_{H_2O} [wt.%]	Ethyl acetate w_{H_2O} [wt.%]
Without oxalic acid	0.1060 (0.0110)	0.0317 (0.0026)	0.0256 (0.0046)	0.0006 (0.0051)
0	0.0808 (0.0017)	0.2095 (0.0620)	0.0000 (0.0315)	0.0000 (0.0148)
1	1.1084 (0.4439)	0.3009 (0.0136)		0.0000 (0.0184)
2	2.0460 (0.0491)	0.4410 (0.0423)	1.4313 (0.1561)	
5	3.0850 (0.1335)	1.0153 (0.0277)	1.8170 (0.0697)	0.0000 (0.0178)
7	3.4510 (0.0759)	1.2028 (0.0597)	1.9342 (0.1470)	0.0000 (0.0345)
9	3.1040 (0.0138)	1.0807 (0.0849)	2.4145 (0.1176)	0.0000 (0.0058)
12	3.4285 (0.2997)	1.5212 (0.0560)	2.2235 (0.0615)	0.0000 (0.0209)
14	3.4405 (0.0622)	1.6630 (0.0118)	2.2672 (0.0807)	0.0000 (0.0215)

Table A-7: Water content of saturated mixtures of oxalic acid in alcohol at 318.15 K over time in days at ambient pressure with the standard deviation in brackets

t [days]	T [K]	Solvent		
		Isopropanol w_{H_2O} [wt.%]	Butanol w_{H_2O} [wt.%]	Ethyl acetate w_{H_2O} [wt.%]
1	318.15	6.5763 (0.5723)		
2	318.15			0.0000 (0.0116)
3	318.15		3.7972 (0.2354)	
4	318.15	7.4137 (0.5556)		
4	318.15	7.4137 (0.5556)		

Table A-8: Water content of oxalic acid in the organic solvents acetonitrile, ethyl acetate, butyl acetate and the mixture of acetonitrile and ethyl acetate (ACN/EA) with a mass ratio of 1:1 over time in days at 298.15 K and ambient pressure with the standard deviation in brackets

	Solvent			
***t* [days]**	**Acetonitrile** w_{H_2O} **[wt.%]**	**Ethyl acetate** w_{H_2O} **[wt.%]**	**Butyl acetate** w_{H_2O} **[wt.%]**	**ACN/EA (1:1)** w_{H_2O} **[wt.%]**
1	0.1163 (0.0687)			
2	0.2553 (0.0000)	0.0000 (0.0123)	0.0000 (0.0167)	
3	0.3305 (0.0194)			
4				
5		0.0000 (0.0116)		0.0000 (0.0039)
6			0.0358 (0.0043)	
7	0.1747 (0.0211)	0.0000 (0.0098)		0.0000 (0.0112)
8			0.0000 (0.0371)	
9	0.0985 (0.0120)	0.0000 (0.0255)		
10			0.0000 (0.0232)	0.1121 (0.0333)
11	0.0384 (0.0230)			
12		0.0391 (0.0455)		0.1161 (0.0346)
13			0.0288 (0.0107)	
14	0.0413 (0.0109)	0.0000 (0.0148)		0.0553 (0.0173)
15				
16		0.0144 (0.0216)		
17				0.0590 (0.0228)

A.3.1.2 Mass Balance for Dibutyl Oxalate Determination

This chapter focuses on the setup of a mass balance to determine dibutyl oxalate. Therefore, a calibration curve of oxalic acid in butanol is used (Appendix A.2.1). Afterwards, a defined dibutyl oxalate amount in butanol was analyzed. The results of this analysis are presented in Table A-9. It is shown that dibutyl oxalate has a higher absorbance in comparison to oxalic acid in butanol. The average relative deviation (ARD) between the weighted mass and the calculation via the UV/VIS spectroscopy is 30%. By an analysis of mixtures of oxalic acid and dibutyl oxalate in butanol with a mass ratio of 1:1, the ARD is 10% higher than the weighted values which is based on oxalic acid and the "oxalate part" of dibutyl oxalate. By an application of the water content of the saturated solution of oxalic acid in butanol (3.8 wt.%), one can estimate the amount of produced ester. This calculation is based on the water content of the mixture, the measured absorbance of the sample at 318.15 K and the 10% higher absorbance of the mixture. Therefore, the following equations are used:

$$w_{UV/VIS} = w_{OxA} + w_{oxalate} + 0.1 \cdot (w_{OxA} + w_{oxalate}) \quad \textbf{(A-4)}$$

$$w_{oxalate} = w_{dibutyl\ oxalate} \cdot \frac{M_{OxA}}{M_{dibutyl\ oxalate}} = w_{dibutyl\ oxalate} \cdot 0.4452 \quad \textbf{(A-5)}$$

$$n_{H_2O} = n_{dibutyl\ oxalate} \cdot 2 \quad \textbf{(A-6)}$$

Based on the assumption that the complete water content arose from esterification, the mass balance of the equation system can be solved. Therefore, the mass of oxalic acid, dibutyl oxalate and butanol are varied to fit the conditions of the water content and the measured UV/VIS weight fraction. The results of the liquid phase are also presented in Table A-9. Hence, butanol and the other alcohols are not suited for temperature-solubility experiments with oxalic acid.

Table A-9: Average relative deviation of oxalic acid and dibutyl oxalate and the mixture of both with a mass ratio of 1:1 in butanol based on the calibration curve of anhydrous oxalic acid in butanol. Furthermore, the calculated composition of the liquid phase is presented.

	ARD [%]		w_i [wt.%]
Oxalic acid in butanol	< 1.0	Oxalic acid	32.97
Dibutyl oxalate in butanol	≈ 30.0	Dibutyl oxalate	21.33
Mixture of oxalic acid and dibutyl oxalate in butanol	≈ 10.0	Butanol	41.90
		Water	3.80

A.3.1.3 DSC Analysis of Oxalic Acid and Organic Solvents

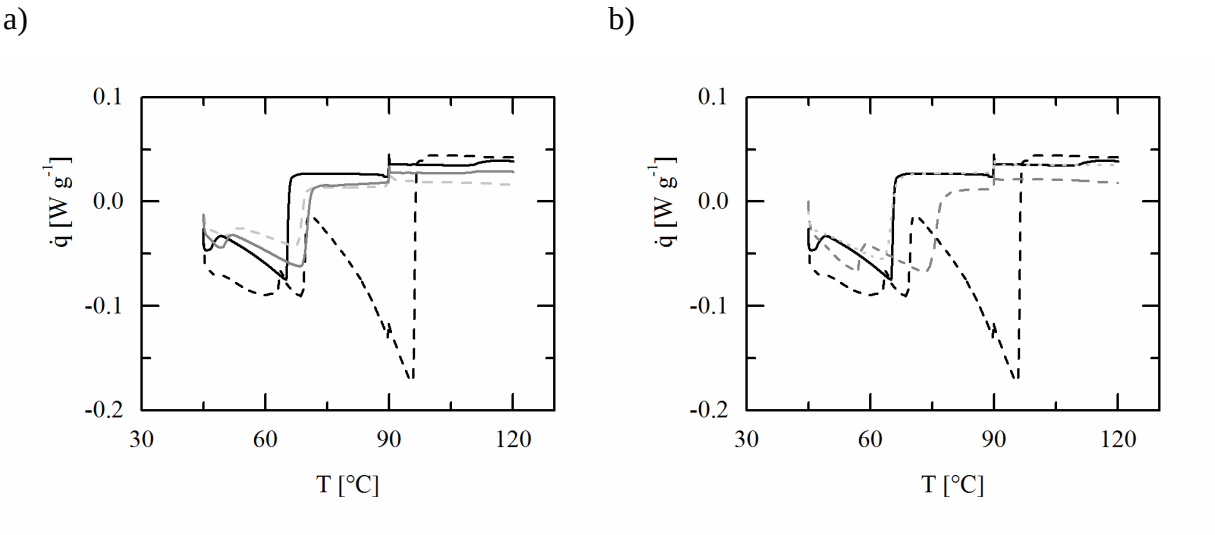

Figure A-7: Mass specified heat flow $\dot{q}$ of the references oxalic acid in ethyl acetate (black solid line) and oxalic acid dihydrate in ethyl acetate (black dashed line) depending on the temperature T. a) DSC analysis of a suspension of oxalic acid and ethyl acetate at 25 °C (light grey dashed line), 30 °C (grey solid line). b) DSC analysis of a suspension of oxalic acid and ethyl acetate at 37 °C (grey dashed line) and 45 °C (light grey dotted line)

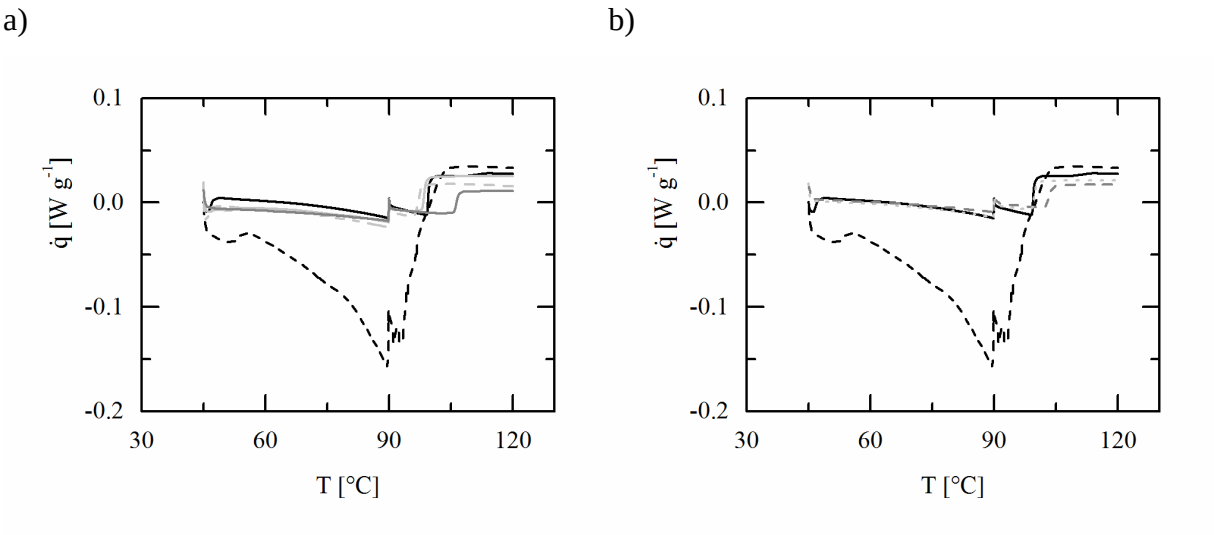

Figure A-8: Mass specified heat flow $\dot{q}$ of the references oxalic acid in butyl acetate (black solid line) and oxalic acid dihydrate in butyl acetate (black dashed line) depending on the temperature T. a) DSC analysis of a suspension of oxalic acid and butyl acetate at 20 °C (light grey solid line), 25 °C (light grey dashed line), 30 °C (grey solid line). b) DSC analysis of a suspension of oxalic acid and butyl acetate at 37 °C (grey dashed line) and 45 °C (light grey dotted line)

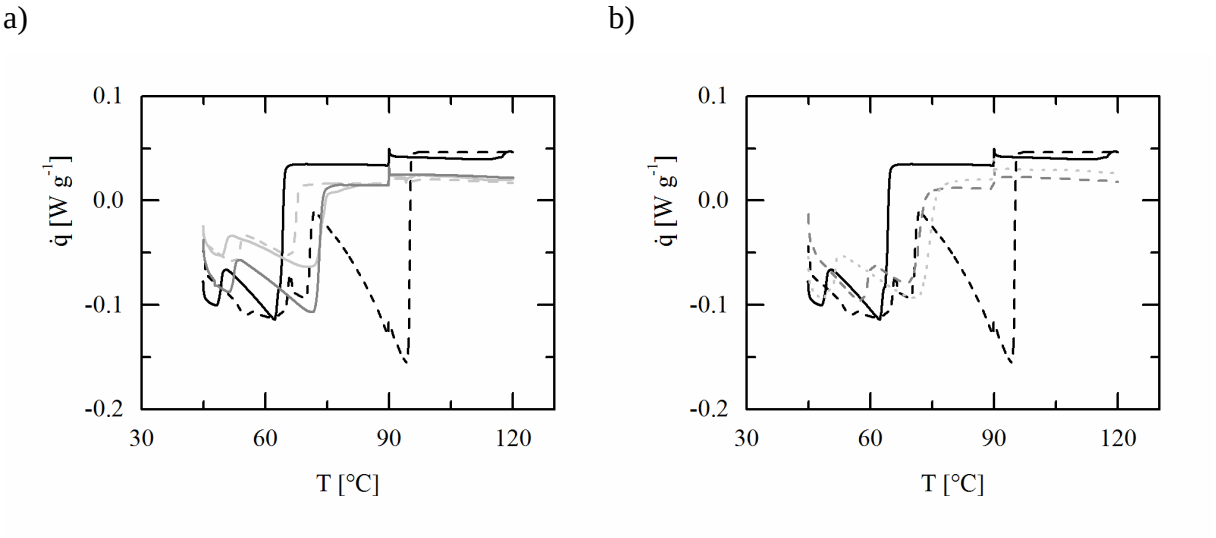

Figure A-9: Mass specified heat flow $\dot{q}$ of the references oxalic acid in the mixture of acetonitrile and ethyl acetate with a mass ratio of 1:1 (ACN/EA) (black solid line) and oxalic acid dihydrate in ACN/EA (black dashed line) depending on the temperature T. a) DSC analysis of a suspension of oxalic acid and ACN/EA at 20 °C (light grey solid line), 25 °C (light grey dashed line), 30 °C (grey solid line). b) DSC analysis of a suspension of oxalic acid and ACN/EA at 37 °C (grey dashed line) and 45 °C (light grey dotted line)

A.3.1.4 Experimental Solubility Data of Oxalic Acid in Organic Solvents

Table A-10: Temperature-dependent solubility of oxalic acid in the organic solvents acetonitrile, ethyl acetate, butyl acetate and the mixture of acetonitrile and ethyl acetate (ACN/EA) with a mass ratio of 1:1 at ambient pressure with the standard deviation in brackets

	Solvent			
***T* [K]**	**Acetonitrile**	**Ethyl acetate**	**Butyl acetate**	**ACN/EA (1:1)**
	$x^L_{oxalic\ acid}$	$x^L_{oxalic\ acid}$	$x^L_{oxalic\ acid}$	$x^L_{oxalic\ acid}$
293.15	$5.81 \cdot 10^{-2}$	$9.81 \cdot 10^{-2}$	$6.43 \cdot 10^{-2}$	$8.23 \cdot 10^{-2}$
(0.50)	$(7.05 \cdot 10^{-4})$	$(7.24 \cdot 10^{-4})$	$(4.68 \cdot 10^{-4})$	$(6.68 \cdot 10^{-4})$
298.15	$6.47 \cdot 10^{-2}$	$9.81 \cdot 10^{-2}$	$6.97 \cdot 10^{-2}$	$8.40 \cdot 10^{-2}$
(0.50)	$(9.94 \cdot 10^{-4})$	$(1.14 \cdot 10^{-3})$	$(5.88 \cdot 10^{-4})$	$(6.94 \cdot 10^{-4})$
303.15	$7.11 \cdot 10^{-2}$	$1.08 \cdot 10^{-1}$	$7.31 \cdot 10^{-2}$	$9.22 \cdot 10^{-2}$
(0.50)	$(3.63 \cdot 10^{-3})$	$(2.90 \cdot 10^{-3})$	$(2.27 \cdot 10^{-3})$	$(1.56 \cdot 10^{-3})$
310.15	$7.92 \cdot 10^{-2}$	$1.19 \cdot 10^{-1}$	$8.34 \cdot 10^{-2}$	$1.02 \cdot 10^{-1}$
(0.50)	$(4.81 \cdot 10^{-3})$	$(5.70 \cdot 10^{-4})$	$(2.32 \cdot 10^{-3})$	$(4.65 \cdot 10^{-4})$
318.15	$9.18 \cdot 10^{-2}$	$1.40 \cdot 10^{-1}$	$8.91 \cdot 10^{-2}$	$1.18 \cdot 10^{-1}$
(0.50)	$(2.16 \cdot 10^{-3})$	$(1.52 \cdot 10^{-3})$	$(6.06 \cdot 10^{-4})$	$(1.24 \cdot 10^{-3})$

A.3.1.5 Experimental Densities of Oxalic Acid in Water

Table A-11: Density of oxalic acid and water mixtures at five temperatures and ambient pressure [26]

T [K]	283.15	293.15	303.15	313.15	323.15
$x^L_{oxalic\ acid}$	**ρ [kg m^{-3}]**	**ρ [kg m^{-3}]**	**ρ [kg m^{-3}]**	**ρ [kg m^{-3}]**	**ρ [kg m^{-3}]**
0.00	999.70	998.20	995.64	992.21	988.03
$2.00 \cdot 10^{-3}$	1004.54	1002.96	1000.30	996.67	991.26
$3.99 \cdot 10^{-3}$	1009.10	1007.38	1004.60	1000.72	996.27
$7.95 \cdot 10^{-3}$	1018.21	1016.19	1013.15	1009.19	1003.48
$1.58 \cdot 10^{-2}$	1036.34	1033.78	1030.28	1025.95	1019.69

A.3.1.6 Experimental Data for Binary Phase Diagrams

Table A-12: Temperature-dependent solubility of oxalic acid dihydrate in water at ambient pressure

***T* [K]**	**Water $x^L_{oxalic\ acid}$**	**Ref for exp data**	***T* [K]**	**Water $x^L_{oxalic\ acid}$**	**Ref for exp data**
293.15	$1.75 \cdot 10^{-2}$	[26]	278.15	$9.24 \cdot 10^{-3}$	[27]
298.15	$2.20 \cdot 10^{-2}$	[26]	283.15	$1.24 \cdot 10^{-2}$	[27]
303.15	$2.49 \cdot 10^{-2}$	[26]	288.15	$1.48 \cdot 10^{-2}$	[27]
308.15	$3.18 \cdot 10^{-2}$	[26]	293.15	$1.86 \cdot 10^{-2}$	[27]
313.15	$3.66 \cdot 10^{-2}$	[26]	298.15	$2.30 \cdot 10^{-2}$	[27]
			303.15	$2.69 \cdot 10^{-2}$	[27]
373.15	1	[38]	308.15	$3.42 \cdot 10^{-2}$	[27]
373.15	1	this work	313.15	$4.13 \cdot 10^{-2}$	[27]
393.20	1	[39]	318.15	$4.93 \cdot 10^{-2}$	[27]
462.65	1	[25]	323.15	$5.89 \cdot 10^{-2}$	[27]
			328.15	$6.96 \cdot 10^{-2}$	[27]
			333.15	$7.81 \cdot 10^{-2}$	[27]
			338.15	$9.83 \cdot 10^{-2}$	[27]

Table A-13: Temperature-dependent solubility of caffeine hydrate (1:0.8) and anhydrous caffeine in water at ambient pressure

T [K]	Water $x^L_{caffeine}$	Ref for exp data	T [K]	Water $x^L_{caffeine}$	Ref for exp data
293.15	$1.42 \cdot 10^{-3}$	[26]	343.82	0.03	[28]
298.15	$1.80 \cdot 10^{-3}$	[26]	347.93	0.06	[28]
303.15	$2.15 \cdot 10^{-3}$	[26]	366.02	0.08	[28]
308.15	$3.10 \cdot 10^{-3}$	[26]	371.78	0.09	[28]
313.15	$3.90 \cdot 10^{-3}$	[26]	373.42	0.10	[28]
343.82	$2.70 \cdot 10^{-2}$	[26]	380.00	0.13	[28]
347.93	$6.02 \cdot 10^{-2}$	[26]	390.69	0.17	[28]
			397.27	0.21	[28]
273.15	0.00	[28]	424.41	0.36	[28]
353.15	1.00	[28]	444.97	0.45	[28]
414.15	1.00	[24]	446.61	0.49	[28]
509.15	1.00	[24]	451.55	0.50	[28]
			453.19	0.52	[28]
			458.13	0.53	[28]
			458.13	0.55	[28]
			457.31	0.55	[28]
			462.24	0.57	[28]
			458.95	0.58	[28]
			480.33	0.69	[28]
			484.44	0.73	[28]
			495.13	0.79	[28]

A.3.2 pH-Dependent Solubility of Oxalic Acid and Caffeine in Water

Table A-14: Experimental pH-dependent solubility data of oxalic acid in water at 298.15 K and ambient pressure with the standard deviation in brackets (*measured in this work)

pH_{exp}	$x^{L}_{oxalic\ acid}$	Solid phase	Ref.
0.68	$1.84 \cdot 10^{-2}$ (-)	oxalic acid dihydrate	[29]
0.72	$2.36 \cdot 10^{-2}$ (-)	oxalic acid dihydrate	[29]
0.84	$1.71 \cdot 10^{-2}$ ($5.07 \cdot 10^{-4}$)	oxalic acid dihydrate	[29]
0.94	$1.38 \cdot 10^{-2}$ ($7.18 \cdot 10^{-4}$)	oxalic acid dihydrate	[29]
1.06	$8.02 \cdot 10^{-3}$ ($3.50 \cdot 10^{-3}$)	sodium hydrogen oxalate monohydrate	[29]
1.07	$8.41 \cdot 10^{-3}$ ($1.05 \cdot 10^{-4}$)	sodium hydrogen oxalate monohydrate	*
1.26	$6.50 \cdot 10^{-3}$ ($1.58 \cdot 10^{-3}$)	sodium hydrogen oxalate monohydrate	[29]
1.41	$4.82 \cdot 10^{-3}$ ($1.56 \cdot 10^{-3}$)	sodium hydrogen oxalate monohydrate	[29]
1.70	$4.71 \cdot 10^{-3}$ ($3.42 \cdot 10^{-4}$)	sodium hydrogen oxalate monohydrate	[29]
1.89	$3.99 \cdot 10^{-3}$ ($3.74 \cdot 10^{-4}$)	sodium hydrogen oxalate monohydrate	[29]
2.09	$3.71 \cdot 10^{-3}$ ($2.35 \cdot 10^{-4}$)	sodium hydrogen oxalate monohydrate	*
4.08	$5.65 \cdot 10^{-3}$ ($2.22 \cdot 10^{-4}$)	sodium hydrogen oxalate monohydrate	[29]
3.28	$3.29 \cdot 10^{-3}$ ($4.29 \cdot 10^{-4}$)	sodium hydrogen oxalate monohydrate	[29]
4.08	$5.65 \cdot 10^{-3}$ ($2.22 \cdot 10^{-4}$)	sodium hydrogen oxalate monohydrate	*
4.13	$4.40 \cdot 10^{-3}$ ($1.98 \cdot 10^{-3}$)	sodium hydrogen oxalate monohydrate	[29]
5.00	$4.85 \cdot 10^{-3}$ ($6.53 \cdot 10^{-5}$)	disodium oxalate	*
5.67	$4.89 \cdot 10^{-3}$ ($3.27 \cdot 10^{-4}$)	disodium oxalate	*
7.10	$4.86 \cdot 10^{-3}$ ($9.01 \cdot 10^{-5}$)	disodium oxalate	*
7.15	$4.98 \cdot 10^{-3}$ ($2.70 \cdot 10^{-4}$)	disodium oxalate	*
7.62	$4.89 \cdot 10^{-3}$ ($2.32 \cdot 10^{-4}$)	disodium oxalate	*
9.85	$4.93 \cdot 10^{-3}$ ($2.84 \cdot 10^{-4}$)	disodium oxalate	*

Table A-15: Experimental pH-dependent solubility data of caffeine in water at 298.15 K and ambient pressure with the standard deviation in brackets (*measured in this work)

pH_{exp}	$x^{L}_{caffeine}$	Solid phase	Ref.
1.00	$2.41 \cdot 10^{-3}$ ($1.44 \cdot 10^{-5}$)	caffeine hydrate (1:0.8)	*
2.20	$1.67 \cdot 10^{-3}$ ($8.91 \cdot 10^{-6}$)	caffeine hydrate (1:0.8)	[29]
3.20	$1.76 \cdot 10^{-3}$ ($8.70 \cdot 10^{-5}$)	caffeine hydrate (1:0.8)	[29]
3.40	$1.71 \cdot 10^{-3}$ ($3.20 \cdot 10^{-5}$)	caffeine hydrate (1:0.8)	[29]
4.00	$1.70 \cdot 10^{-3}$ ($2.78 \cdot 10^{-2}$)	caffeine hydrate (1:0.8)	[29]
4.50	$1.81 \cdot 10^{-3}$ ($1.32 \cdot 10^{-4}$)	caffeine hydrate (1:0.8)	[29]
4.75	$1.67 \cdot 10^{-3}$ ($2.84 \cdot 10^{-10}$)	caffeine hydrate (1:0.8)	[29]
5.54	$1.69 \cdot 10^{-3}$ ($1.31 \cdot 10^{-5}$)	caffeine hydrate (1:0.8)	[29]
6.20	$1.67 \cdot 10^{-3}$ ($6.60 \cdot 10^{-6}$)	caffeine hydrate (1:0.8)	[29]
6.75	$1.64 \cdot 10^{-3}$ ($2.97 \cdot 10^{-5}$)	caffeine hydrate (1:0.8)	[29]
6.90	$1.66 \cdot 10^{-3}$ ($1.02 \cdot 10^{-5}$)	caffeine hydrate (1:0.8)	[29]
7.00	$1.75 \cdot 10^{-3}$ ($7.12 \cdot 10^{-5}$)	caffeine hydrate (1:0.8)	[29]
7.30	$1.70 \cdot 10^{-3}$ ($2.47 \cdot 10^{-5}$)	caffeine hydrate (1:0.8)	[29]
9.50	$1.75 \cdot 10^{-3}$ ($6.92 \cdot 10^{-5}$)	caffeine hydrate (1:0.8)	[29]
9.80	$1.68 \cdot 10^{-3}$ ($1.40 \cdot 10^{-5}$)	caffeine hydrate (1:0.8)	[29]
10.30	$1.69 \cdot 10^{-3}$ ($5.02 \cdot 10^{-5}$)	caffeine hydrate (1:0.8)	[29]
10.35	$1.75 \cdot 10^{-3}$ ($5.94 \cdot 10^{-6}$)	caffeine hydrate (1:0.8)	[29]
10.55	$1.70 \cdot 10^{-3}$ ($8.97 \cdot 10^{-5}$)	caffeine hydrate (1:0.8)	[29]
11.30	$2.40 \cdot 10^{-3}$ ($6.18 \cdot 10^{-10}$)	caffeine hydrate (1:0.8)	[29]
12.07	$3.18 \cdot 10^{-3}$ ($7.89 \cdot 10^{-5}$)	caffeine hydrate (1:0.8)	*

A.3.3 pH-Dependent Solubility of the Cocrystal of Oxalic Acid and Caffeine

Table A-16: Experimental pH-dependent solubility data of oxalic acid, caffeine and water at 298.15 K and ambient pressure (part 1) with standard deviation in brackets. CC correspond to cocrystal formation

pH_{exp}	$x^{L}_{oxalic\ acid}$	$x^{L}_{caffeine}$	Solid phase
1.02	$8.30 \cdot 10^{-3}$ ($1.92 \cdot 10^{-4}$)	$2.94 \cdot 10^{-4}$ ($1.43 \cdot 10^{-5}$)	cocrystal
0.98	$8.23 \cdot 10^{-3}$ ($3.84 \cdot 10^{-4}$)	$2.99 \cdot 10^{-4}$ ($3.21 \cdot 10^{-6}$)	cocrystal
1.06	$6.44 \cdot 10^{-3}$ ($1.18 \cdot 10^{-4}$)	$3.01 \cdot 10^{-4}$ ($2.77 \cdot 10^{-6}$)	cocrystal
1.07	$5.96 \cdot 10^{-3}$ ($9.89 \cdot 10^{-5}$)	$3.09 \cdot 10^{-4}$ ($1.59 \cdot 10^{-6}$)	cocrystal
1.07	$2.38 \cdot 10^{-3}$ ($1.77 \cdot 10^{-4}$)	$4.42 \cdot 10^{-4}$ ($2.89 \cdot 10^{-6}$)	cocrystal
1.06	$6.05 \cdot 10^{-4}$ ($2.93 \cdot 10^{-4}$)	$8.89 \cdot 10^{-4}$ ($4.61 \cdot 10^{-5}$)	cocrystal
2.01	$3.63 \cdot 10^{-3}$ ($1.96 \cdot 10^{-4}$)	$5.03 \cdot 10^{-4}$ ($4.71 \cdot 10^{-6}$)	sodium hydrogen oxalate monohydrate
1.97	$3.55 \cdot 10^{-3}$ ($1.46 \cdot 10^{-4}$)	$5.43 \cdot 10^{-4}$ ($3.15 \cdot 10^{-6}$)	sodium hydrogen oxalate monohydrate
2.10	$3.53 \cdot 10^{-3}$ ($1.79 \cdot 10^{-4}$)	$5.32 \cdot 10^{-4}$ ($9.82 \cdot 10^{-6}$)	sodium hydrogen oxalate monohydrate
2.01	$3.46 \cdot 10^{-3}$ ($1.69 \cdot 10^{-4}$)	$7.44 \cdot 10^{-4}$ ($2.80 \cdot 10^{-6}$)	sodium hydrogen oxalate monohydrate
1.94	$3.41 \cdot 10^{-3}$ ($1.99 \cdot 10^{-4}$)	$3.04 \cdot 10^{-4}$ ($2.33 \cdot 10^{-6}$)	sodium hydrogen oxalate monohydrate
2.00	$3.33 \cdot 10^{-3}$ ($1.92 \cdot 10^{-4}$)	$7.80 \cdot 10^{-4}$ ($2.54 \cdot 10^{-6}$)	sodium hydrogen oxalate monohydrate + CC
1.98	$2.81 \cdot 10^{-3}$ ($3.75 \cdot 10^{-4}$)	$9.57 \cdot 10^{-4}$ ($2.44 \cdot 10^{-6}$)	cocrystal
2.01	$2.29 \cdot 10^{-3}$ ($1.60 \cdot 10^{-4}$)	$1.08 \cdot 10^{-3}$ ($3.36 \cdot 10^{-5}$)	cocrystal
1.96	$1.83 \cdot 10^{-3}$ ($2.40 \cdot 10^{-4}$)	$1.16 \cdot 10^{-3}$ ($3.63 \cdot 10^{-6}$)	cocrystal
1.98	$1.33 \cdot 10^{-3}$ ($1.17 \cdot 10^{-4}$)	$1.38 \cdot 10^{-3}$ ($5.28 \cdot 10^{-6}$)	cocrystal
2.06	$1.07 \cdot 10^{-3}$ ($1.25 \cdot 10^{-4}$)	$1.72 \cdot 10^{-3}$ ($3.63 \cdot 10^{-6}$)	cocrystal

Table A-17: Experimental pH-dependent solubility data of oxalic acid, caffeine and water at 298.15 K and ambient pressure (part 2) with standard deviation in brackets

pH_{exp}	$x^{L}_{oxalic\ acid}$	$x^{L}_{caffeine}$	Solid phase
3.99	$4.43 \cdot 10^{-3}$ ($1.12 \cdot 10^{-4}$)	$5.94 \cdot 10^{-4}$ ($2.91 \cdot 10^{-6}$)	sodium hydrogen oxalate monohydrate
3.99	$4.57 \cdot 10^{-3}$ ($1.33 \cdot 10^{-4}$)	$9.93 \cdot 10^{-4}$ ($1.17 \cdot 10^{-6}$)	sodium hydrogen oxalate monohydrate
4.02	$1.70 \cdot 10^{-3}$ ($3.23 \cdot 10^{-4}$)	$1.73 \cdot 10^{-3}$ ($2.33 \cdot 10^{-6}$)	caffeine hydrate (1:0.8)
3.99	$1.04 \cdot 10^{-3}$ ($2.40 \cdot 10^{-4}$)	$1.82 \cdot 10^{-3}$ ($2.14 \cdot 10^{-6}$)	caffeine hydrate (1:0.8)
5.02	$4.45 \cdot 10^{-3}$ ($2.37 \cdot 10^{-4}$)	$1.02 \cdot 10^{-3}$ ($2.31 \cdot 10^{-6}$)	disodium oxalate
5.00	$4.10 \cdot 10^{-3}$ ($1.82 \cdot 10^{-4}$)	$1.11 \cdot 10^{-3}$ ($3.30 \cdot 10^{-6}$)	disodium oxalate
5.01	$2.08 \cdot 10^{-3}$ ($1.42 \cdot 10^{-4}$)	$1.61 \cdot 10^{-3}$ ($3.99 \cdot 10^{-6}$)	caffeine hydrate (1:0.8)
5.00	$3.52 \cdot 10^{-3}$ ($2.10 \cdot 10^{-4}$)	$1.73 \cdot 10^{-3}$ ($4.27 \cdot 10^{-6}$)	caffeine hydrate (1:0.8)
6.86	$4.22 \cdot 10^{-3}$ ($3.11 \cdot 10^{-4}$)	$4.45 \cdot 10^{-4}$ ($7.95 \cdot 10^{-6}$)	disodium oxalate
7.02	$4.62 \cdot 10^{-3}$ ($1.66 \cdot 10^{-4}$)	$5.99 \cdot 10^{-4}$ ($2.88 \cdot 10^{-6}$)	disodium oxalate
7.00	$4.64 \cdot 10^{-3}$ ($2.49 \cdot 10^{-4}$)	$1.15 \cdot 10^{-3}$ ($6.03 \cdot 10^{-6}$)	disodium oxalate
7.11	$4.63 \cdot 10^{-3}$ ($1.23 \cdot 10^{-4}$)	$1.31 \cdot 10^{-3}$ ($9.36 \cdot 10^{-6}$)	caffeine hydrate (1:0.8)
6.94	$2.56 \cdot 10^{-3}$ ($4.03 \cdot 10^{-4}$)	$1.47 \cdot 10^{-3}$ ($2.70 \cdot 10^{-6}$)	caffeine hydrate (1:0.8)
7.02	$1.76 \cdot 10^{-3}$ ($2.73 \cdot 10^{-4}$)	$1.70 \cdot 10^{-3}$ ($8.07 \cdot 10^{-6}$)	caffeine hydrate (1:0.8)
7.14	$1.95 \cdot 10^{-3}$ ($2.49 \cdot 10^{-4}$)	$1.61 \cdot 10^{-3}$ ($5.45 \cdot 10^{-6}$)	caffeine hydrate (1:0.8)
7.03	$2.62 \cdot 10^{-3}$ ($3.51 \cdot 10^{-4}$)	$1.68 \cdot 10^{-3}$ ($7.90 \cdot 10^{-6}$)	caffeine hydrate (1:0.8)

A.3.4 PXRD Analysis of Solid Phases

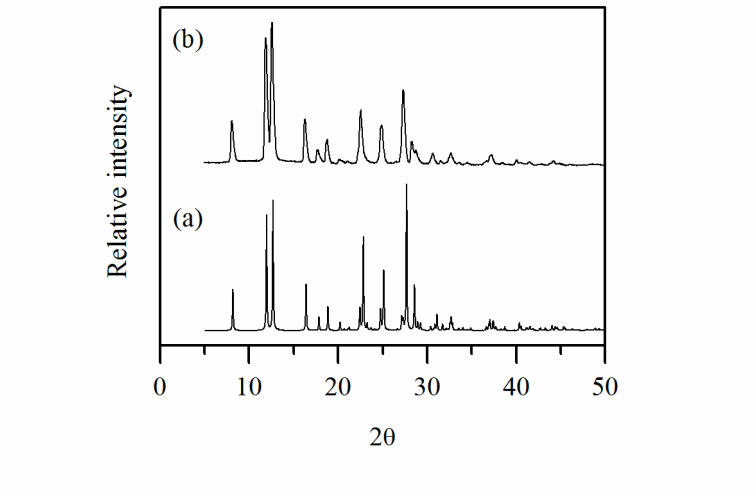

Figure A-10: a) Reference spectrum of caffeine and oxalic acid (2:1) cocrystal by CSD [54] and b) sample spectrum of caffeine and oxalic acid (2:1) cocrystal measured at T = 298.15 K and pH 1

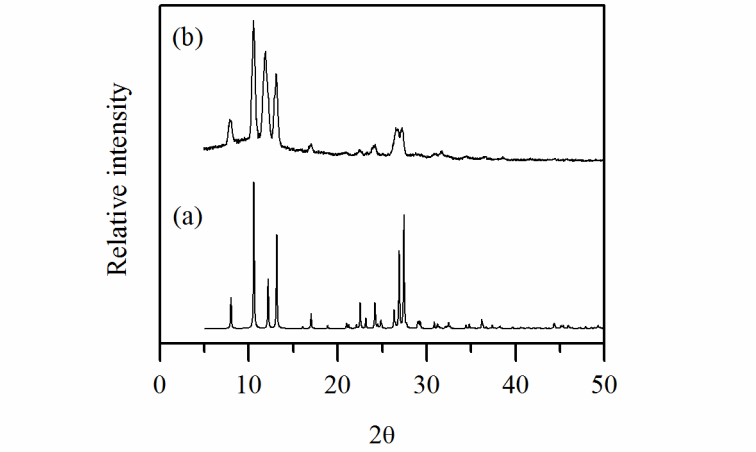

Figure A-11: a) Reference spectrum of caffeine hydrate (1:0.8) by CSD [54] and b) sample spectrum of caffeine hydrate (1:0.8) measured at T = 298.15 K and pH 7

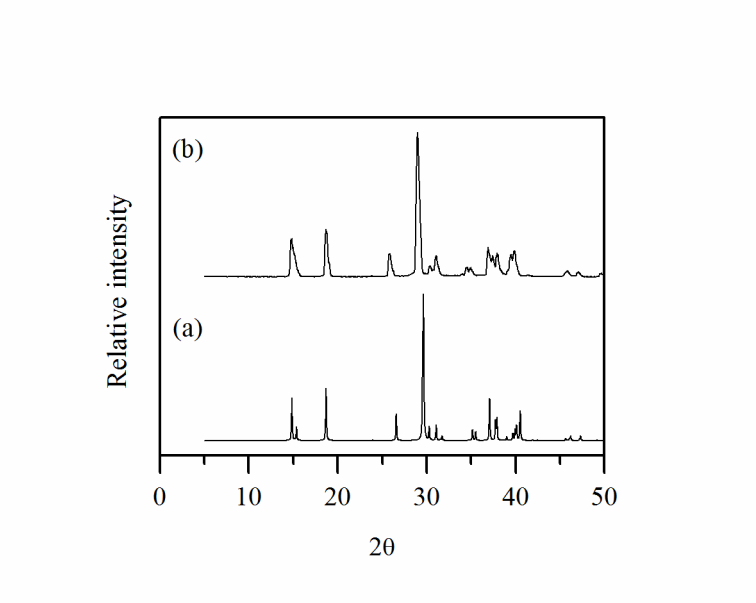

Figure A-12: a) Reference spectrum of oxalic acid dihydrate by CSD [54] and b) sample spectrum of oxalic acid dihydrate at T = 298.15 K and pH 0.7 [29]

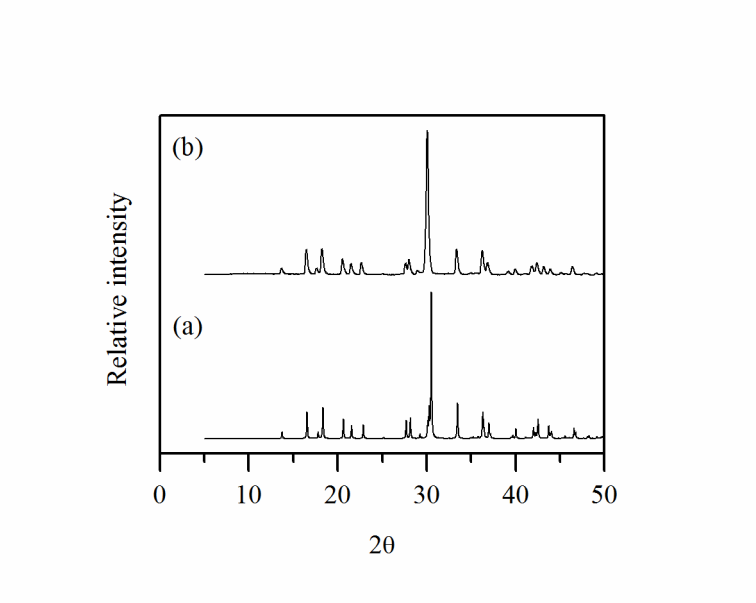

Figure A-13: a) Reference spectrum of sodium hydrogen oxalate monohydrate by CSD [54] and b) sample spectrum of sodium hydrogen oxalate monohydrate measured at T = 298.15 K and pH 2

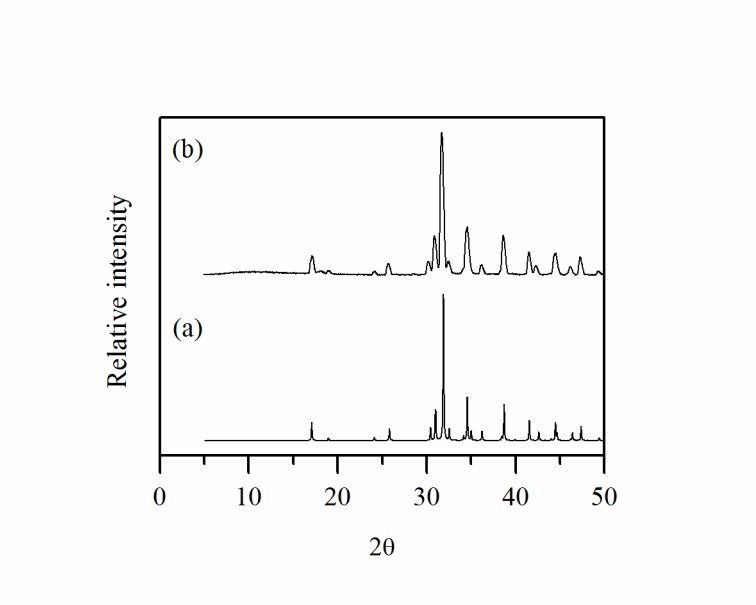

Figure A-14: a) Reference spectrum of disodium oxalate by CSD [54] and b) sample spectrum of disodium oxalate measured at T = 298.15 K and pH 5

A.4 Modeling

A.4.1 Modeling Parameters

Table A-18: PC-SAFT pure component parameters of the solvents for the temperature-dependent solubility modeling of oxalic acid and binary interaction parameters between oxalic acid and solvents (*determined in this work)

Component	**Acetonitrile** [59]	**Ethyl acetate** [17]	**Butyl acetate** [17]
M_i [g mol^{-1}]	41.05	88.11	116.16
$m_{seg,i}$ [-]	2.33	3.54	3.98
σ_{ii} [Å]	3.1898	3.31	3.54
u_{ii} [K]	311.31	230.80	242.52
ε^{AiBi} [K]	0.00	0.00	-
κ^{AiBi} [-]	0.01	0.01	-
$as.scheme$ [-]	1/1	1/1	-
$k_{i,OxA,m}$ [K^{-1}]	$1.41 \cdot 10^{-4}$*	$3.02 \cdot 10^{-4}$*	$6.91 \cdot 10^{-4}$*
$k_{i,OxA,b}$ [-]	$-5.23 \cdot 10^{-2}$*	$-1.34 \cdot 10^{-1}$*	$-2.55 \cdot 10^{-1}$*

Table A-19: PC-SAFT and pure component parameters of caffeine, oxalic acid and water for the modeling of the temperature- and pH-dependent solubility in this work (*determined in this work)

Component	**Caffeine** [9]	**Oxalic Acid**	**Water** [20]
M_i [g mol^{-1}]	194.19	90.04	18.02
$m_{seg,i}$ [-]	9.56	3.36*	1.20
σ_{ii} [Å]	2.96	2.75*	2.79
u_{ii} [K]	428.51	180.14*	353.94
ε^{AiBi} [K]	827.69	1654.78*	2425.67
κ^{AiBi} [-]	0.02	0.02*	0.05
$as.scheme$ [-]	2/2	2/2*	1/1
$\Delta c_{p,i}$ [J mol^{-1} K^{-1}]	101.52 [21]	93.00 [22]	0.00
Δh_{0i}^{SL} [J mol^{-1}]	21600.00 [23]	18578.00 [22]	0.00
$T_{m,i}$ [K]	509.15 [24]	462.65 [25]	273.15
$pK_{a,1}$ [-]	0.6*	1.23*	-
$pK_{a,2}$ [-]	12.15*	4.3*	-

Table A-20: Reference parameter for the modeling of the temperature-dependent solubility of oxalic acid dihydrate and caffeine hydrate (1:0.8)

Component	**Oxalic acid**	**Caffeine**
Δh_i^{ref} [J mol^{-1}]	15300.00	73000.00
T_i^{ref} [K]	313.15	313.15
$K_{a,i}^{ref}$ [-]	0.127586	0.010110

Table A-21: Binary interaction parameters of oxalic acid, caffeine and ions with water

Component	**Oxalic acid**	**Caffeine**	**HOxA$^-$**	**(Caffeine)$^-$**
$k_{i,H_2O,m}$ [K^{-1}]	$0.00 \cdot 10^{-0}$	$0.00 \cdot 10^{-0}$	$0.00 \cdot 10^{-0}$	$0.00 \cdot 10^{-0}$
$k_{i,H_2O,b}$ [-]	$-2.56 \cdot 10^{-2}$	$-3.95 \cdot 10^{-2}$	$5.00 \cdot 10^{-2}$	$8.00 \cdot 10^{-2}$

Table A-22: Dissociation constants for modeling the pH-dependent solubility of oxalic acid and caffeine in water at 298.15 K and ambient pressure. In case of oxalic acid, K_{a1i} corresponds to the first dissociation step from neutral oxalic acid to hydrogen oxalate and $K_{a2,i}$ corresponds to the second step from hydrogen oxalate to oxalate. In case of caffeine, $K_{a1,i}$ corresponds to the first dissociation step from neutral caffeine to protonated caffeine at a low pH value and $K_{a2,i}$ corresponds to the second dissociation step at a high pH value. The modeled dissociation constants are compared with the literature data

Component	**Oxalic acid**		**Caffeine**	
	Modeled	Literature [40]	Modeled	Literature [45]
$K_{a1,i}$ [-]	$0.70 \cdot 10^{-0}$	$5.37 \cdot 10^{-2}$	$1.0234 \cdot 10^{-05}$	$1.00 \cdot 10^{-01}$
$K_{a2,i}$ [-]	$2.00 \cdot 10^{-4}$	$6.31 \cdot 10^{-5}$	$4.3521 \cdot 10^{-16}$	$1.00 \cdot 10^{-14}$

Table A-23: Solubility products of the hydrates, salts and the cocrystal of oxalic acid and caffeine at 298.15 K and ambient pressure

Component	**Complex stoichiometry**	$\boldsymbol{K_{s,i}}$ **[-]**
A/B or A/B/ H_2O	**A:B or A:B:H_2O**	
Caffeine / H_2O		
Caffeine hydrate	1:0.8	$5.49825 \cdot 10^{-3}$
OxA / H_2O		
Oxalic acid dihydrate	1:2	$5.64259 \cdot 10^{-2}$
OxA H_2 / H_2O		
Sodium hydrogen oxalate monohydrate	1:1:1	$1.66903 \cdot 10^{-1}$
Disodium oxalate	1:2:0	$1.00435 \cdot 10^{-0}$
Cocrystal		
Caffeine / OxA	2:1	$1.65119 \cdot 10^{-8}$

A.4.2 Modeling of the Solubility of Oxalic Acid and Caffeine in Solvents

Table A-24: Modeling of the temperature-dependent solubility of oxalic acid in the organic solvents acetonitrile, ethyl acetate, butyl acetate and the mixture of acetonitrile and ethyl acetate (ACN/EA) with a mass ratio of 1:1 at ambient pressure

T [K]	Solvent			
	Acetonitrile	Ethyl acetate	Butyl acetate	ACN/EA (1:1)
	$x^L_{oxalic\ acid}$	$x^L_{oxalic\ acid}$	$x^L_{oxalic\ acid}$	$x^L_{oxalic\ acid}$
293.15	$5.64 \cdot 10^{-2}$	$9.17 \cdot 10^{-2}$	$6.49 \cdot 10^{-2}$	$8.60 \cdot 10^{-2}$
298.15	$6.15 \cdot 10^{-2}$	$9.82 \cdot 10^{-2}$	$6.91 \cdot 10^{-2}$	$9.19 \cdot 10^{-2}$
303.15	$6.72 \cdot 10^{-2}$	$1.05 \cdot 10^{-1}$	$7.38 \cdot 10^{-2}$	$9.86 \cdot 10^{-2}$
310.15	$7.63 \cdot 10^{-2}$	$1.17 \cdot 10^{-1}$	$8.11 \cdot 10^{-2}$	$1.09 \cdot 10^{-1}$
318.15	$8.87 \cdot 10^{-2}$	$1.32 \cdot 10^{-1}$	$9.07 \cdot 10^{-2}$	$1.23 \cdot 10^{-1}$

Table A-25: Modeling of the density of oxalic acid and water mixtures at five temperatures and ambient pressure

T [K]	283.15	293.15	303.15	313.15	323.15
$x^L_{oxalic\ acid}$	ρ [kg m^{-3}]	ρ [kg m^{-3}]	ρ [kg m^{-3}]	ρ [kg m^{-3}]	ρ [kg m^{-3}]
0.00	999.48	998.13	995.61	992.13	987.87
$2.00 \cdot 10^{-3}$	1003.88	1002.49	999.93	996.40	992.10
$3.99 \cdot 10^{-3}$	1008.23	1006.80	1004.19	1000.63	996.28
$7.95 \cdot 10^{-3}$	1016.80	1015.28	1012.59	1008.94	1004.51
$1.58 \cdot 10^{-2}$	1033.43	1031.74	1028.88	1025.06	1020.46

Table A-26: Modeling of the temperature-dependent solubility of oxalic acid dihydrate and amorphous oxalic acid in water at ambient pressure

T [K]	Water $x^L_{OxA\ dihydrate}$	T [K]	Water $x^L_{oxalic\ acid}$	T [K]	Water $x^L_{oxalic\ acid}$
273.15	$9.41 \cdot 10^{-3}$	373.15	0.33	417.90	0.59
279.82	$1.17 \cdot 10^{-2}$	376.13	0.35	420.88	0.61
286.48	$1.46 \cdot 10^{-2}$	379.12	0.36	423.87	0.64
293.15	$1.81 \cdot 10^{-2}$	382.10	0.38	426.85	0.66
299.82	$2.25 \cdot 10^{-2}$	385.08	0.39	429.83	0.68
306.48	$2.80 \cdot 10^{-2}$	388.07	0.41	432.82	0.71
313.15	$3.49 \cdot 10^{-2}$	391.05	0.42	435.80	0.74
319.82	$4.38 \cdot 10^{-2}$	394.03	0.44	438.78	0.76
326.48	$5.54 \cdot 10^{-2}$	397.02	0.46	441.77	0.79
333.15	$7.08 \cdot 10^{-2}$	400.00	0.47	444.75	0.82
339.82	$9.12 \cdot 10^{-2}$	402.98	0.49	447.73	0.85
346.48	$1.19 \cdot 10^{-1}$	405.97	0.51	450.72	0.88
353.15	$1.54 \cdot 10^{-1}$	408.95	0.53	453.70	0.91
359.82	$1.99 \cdot 10^{-1}$	411.93	0.55	456.68	0.94
366.48	$2.57 \cdot 10^{-1}$	414.92	0.57	459.67	0.97
373.15	$3.33 \cdot 10^{-1}$	416.41	0.58	462.65	1.00

Table A-27: Modeling of the temperature-dependent solubility of caffeine hydrate and amorphous caffeine in water at ambient pressure

T [K]	Water $x^L_{caffeine\ hydrate}$	T [K]	Water $x^L_{caffeine}$	T [K]	Water $x^L_{caffeine}$
273.15	$2.79 \cdot 10^{-5}$	353.15	$7.13 \cdot 10^{-2}$	431.15	0.36
279.82	$7.50 \cdot 10^{-5}$	355.75	$7.45 \cdot 10^{-2}$	436.35	0.40
286.48	$1.89 \cdot 10^{-4}$	358.35	$7.79 \cdot 10^{-2}$	441.55	0.43
293.15	$4.48 \cdot 10^{-4}$	363.55	$8.55 \cdot 10^{-2}$	446.75	0.47
299.82	$9.95 \cdot 10^{-4}$	368.75	$9.42 \cdot 10^{-2}$	451.95	0.50
306.48	$2.05 \cdot 10^{-3}$	373.95	$1.04 \cdot 10^{-2}$	457.15	0.54
313.15	$3.91 \cdot 10^{-3}$	379.15	$1.16 \cdot 10^{-2}$	462.35	0.58
319.82	$6.90 \cdot 10^{-3}$	384.35	$1.30 \cdot 10^{-2}$	467.55	0.62
326.48	$1.14 \cdot 10^{-2}$	389.55	0.15	472.75	0.67
333.15	$1.78 \cdot 10^{-2}$	394.75	0.17	477.95	0.71
336.48	$2.21 \cdot 10^{-2}$	399.95	0.19	483.15	0.75
339.82	$2.73 \cdot 10^{-2}$	405.15	0.21	488.35	0.80
343.15	$3.39 \cdot 10^{-2}$	410.35	0.24	493.55	0.85
346.48	$4.23 \cdot 10^{-2}$	415.55	0.27	498.75	0.90
349.82	$5.39 \cdot 10^{-2}$	420.75	0.30	503.95	0.95
353.15	$7.16 \cdot 10^{-2}$	425.95	0.33	509.15	1.00

A.4.3 Modeling of the pH-dependent Solubility of Oxalic Acid and Caffeine

Table A-28: Modeling of the pH-dependent solubility data of oxalic acid dihydrate, sodium hydrogen oxalate monohydrate and disodium oxalate in water at 298.15 K and ambient pressure

pH	$x^{L}_{oxalic\ acid}$	Solid phase
0.00	$1.40 \cdot 10^{-2}$	oxalic acid dihydrate
0.10	$1.43 \cdot 10^{-2}$	oxalic acid dihydrate
0.20	$1.48 \cdot 10^{-2}$	oxalic acid dihydrate
0.30	$1.56 \cdot 10^{-2}$	oxalic acid dihydrate
0.40	$1.67 \cdot 10^{-2}$	oxalic acid dihydrate
0.50	$1.83 \cdot 10^{-2}$	oxalic acid dihydrate
0.60	$2.08 \cdot 10^{-2}$	oxalic acid dihydrate
0.70	$2.49 \cdot 10^{-2}$	oxalic acid dihydrate
0.76	$1.31 \cdot 10^{-2}$	sodium hydrogen oxalate monohydrate
0.82	$1.16 \cdot 10^{-2}$	sodium hydrogen oxalate monohydrate
0.89	$1.03 \cdot 10^{-2}$	sodium hydrogen oxalate monohydrate
0.96	$9.16 \cdot 10^{-3}$	sodium hydrogen oxalate monohydrate
1.04	$8.11 \cdot 10^{-3}$	sodium hydrogen oxalate monohydrate
1.23	$6.32 \cdot 10^{-3}$	sodium hydrogen oxalate monohydrate
1.50	$5.56 \cdot 10^{-3}$	sodium hydrogen oxalate monohydrate
2.02	$3.78 \cdot 10^{-3}$	sodium hydrogen oxalate monohydrate
2.64	$3.43 \cdot 10^{-3}$	sodium hydrogen oxalate monohydrate
2.94	$3.38 \cdot 10^{-3}$	sodium hydrogen oxalate monohydrate
3.54	$3.59 \cdot 10^{-3}$	sodium hydrogen oxalate monohydrate
3.86	$4.29 \cdot 10^{-3}$	sodium hydrogen oxalate monohydrate
3.95	$4.70 \cdot 10^{-3}$	sodium hydrogen oxalate monohydrate
4.10	$5.58 \cdot 10^{-3}$	sodium hydrogen oxalate monohydrate
4.30	$5.29 \cdot 10^{-3}$	disodium oxalate
4.40	$5.21 \cdot 10^{-3}$	disodium oxalate
5.00	$4.96 \cdot 10^{-3}$	disodium oxalate
6.00	$4.88 \cdot 10^{-3}$	disodium oxalate
8.00	$4.87 \cdot 10^{-3}$	disodium oxalate
10.00	$4.87 \cdot 10^{-3}$	disodium oxalate
12.00	$4.87 \cdot 10^{-3}$	disodium oxalate
14.00	$4.87 \cdot 10^{-3}$	disodium oxalate

Table A-29: Modeling of the pH-dependent solubility data of caffeine hydrate (1:0.8) in water at 298.15 K and ambient pressure

pH	$x^{L}_{caffeine}$	Solid phase
0.00	$1.79 \cdot 10^{-2}$	caffeine hydrate (1:0.8)
0.20	$8.45 \cdot 10^{-3}$	caffeine hydrate (1:0.8)
0.40	$5.20 \cdot 10^{-3}$	caffeine hydrate (1:0.8)
0.60	$3.69 \cdot 10^{-3}$	caffeine hydrate (1:0.8)
0.80	$2.89 \cdot 10^{-3}$	caffeine hydrate (1:0.8)
1.00	$2.43 \cdot 10^{-3}$	caffeine hydrate (1:0.8)
1.40	$2.00 \cdot 10^{-3}$	caffeine hydrate (1:0.8)
1.80	$1.84 \cdot 10^{-3}$	caffeine hydrate (1:0.8)
2.20	$1.77 \cdot 10^{-3}$	caffeine hydrate (1:0.8)
3.00	$1.73 \cdot 10^{-3}$	caffeine hydrate (1:0.8)
4.00	$1.73 \cdot 10^{-3}$	caffeine hydrate (1:0.8)
5.00	$1.73 \cdot 10^{-3}$	caffeine hydrate (1:0.8)
6.00	$1.73 \cdot 10^{-3}$	caffeine hydrate (1:0.8)
7.00	$1.73 \cdot 10^{-3}$	caffeine hydrate (1:0.8)
8.00	$1.73 \cdot 10^{-3}$	caffeine hydrate (1:0.8)
9.00	$1.74 \cdot 10^{-3}$	caffeine hydrate (1:0.8)
10.00	$1.73 \cdot 10^{-3}$	caffeine hydrate (1:0.8)
11.00	$1.82 \cdot 10^{-3}$	caffeine hydrate (1:0.8)
11.60	$2.15 \cdot 10^{-3}$	caffeine hydrate (1:0.8)
11.80	$2.44 \cdot 10^{-3}$	caffeine hydrate (1:0.8)
12.00	$2.96 \cdot 10^{-3}$	caffeine hydrate (1:0.8)
12.20	$3.86 \cdot 10^{-3}$	caffeine hydrate (1:0.8)
12.40	$5.37 \cdot 10^{-3}$	caffeine hydrate (1:0.8)
12.60	$7.75 \cdot 10^{-3}$	caffeine hydrate (1:0.8)
12.80	$1.12 \cdot 10^{-2}$	caffeine hydrate (1:0.8)
13.00	$1.60 \cdot 10^{-2}$	caffeine hydrate (1:0.8)
13.20	$2.21 \cdot 10^{-2}$	caffeine hydrate (1:0.8)
13.40	$2.97 \cdot 10^{-2}$	caffeine hydrate (1:0.8)
13.60	$3.92 \cdot 10^{-2}$	caffeine hydrate (1:0.8)
13.80	$5.08 \cdot 10^{-2}$	caffeine hydrate (1:0.8)
14.00	$6.51 \cdot 10^{-2}$	caffeine hydrate (1:0.8)

A.4.4 Modeling of the pH-dependent Cocrystal Solubility

Table A-30: Prediction of the pH-dependent solubility data of sodium hydrogen oxalate monohydrate and caffeine hydrate (1:0.8) in water at 298.15 K, ambient pressure and pH 1

$x^L_{OxA,total}$	$x^L_{caffeine,total}$	Solid phase
$8.89 \cdot 10^{-3}$	$0.00 \cdot 10^{-0}$	sodium hydrogen oxalate monohydrate
$8.77 \cdot 10^{-3}$	$3.53 \cdot 10^{-4}$	sodium hydrogen oxalate monohydrate
$0.00 \cdot 10^{-0}$	$2.43 \cdot 10^{-3}$	caffeine hydrate (1:0.8)
$1.74 \cdot 10^{-4}$	$2.43 \cdot 10^{-3}$	caffeine hydrate (1:0.8)

Table A-31: Prediction of the pH-dependent cocrystal solubility data of caffeine and oxalic acid (2:1) in water at 298.15 K, ambient pressure and pH 1

$x^L_{OxA,0}$	$x^L_{caffeine,0}$	$x^L_{OxA,total}$	$x^L_{caffeine,total}$	Solid phase
$9.73 \cdot 10^{-5}$	$1.73 \cdot 10^{-3}$	$1.74 \cdot 10^{-4}$	$2.43 \cdot 10^{-3}$	cocrystal
$1.22 \cdot 10^{-4}$	$1.50 \cdot 10^{-3}$	$2.19 \cdot 10^{-4}$	$2.10 \cdot 10^{-3}$	cocrystal
$2.75 \cdot 10^{-4}$	$1.00 \cdot 10^{-3}$	$4.92 \cdot 10^{-4}$	$1.40 \cdot 10^{-3}$	cocrystal
$3.39 \cdot 10^{-4}$	$9.00 \cdot 10^{-4}$	$6.07 \cdot 10^{-4}$	$1.26 \cdot 10^{-3}$	cocrystal
$4.30 \cdot 10^{-4}$	$8.00 \cdot 10^{-4}$	$7.69 \cdot 10^{-4}$	$1.12 \cdot 10^{-3}$	cocrystal
$5.61 \cdot 10^{-3}$	$7.00 \cdot 10^{-4}$	$1.00 \cdot 10^{-3}$	$9.81 \cdot 10^{-4}$	cocrystal
$7.64 \cdot 10^{-4}$	$6.00 \cdot 10^{-4}$	$1.37 \cdot 10^{-3}$	$8.41 \cdot 10^{-4}$	cocrystal
$1.10 \cdot 10^{-3}$	$5.00 \cdot 10^{-4}$	$1.97 \cdot 10^{-3}$	$7.01 \cdot 10^{-4}$	cocrystal
$1.72 \cdot 10^{-3}$	$4.00 \cdot 10^{-4}$	$3.07 \cdot 10^{-3}$	$5.61 \cdot 10^{-4}$	cocrystal
$3.06 \cdot 10^{-3}$	$3.00 \cdot 10^{-4}$	$5.45 \cdot 10^{-3}$	$4.21 \cdot 10^{-4}$	cocrystal
$4.92 \cdot 10^{-3}$	$2.51 \cdot 10^{-4}$	$8.77 \cdot 10^{-3}$	$3.53 \cdot 10^{-4}$	cocrystal

Table A-32: Prediction of the pH-dependent solubility data of sodium hydrogen oxalate monohydrate and caffeine hydrate (1:0.8) in water at 298.15 K, ambient pressure and pH 2

$x^L_{OxA,total}$	$x^L_{caffeine,total}$	Solid phase
$3.72 \cdot 10^{-3}$	$0.00 \cdot 10^{-0}$	sodium hydrogen oxalate monohydrate
$3.71 \cdot 10^{-3}$	$8.51 \cdot 10^{-3}$	sodium hydrogen oxalate monohydrate
$0.00 \cdot 10^{-0}$	$1.80 \cdot 10^{-3}$	caffeine hydrate (1:0.8)
$5.00 \cdot 10^{-4}$	$1.80 \cdot 10^{-3}$	caffeine hydrate (1:0.8)
$8.31 \cdot 10^{-4}$	$1.80 \cdot 10^{-3}$	caffeine hydrate (1:0.8)

Table A-33: Modeling of the pH-dependent cocrystal solubility data of caffeine and oxalic acid (2:1) in water at 298.15 K, ambient pressure and pH 2

$x^L_{OxA,0}$	$x^L_{caffeine,0}$	$x^L_{OxA,total}$	$x^L_{caffeine,total}$	Solid phase
$9.27 \cdot 10^{-5}$	$1.73 \cdot 10^{-3}$	$8.31 \cdot 10^{-4}$	$1.80 \cdot 10^{-3}$	cocrystal
$1.07 \cdot 10^{-4}$	$1.60 \cdot 10^{-3}$	$9.62 \cdot 10^{-4}$	$1.66 \cdot 10^{-3}$	cocrystal
$1.40 \cdot 10^{-4}$	$1.40 \cdot 10^{-3}$	$1.26 \cdot 10^{-3}$	$1.46 \cdot 10^{-3}$	cocrystal
$1.91 \cdot 10^{-4}$	$1.20 \cdot 10^{-3}$	$1.71 \cdot 10^{-3}$	$1.25 \cdot 10^{-3}$	cocrystal
$2.75 \cdot 10^{-4}$	$1.00 \cdot 10^{-3}$	$2.46 \cdot 10^{-3}$	$1.04 \cdot 10^{-3}$	cocrystal
$4.15 \cdot 10^{-4}$	$8.18 \cdot 10^{-4}$	$3.71 \cdot 10^{-3}$	$8.51 \cdot 10^{-4}$	cocrystal

Table A-34: Prediction of the pH-dependent solubility data of sodium hydrogen oxalate monohydrate and caffeine hydrate (1:0.8) in water at 298.15 K, ambient pressure and pH 2.6

$x^L_{OxA,total}$	$x^L_{caffeine,total}$	Solid phase
$3.42 \cdot 10^{-3}$	$0.00 \cdot 10^{-0}$	sodium hydrogen oxalate monohydrate
$3.42 \cdot 10^{-3}$	$1.66 \cdot 10^{-3}$	sodium hydrogen oxalate monohydrate
$0.00 \cdot 10^{-0}$	$1.75 \cdot 10^{-3}$	caffeine hydrate (1:0.8)
$1.50 \cdot 10^{-3}$	$1.75 \cdot 10^{-3}$	caffeine hydrate (1:0.8)
$3.10 \cdot 10^{-3}$	$1.75 \cdot 10^{-3}$	caffeine hydrate (1:0.8)

Table A-35: Prediction of the pH-dependent cocrystal solubility data of caffeine and oxalic acid (2:1) in water at 298.15 K, ambient pressure and pH 2.6

$x^L_{OxA,0}$	$x^L_{caffeine,0}$	$x^L_{OxA,total}$	$x^L_{caffeine,total}$	Solid phase
$9.25 \cdot 10^{-5}$	$1.73 \cdot 10^{-3}$	$3.10 \cdot 10^{-3}$	$1.75 \cdot 10^{-3}$	cocrystal
$9.51 \cdot 10^{-5}$	$1.70 \cdot 10^{-3}$	$3.19 \cdot 10^{-3}$	$1.72 \cdot 10^{-3}$	cocrystal
$1.02 \cdot 10^{-4}$	$1.64 \cdot 10^{-3}$	$3.42 \cdot 10^{-3}$	$1.66 \cdot 10^{-3}$	cocrystal

Table A-36: Prediction of the pH-dependent solubility data of sodium hydrogen oxalate monohydrate and caffeine hydrate (1:0.8) in water at 298.15 K, ambient pressure and pH 4

$x^{L}_{OxA,total}$	$x^{L}_{caffeine,total}$	**Solid phase**
$4.70 \cdot 10^{-3}$	$0.00 \cdot 10^{-0}$	sodium hydrogen oxalate monohydrate
$4.70 \cdot 10^{-3}$	$1.73 \cdot 10^{-3}$	sodium hydrogen oxalate monohydrate
$0.00 \cdot 10^{-0}$	$1.73 \cdot 10^{-3}$	caffeine hydrate (1:0.8)
$2.50 \cdot 10^{-3}$	$1.73 \cdot 10^{-3}$	caffeine hydrate (1:0.8)
$4.70 \cdot 10^{-3}$	$1.73 \cdot 10^{-3}$	caffeine hydrate (1:0.8)

Table A-37: Prediction of the pH-dependent solubility data of disodium oxalate and caffeine hydrate (1:0.8) in water at 298.15 K, ambient pressure and pH 5

$x^{L}_{OxA,total}$	$x^{L}_{caffeine,total}$	**Solid phase**
$4.95 \cdot 10^{-3}$	$0.00 \cdot 10^{-0}$	disodium oxalate
$4.95 \cdot 10^{-3}$	$1.73 \cdot 10^{-3}$	disodium oxalate
$0.00 \cdot 10^{-0}$	$1.73 \cdot 10^{-3}$	caffeine hydrate (1:0.8)
$2.50 \cdot 10^{-3}$	$1.73 \cdot 10^{-3}$	caffeine hydrate (1:0.8)
$4.95 \cdot 10^{-3}$	$1.73 \cdot 10^{-3}$	caffeine hydrate (1:0.8)

Table A-38: Prediction of the pH-dependent solubility data of disodium oxalate and caffeine hydrate (1:0.8) in water at 298.15 K, ambient pressure and pH 7

$x^{L}_{OxA,total}$	$x^{L}_{caffeine,total}$	**Solid phase**
$4.87 \cdot 10^{-3}$	$0.00 \cdot 10^{-0}$	disodium oxalate
$4.87 \cdot 10^{-3}$	$1.73 \cdot 10^{-3}$	disodium oxalate
$0.00 \cdot 10^{-0}$	$1.73 \cdot 10^{-3}$	caffeine hydrate (1:0.8)
$2.50 \cdot 10^{-3}$	$1.73 \cdot 10^{-3}$	caffeine hydrate (1:0.8)
$4.87 \cdot 10^{-3}$	$1.73 \cdot 10^{-3}$	caffeine hydrate (1:0.8)

A. Lists of Figures and Tables

List of Figures

List of Tables